Structural and functional roles of free mRNAs during proteostasis stress and amyloidogenesis

Dissertation

zur Erlangung des Doktorgrades

der Naturwissenschaften

vorgelegt beim Fachbereich Biochemie, Chemie und Pharmazie (FB 14)

der Johann Wolfgang Goethe -Universität

in Frankfurt am Main

von

Marion Alriquet

aus Rodez

Frankfurt 2019

(D30)

vom Fachbereich Biochemie, Chemie und Pharmazie (FB 14)

der Johann Wolfgang Goethe -Universität als Dissertation angenommen

Dekan: Prof. Dr. Clemens Glaubitz

Gutachter: Dr. Martin Vabulas

Prof. Dr. Volker Dötsch

Datum der Disputation:

Abstract

Proteostasis stressors that destabilize the cellular proteome, like heat shock, trigger transcription and translational reactions leading to the accumulation of heat shock proteins, also called molecular chaperones. During stress, induction of stress response genes is prioritized so that molecular chaperones and other stress response proteins are synthesized to cope with proteome misfolding and aggregation. In order to promote the selective translation of stress-specific genes, translation of others genes that are nonessential for cell survival has to stop. Nonessential protein-coding mRNAs accumulate in the cytosol with the associated proteins to form granular structures called stress granules (SG). These membrane-less organelles are thought to be involved in cell survival, mRNA stabilization and mRNA triage. They were proposed to form via the liquid-liquid phase separation which can be triggered by the high local concentration of RNA-binding proteins. mRNAs were long thought to simply play a scaffolding role by bringing RNA-binding proteins together and allowing their concentration and local aggregation. Recently, the active role of mRNAs in the SG assembly became apparent, too. For example, the spontaneous assembly of total yeast RNA into granules was observed, and these RNA granules showed a large overlap with SG transcriptome. Furthermore, cytosolic mRNAs can be released from polyribosomes under stress and be exposed to the cytosolic contents as free mRNAs. It has been suggested that this massive increase of free mRNA in the cytosol might overload the capacities of RNA-stabilizing proteins. The remaining free mRNA molecules would then become exposed to misfolded and aggregation-prone proteins and trigger granulation.

We investigated the role of free mRNAs in different stress conditions during the early and chronic phases of stress response and explored their involvement in SGs assembly and amlyoidogenesis. We identified and studied the interactome of a free mRNA probe incubated with heat shocked cell lysate by means of quantitative mass spectrometry. Proteomics analysis allowed us to identify 79 interactors of free mRNA. Among these interactors, we focused on the translation initiation factor eIF2α and on the RNA methyltransferase TRMT6/61A. Both interactions were verified biochemically, which confirmed that the association is enhanced in heat shocked lysate. *In vitro* reconstitution showed that free mRNA and TRMT6 interact directly. *Ex vivo* pulldowns revealed

that eIF2α and TRMT6/61A interact under stress conditions and that this interaction is RNA-dependent.

TRMT6/61A is a tRNA methytransferase responsible for the methylation of the adenosine 58 at the position 1 producing m^1A. However, also mRNAs have been recently found to be methylated by TRMT6/61A. Our bioinformatics analyses revealed that significantly more mRNAs enriched in SG contain the motif for methylation than SG-depleted mRNAs. We hypothesized that m^1A methylation of mRNAs could constitute a tag for the mRNAs targeting to SGs. TRMT61A knock-down (KD) cell lines were generated using the CRISPR-Cas9 technique. In TRMT61A KD cells, m^1A was significantly reduced on mRNAs, which correlated with an increased sensitivity of the cells to proteostasis stress. KD cells also showed defects in SG assembly. In heat shocked cells, an m^1A motif-containing mRNA recovered better after returning to normal temperature than a control mRNA with mutated motif. In addition, we could isolate SGs and analyze their m^1A and m^6A content by mass spectrometry. While m^6A content in SG mRNAs was very similar to cytosolic mRNAs, m^1A was almost 8 times enriched in SGs. Thus, we could confirm experimentally the results of the bioinformatics analysis and directly support the hypothesis that m^1A is a tag to direct mRNAs for sequestration. Finally, we compared amyloidogenesis in wild-type and TRMT61A KD cell lines. Cells with reduced levels of TRMT61A demonstrated an increased accumulation of transfected Aβ and an impaired aggregate clearance. Various assays led us to conclude that the lack of m^1A deposition on mRNAs enhanced RNA co-aggregation with amyloids.

Based on our results, we propose a model explaining the fate of free mRNA during proteostasis stress. Upon polysome disassembly, free mRNA is released and becomes free to interact with other proteins, including the methyltransferase TRMT6/61A. TRMT6/61A methylates the freed mRNAs containing the cognate motif. The m^1A tag then targets mRNAs to SGs promoting sequestration. Upon stress release, SGs disassemble, thus releasing rescued mRNAs which could now reenter translation and support cell recovery. On the other hand, non-sequestered mRNAs increasingly co-aggregate with aggregating proteins. Thus, deficiency of the N1-adenine methylation of mRNAs due to the lack of TRMT6/61A increases the amount of unpacked mRNAs. The deposition of m^1A on mRNAs could then be a way to protect them during exposure to stress, to limit their co-aggregation with misfolded proteins and to allow a faster recovery upon stress release.

Zusammenfassung

Die richtige Struktur der Proteine ist für ihre Funktion unerlässlich, daher wird die Proteinfaltung streng kontrolliert. Der Faltungsprozess ist fehleranfällig und es entstehen ständig falsch gefaltete Proteine. Eine Fehlfaltung kann ihre Aktivität und Stabilität beeinträchtigen und manchmal toxisch und schädlich für die Zelle sein. Das Gleichgewicht zwischen Proteinsynthese, Faltung und Abbau muss streng reguliert werden, damit die Zellen überleben können. Stressfaktoren, die das Proteom destabilisieren, wie z.B. ein Hitzeschock, lösen eine Reaktion der Zelle aus, die zur Induktion von Hitzeschockproteinen führt, auch molekulare Chaperone genannt. Während des Stresses wird die Translation von Stressreaktionsgenen priorisiert, so dass Chaperone und andere Stressreaktionsproteine synthetisiert werden, um mit der Fehlfaltung von Proteinen fertig zu werden. Um die selektive Translation von stressspezifischen Genen zu fördern, muss die Translation von anderen Genen, die für das Überleben der Zelle unwesentlich sind, eingestellt werden. Nicht essenzielle mRNAs akkumulieren mit den zugehörigen Proteinen zu Granulatstrukturen, den sogenannten Stressgranulaten. Diese Organellen bestehen aus RNA und Proteinen und sind vermutlich am Überleben der Zelle, der mRNA-Stabilisierung und der mRNA-Triage beteiligt. Sie bilden sich bei einem Translationsstopp, der durch die Phosphorylierung des Translationsfaktors eIF2α ausgelöst wird. Die Phosphorylierung von eIF2α Serin 51 hemmt den Austausch von GDP zu GTP und verhindert das Recycling von eIF2α, was zur Blockade der Translationsinitiierung führt. Nach der Phosphorylierung von eIF2α assoziiert TIA-1, ein mRNA-bindendes Protein, das am mRNA-Spleißen beteiligt ist, mit eIF2-defizienten Vorinitiierungskomplexen, die dann das Transkript ablaufen und zur Disassemblierung von Polysomen führen. Stress-Granulat-Proteine sind meist RNA-bindende Proteine (ca. 50 %) mit hoher Aggregationsneigung. Die meisten Proteine aus dem 48S-Pre-Initiationskomplex haben sich als Teil von Stressgranulaten erwiesen, einschließlich der kleinen ribosomalen Untereinheit und Translationsinitiationsfaktoren wie eIF4E, eIF3, eIF4A, eIF4G sowie PolyA Binding Protein. Ihre Instabilität hat lange Zeit die Isolierung von Stressgranulaten erschwert, aber eine jüngste veröffentlichte Proteomanalyse von stabilen Stressgranulatkernen half, eine vollständigere Liste von Stressgranulat-Proteinen zu erstellen. Diese Analyse ergab, dass Stressgranulatekerne ein sehr dichtes Netzwerk von Proteinen bilden. Interessanterweise wurden viele aggregierungsanfällige Proteine, die an Krankheiten wie neurologischen Störungen oder Myopathien beteiligt sind, in Stressgranulaten identifiziert. Die mRNA-Zusammensetzung von Stressgranulaten wurde kürzlich

in Hefe- und Säugetierzellen entdeckt. Obwohl die meisten mRNAs in Stressgranulaten vorkommen können, werden sie mit sehr unterschiedlicher Effizienz, im Bereich von 1 % bis 95 %, rekrutiert.

Die Bildung und Zusammensetzung von Stressgranulaten bleibt ein Bereich der aktiven Forschung. Es wird angenommen, dass sie sich über einen Flüssig-Flüssig-Phasentrennungsmechanismus bilden, der durch eine lokale Konzentration von RNA-Bindungsproteinen ausgelöst wird. Bis vor Kurzem wurde davon ausgegangen, dass mRNAs nur eine Gerüstrolle spielen, indem sie RNA-Bindungsproteine zusammenbringen und ihre Konzentration und lokale Aggregation ermöglichen. Diese Hypothese wurde durch die spontanen Aggregation einiger Stressgranulatproteine *in vitro*, in Abwesenheit von mRNA untermauert. Die Rolle der mRNAs bei der Bildung von Stressgranulaten wurde jedoch erst kürzlich durch die Beobachtung der spontanen Assemblierung der gesamten Hefe-RNA zu Granulaten interessant, welche eine große Überschneidung mit dem Transkriptom der Stressgranulate aufwiesen. Darüber hinaus hat sich kürzlich gezeigt, dass RNA die biophysikalischen Eigenschaften und die Zusammensetzung von RNA-Granulaten beeinflusst. Schließlich wurde vorgeschlagen, dass freie mRNAs, die bei Stress freigesetzt werden, die Bildung von Stressgranulaten initiieren könnt. Unter normalen Bedingungen, vor der Translation, sind mRNAs mit RNA-bindenden Proteinen assoziiert, die an der mRNA-Prozessierung beteiligt sind. Unter bestimmten Bedingungen können zytosolische mRNAs aus Polyribosomen freigesetzt und als freie mRNA ins Zytosol abgegeben werden. Es wurde vermutet, dass dieser Anstieg der freien mRNA-Mengen im Zytosol eine Sättigung von RNA-Stabilisierungsproteinen wie YB-1 erzeugt. Die verbleibenden freien mRNA-Moleküle würden im Zytosol falsch gefalteten und aggregierungsanfälligen Proteinen ausgesetzt werden und die Bildung von Stressgranulaten auslösen.

Wir untersuchten die Rolle der freien mRNAs unter Stressbedingungen in der frühen Phase der Stressreaktion, in Hinblick auf ihre Beteiligung an der Bildung von Stressgranulaten. Die Exposition der freien mRNA mit dem Zytosol könnte Möglichkeiten der Interaktion mit zytosolischen Proteinen eröffnen. Für diese Studie haben wir zunächst Stressbedingungen festgelegt, die es uns ermöglichten, das frühe Stadium der Stressreaktion zu untersuchen, in dem Stressgranulate assembliert werden. Zu diesem Zweck haben wir Zellen Hitzeschockbedingungen ausgesetzt und verschiedene Kriterien untersucht, um die optimale Belastungsbedingung für unsere

Studie zu bestimmen. So haben wir beispielsweise die Induktion des Chaperons HSP70, den Phosphorylierungsstatus von eIF2α, die Bildung von Stressgranulaten und Polysomenprofile bei Stressbelastung überwacht. Nachdem wir die richtigen Hitzeschockbedingungen bestimmt hatten, um die Bildung von Stressgranulaten zu untersuchen, untersuchten wir das Zusammenspiel einer freien mRNA-Sonde, die mit Zelllysat aus Stress exponierten Zellen, inkubiert wurde, mittels quantitativer Massenspektrometrie. Diese Sonde bestand aus kodierenden Sequenz der HSP70 mRNA, unter Deletion der 3' und 5' -UTR-Regulierungsregionen. Dadurch wurde diese mRNA zu einer idealen Modell-mRNA und wir konnten ihre spontane Granulation nach der Transfektion in Zellen verifizieren. Die Proteomanalyse der Stressgranulate erlaubte es uns, 79 Interaktoren der freien mRNA zu identifizieren. Dieses Ergebnis wurde mit einer weiteren mRNA-Sonde ähnlicher Länge verifiziert, die aus der kodierenden Sequenz von B-Raf besteht. Etwa die Hälfte der Interaktoren zeigte eine Schnittmenge mit der RNA-Sonde von HSP70, wordurch unsere Interaktionliste in Bezug auf den minimalen sequenzspezifischen Bias und Relevanz untermauert wurde.

Unter diesen Interaktionen konzentrierten wir uns auf den Translationsinitiationsfaktor eIF2α und auf die Methyltransferase TRMT6/61A. Die Interaktion der freien mRNA mit der Untereinheit eIF2α wurde biochemisch verifiziert und wir beobachteten, dass nur die nicht-phosphorylierte Form (an Serin 51) des Proteins beteiligt war, obwohl die Phosphorylierung von eIF2α nicht beeinträchtigt war. Wir konnten außerdem zeigen, dass diese Interaktion nur bei hitzeschockbehandeltem Lysat stattfand. Wir konnten die Interaktion der freien mRNA mit TRMT6/61A biochemisch überprüfen und zeigten, dass sie ebenfalls durch Hitzeschock induziert wird. Dieses Protein ist vor allem als tRNA-Methyltransferase bekannt, dass für die Methylierung des Adenosins 58 an der Position 1 (m^1A) verantwortlich ist. Diese Modifikation ist notwendig für die Stabilität der Initiator tRNA, auch bekannt als tRNA-iMet. Es wurde jedoch auch festgestellt, dass mRNAs methyliert sind, und in einer kürzlich veröffentlichten Studie konnte TRMT6/61A als Methyltransferase identifiziert werden, die die m^1A-Modifikation katalysiert. Weiterführend konnten wir die Interaktion von TRMT6/61A mit endogener mRNA während des Hitzeschocks mittels PolyA mRNA Pulldowns verifizieren. Interessanterweise konnten freie mRNA und TRMT6 direkt *in vitro* interagieren, die Interaktion ging jedoch bei 45 °C verloren. *In vitro* Strukturanalysen zeigten eine lokale Entfaltung in der TRMT6 Untereinheit bei 45 °C, die die Affinität des Heterodimers zu seinem Hauptsubstrat tRNA nicht verminderte. *Ex vivo* Pulldowns

zeigten, dass eIF2α und TRMT6/61A miteinander interagieren und dass diese Interaktion RNA-abhängig ist, was darauf hindeutet, dass mRNA, eIF2α und TRMT6/61A Teil eines großen Multiproteinkomplexes sein könnten. Das Fehlen einiger Schlüsselkomponenten würde erklären, warum wir die erhöhte Interaktion beim Hitzeschock *in vitro* nicht beobachten konnten.

Wir führten eine bioinformatische Analyse durch, die ergab, dass deutlich mehr mRNAs, die in Stressgranulaten angereichert sind, das Motiv der Methylierung enthalten, als mRNAs, die nicht mit Stressgranulaten assoziiert sind. Wir formulierten die Hypothese, dass die m^1A-Methylierung von mRNAs ein Marker für die mRNAs darstellt, der sie zu Stressgranulate rekrutiert. Eine mikroskopische Evaluation von überexprimiertem TRMT6/61A in HeLa Zellen, zeigte eine Kolokalisierung der Methyltransferase mit dem Stress-Granulat-Marker TIAR bei Behandlung mit Arsenit, obwohl weder TRMT6 noch TRMT61A bisher als Komponenten von Stressgranulaten identifiziert wurden. Die funktionelle Konsequenz der m^1A-Deposition auf mRNAs während der Stressreaktion wurde mit TRMT61A Knock-Down (KD) Zelllinien analysiert, die mit der CRISPR-Cas9-Technik erzeugt wurden. Der Mangel an m^1A auf mRNAs führte zu einer erhöhten Empfindlichkeit der Zellen gegenüber proteostatischem Stress. In TRMT61A KD-Zellen wurde m^1A auf PolyA mRNAs signifikant reduziert, was uns ermöglichte, diese neuartige Funktion der Methyltransferase zu untersuchen. In hitzeschockbehandelten Zellen waren mRNAs, die das m^1A-Motiv enthielten, stabiler und wurde unmittelbar nach der Rückkehr zur Normaltemperatur besser translatiert als Kontroll-RNA mit mutiertem Motiv. Eine mögliche Erklärung hierfür ist, dass die m^1A-haltige mRNA zu Stressgranulaten rekrutiert wurde und somit vor dem Abbauprozess geschützt war. Darüber hinaus konnten wir Stressgranulate isolieren und deren m^1A- und m^6A-Gehalt (eine Modifikation von mRNAs, die durch eine andere Methyltransferase deponiert wird) mittels Massenspektrometrie analysieren. Dabei zeigte sich, dass der m^6A-Gehalt in Stressgranulaten mRNAs sehr ähnlich zu PolyA mRNAs war, während m^1A fast 8-fach angereichert war. Wir konnten somit die Ergebnisse der Bioinformatik-Analyse biochemisch bestätigen und die Hypothese direkt unterstützen, dass m^1A ein Marker ist, um mRNAs zu Stressgranulaten zu rekrutieren.

Da Zellen ohne TRMT61A eine erhöhte Empfindlichkeit gegenüber proteostatzischem Stress zeigten, verglichen wir die Amyloidogenese in wildtyp und TRMT61A KD-Zelllinien. Interessanterweise zeigten Zellen mit reduziertem TRMT61A Expressionslevel eine erhöhte

Akkumulation von transfiziertem Aβ und eine beeinträchtigte Beseitigung der Aβ-Aggregate. Die Analyse der Interaktoren von Amyloiden ergab die Koaggregation von mRNA-bindenden Proteinen, was auf das Vorhandensein von mRNA in den Aggregaten hindeutet. Wir konnten diese Annahme direkt beweisen, indem wir PolyA mRNA Pulldowns durchführten und eine erhöhte Assoziation von Aβ mit mRNA aus Zellen ohne TRMT61A fanden. Diese beiden Ergebnisse führten uns zu dem Schluss, dass der Mangel an m^1A-Modifikationen auf mRNAs die Koaggregation von RNA mit Amyloiden verstärkt. Wir konnten außerdem zeigen, dass eine m^1A mRNA bei Kotransfektion mit Aβ effizienter gerettet und translatiert wurde als eine mRNA mit einem mutierten m^1A-Motiv. Dieses Ergebnis wurde zusätzlich in einer weiteren Zelllinie, der murinen Melanom-Zelllinie B16F10, bestätigt.

Wir schlagen ein Modell für das Verhalten von freien mRNAs bei proteostatischem Stress vor. Bei der stressinduzierten Disassemblierung von Polysomen entsteht freie mRNA, die dem Inhalt des Zytosols ausgesetzt ist. Dardurch werden Interaktionen mit anderen Proteinen ermöglicht, einschließlich der Methyltransferase TRMT6/61A. Auf der Basis unserer Ergebnisse ist anzunehmen, dass TRMT6/61A die durch Stressexposition freigesetzten mRNAs erkennt und modifiziert, wenn diese ein bestimmtes m^1A-Motiv enthalten. Das m^1A Motiv könnte dann als Marker dienen, der mRNAs zu Stressgranulaten rekrutiert und deren Assemblierung fördert. Nach dem Ende des Stressexposition zerfallen Stressgranulate schnell und setzen so m^1A-haltige mRNAs frei, die wiederum translatiert werden können, um die Zelle bei der Erholung vom Stress zu unterstützen. Andererseits könnten mRNAs, denen die m^1A-Methylierung fehlt, von aggregierenden Proteinen eingeschlossen werden, die durch Konformationsstress erzeugt werden. Ein Mangel an der N1-Adenin-Methylierung von mRNAs aufgrund des Fehlens von TRMT6/61A könnte die Menge an freien, unverpackten mRNAs, die aggregierenden Proteinen ausgesetzt sind, erhöhen und so die Amyloidogenese fördern. Die Deposition von m^1A auf mRNAs könnte somit ein Weg sein, mRNAs während der Stressexposition zu schützen, ihre Koaggregation mit falsch gefalteten Proteinen zu begrenzen und eine schnellere Erholung der Zelle nach der Stressexposition zu ermöglichen.

Contents

List of figures

List of tables

Abbreviations

Abbreviation	Meaning
Aβ	Amyloid beta
A-bodies	Amyloid nuclear bodies
ACM	Amyloid Converting Motifs
ADP	Adenosine diphosphate
ALS	Amyotrophic Lateral Sclerosis
APP	Amyloid Precursor Protein
ATP	Adenosine triphosphate
AVG	Average
Cas9	CRISPR associated protein 9
cDNA	Complementary DNA
CDS	Coding sequence
CRISPR	Clustered Regularly Interspaced Short Palindromic Repeats
ddH_2O	Double-distilled water
DNA	Desoxyribonucleic acid
eIF	Eukaryotic Initiation Factor
FA	Formaldehyde
FDR	False Discovery Rate
FTD	Frontotemporal dementia
Fig.	Figure
FRAP	Fluorescence Recovery After Photobleaching
GCN2	General Control Non-derepressible protein 2
GDP	Guanosine diphosphate
GEF	Guanine Nucleotide Exchange Factor
GFP	Green Fluorescent Protein
GMP	Guanosine monophosphate
GO	Gene Ontology
GTP	Guanosine triphosphate
h	Hour (s)
HS	Heat Shock
HSF1	Heat Shock Factor 1
HRI	Heme-Regulated Inhibitor
HSP	Heat Shock Protein
IDR	Intrinsically Disordered Region
IAPP	Island Amyloid PolyPeptide
KD	Knock-down
kDa	kilo Dalton
KO	Knock-out

Abbreviation	Meaning
LC	Low Complexity
LFQ	Label-free Quantification
LLPS	Liquid-Liquid Phase Transition
m^1A	N1-methyladenosine
m^6A	N6-methyladenosine
min	Minute (s)
MS	Mass Spectrometry
mRNA	messenger RNA
ncRNA	non coding RNA
mRNP	messenger ribonucleoprotein
OD	Optical Density
P-bodies	Processing bodies
PERK	Protein kinase R-like Endoplasmic Reticulum Kinase
PKR	Protein Kinase RNA-activated
SDS-PAGE	Sodium Dodecyl Sulfate-Polyacrylamide Gel Electrophoresis
PCR	Polymerase Chain Reaction
qPCR	quantitative PCR
RACK-1	Receptor of Activated protein C Kinase 1
RBD	RNA-Binding Domain
RBP	RNA-Binding Protein
RNP	Ribonucleoprotein
RNA	Ribonucleic acid
ROS	Reactive Oxygen Species
RT	Room Temperature
SAM	S-Adenosyl methionine
sec	Second (s)
SG	Stress Granule
rRNA	Ribosomal RNA
tRNA	Transfer RNA
TDP-43	Tar DNA-binding Protein 43
TIA-1	T-cell-restricted Intracellular Antigen 1
TIAR	TIA-1-Related protein
UTR	Untranslated Region
UV	Ultra Violet
WT	Wild Type
ZBP1	Zipcode Binding Protein 1

CHAPTER 1. INTRODUCTION

I. Stress granules formation

I. A. Stress granules and stress response

I. A. 1. Heat shock response

The correct structure of proteins is essential for function, therefore protein folding is tightly controlled. The folding process is error-prone and misfolded proteins are constantly produced. Misfolding can affect their activity and stability and sometimes be toxic and detrimental for the cell. The balance between protein synthesis, folding and degradation has to be tightly regulated to allow cell survival. Stressors that destabilize the proteome, like heat shock (HS), trigger a response from the cell that leads to the induction of heat shock proteins (HSP), also called molecular chaperones. This phenomenon is called the HS response and was described in 1962 in drosophila (Ritossa, 1962). This adaptation to stress is controlled by transcription factors, highly conserved among species (Kingston et al., 1987). They are activated upon HS, bind to HSPs promoter regions and are called Heat Shock Factors (HSF). Among them, HSF1 is a key regulator of stress response in mammals. After trimerization, HSF1 is translocated to the nucleus (Baler et al., 1993) and is post-translationally modified (Larson et al., 1988). The activated form of HSF1 can bind HS response elements and promote the transcription of the corresponding genes, leading to the synthesis of HSPs (Fig. 1). HSF1 is constitutively expressed in normal conditions but is thought to be repressed by interactions with HSPs, like constitutive HSP70 (Abravaya et al., 1992; Shi et al., 1998) and HSP90 (Zou et al., 1998). Misfolded proteins generated upon stress are known to induce HSF1 and HSPs gene expression (Ananthan et al., 1986; Hightower, 1980; Kelley and Schlesinger, 1978). When the concentration of misfolded proteins increases, they compete with HSF1 for interaction with HSPs. As a result, the concentration of free HSF1 in the cytosol increases, it becomes free to oligomerize, relocalize to the nucleus, undergo post-translational modifications and bind HS response elements.

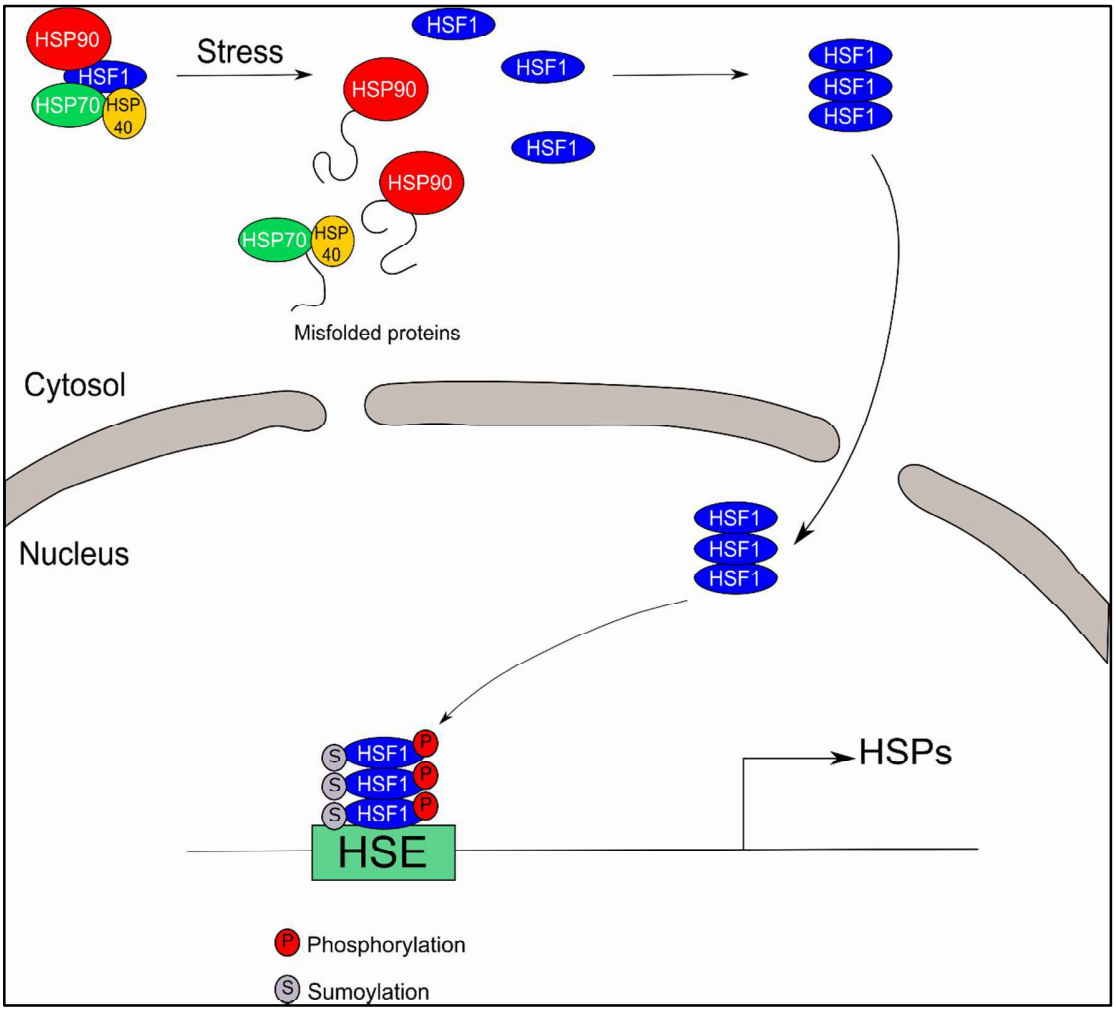

Figure 1. Heat shock response in eukaryotes is regulated by HSF1 activation
Upon stress, misfolded proteins are generated and accumulate. They are bound by HSPs and HSF1 becomes free to oligomerize and relocalize to the nucleus where it is post-translationally modified. The activated form of HSF1 binds to Heat Shock response Elements (HSE), which leads to an increased synthesis of HSPs.

I. A. 2. Fate of untranslated mRNAs during heat shock

During stress, translation of stress response genes is prioritized so that chaperones and other stress response proteins are synthesized to cope with protein misfolding. In order to promote the selective translation of stress-specific genes, translation of others genes that are nonessential for cell survival has to stop.

I. A. 2. a. Translation arrest

eIF2α is a component of the translation initiation machinery and forms a ternary complex with the initiator tRNA, so called tRNA-iMet, and GTP. This complex is recruited to the 40S ribosomal subunit associated with eIF3 and eIF1A to form the 43S pre-initiation complex. 43S in turn associates with mRNA via interaction with eIF4G and eIF3 to form the 48S complex. After scanning of the mRNA and an AUG codon is found, the 60S ribosomal subunit is recruited and initiation factors are released following GTP hydrolysis by eIF2. The 80S initiation complex is ready and translation can start (reviewed in Holcik & Sonenberg, 2005). Phosphorylation of eIF2α is responsible for the inhibition of tRNA-iMet binding to the 40S ribosomal subunit and consequently for the reduced translation initiation upon stress. The serine at the position 51 was identified as the residue phosphorylated upon stress (Colthurst et al., 1987; Pathak et al., 1988). Phosphorylation at this position inhibits GDP exchange to GTP via the Guanine nucleotide Exchange Factor (GEF) eIF2B. eIF2B has an affinity for the phosphorylated form of eIF2α (Ser 51) more than 150 times higher than for its non-phosphorylated form, such that its release from the eIF2-GDP complex is impeded and nucleotide exchange does not take place (Clemens et al., 1982; Ramaiah et al., 1994; Rowlands et al., 1988). Recycling of eIF2α is thus affected and translation initiation inhibited. As a consequence polysomes disassemble, and free RNA is released into cytosol (Kedersha et al., 2000, 1999) (Fig. 2).

Various stressors can induce eIF2α phosphorylation by activating four stress-specific kinases (Fig. 2). Amino acid starvation or exposure to UV light activates the General Control Non-derepressible protein 2 (GCN2) kinase (Deng et al., 2002; Wek et al., 1995). In the case of oxidative stress, osmotic stress, heme deficiency or HS, Heme-Regulated Inhibitor (HRI) is activated (Lu et al., 2001; Mcewen et al., 2005), while it is Protein kinase R-like Endoplasmic Reticulum Kinase (PERK) in the case of ER stress (Harding et al., 2000). Finally, when cells are exposed to double stranded RNA, e.g. during viral infection, Protein Kinase RNA-activated (PKR) is stimulated (Lebleu et al., 1976; Roberts et al., 1976). Following eIF2α phosphorylation, T-cell-restricted Intracellular Antigen 1 (TIA-1) associates with eIF2-deficient pre-initiation complexes which then run off the transcript and leads to polysomes disassembly (Kedersha, et al., 2002).

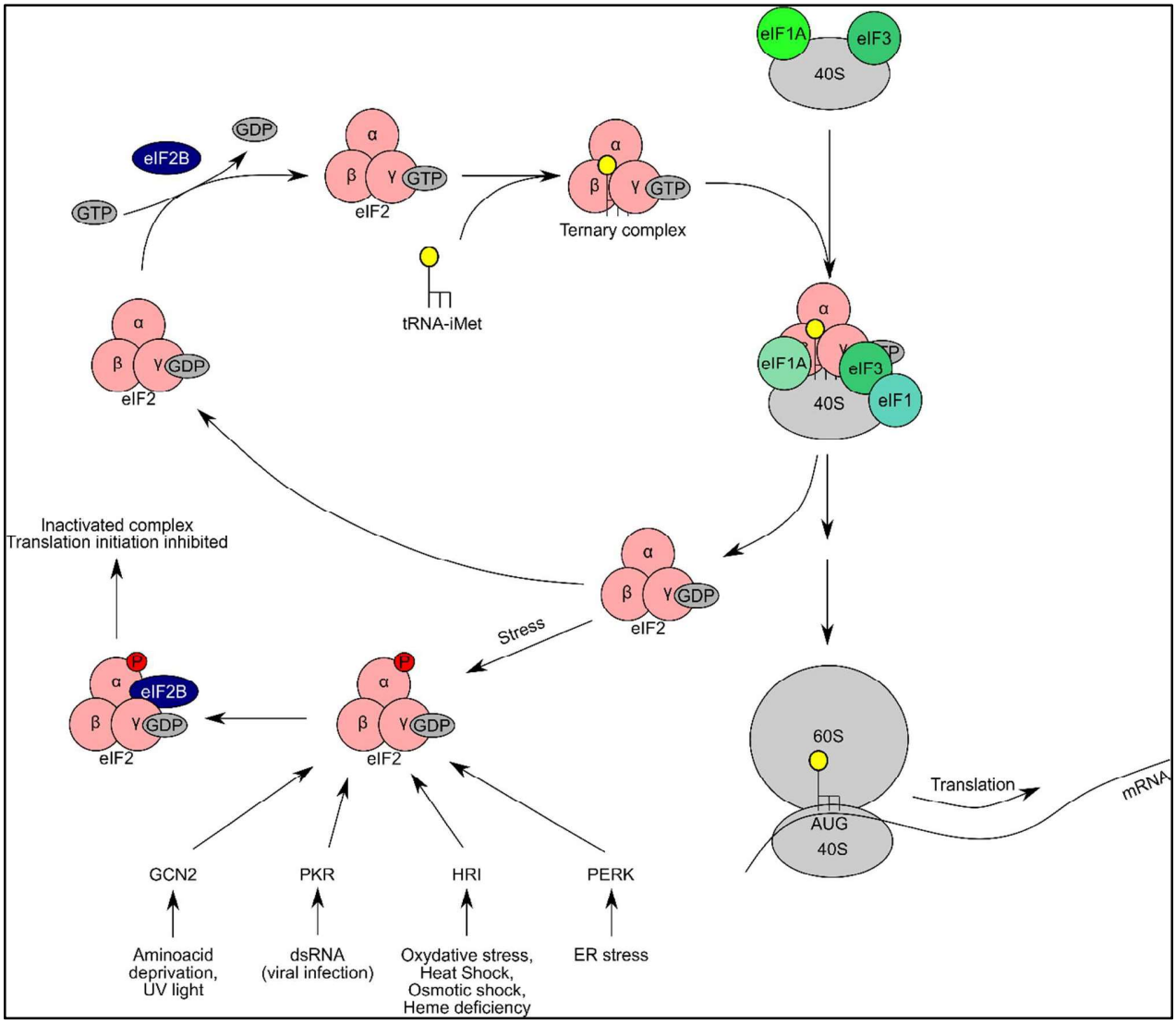

Figure 2. Translation inhibition upon stress via eIF2α phosphorylation, adapted from (Holcik and Sonenberg, 2005).

GTP-bound eIF2 is loaded with tRNA-iMet to form a ternary complex. The 40S ribosomal subunit associated with eIF1A and eIF3 recruits the complex to form the 43S pre-initiation complex. Its association with mRNA to form the 48S pre-initiation complex is followed by the scanning of the mRNA molecule until an AUG codon is found. At this stage, the 60S ribosomal subunit is recruited, GTP is hydrolyzed by eIF2 and the initiation factors are released. The 80S initiation complex is ready to initiate translation. Upon stress, eIF2α can be phosphorylated by four kinases. This leads to the formation of an inactivated complex via interaction with eIF2B and translation is inhibited.

I. A. 2. b. Nuclear pool of mRNAs

While mRNA is being transcribed, it becomes associated with many proteins that play roles in its export, stability and translation. Before being exported to the cytosol, pre-mRNA has to be processed into mature mRNA. Maturation requires the addition of a 5' cap, splicing of introns, and the polyadenylation of the 3' end (Fasken and Corbett, 2009; Zander et al., 2016). The mRNA quality has to be verified to ensure that no improper mRNA reaches the cytosol. The mechanism of this RNA quality control was first identified in yeast and was later shown to be conserved in humans. It involves the loading of mRNA with adaptor proteins at the different key steps of maturation, which subsequently recruit an export receptor heterodimer (Mex67-Mtr2 in yeast, TAP-p15 in human) (Katahira et al., 1999; Tutucci and Stutz, 2011).

It was observed in yeast (Saavedra et al., 1996) that upon stress, export of nuclear mRNAs becomes selective. Most mRNAs are sequestered in the nucleus while stress-specific mRNAs continue being exported from the nucleus and actively translated. Actually stress-specific mRNAs in yeast bypass mRNA quality control and are exported directly for faster translation and synthesis of stress-induced proteins in the cytosol (Zander et al., 2016).

I. A. 2. c. Cytosolic mRNAs

On the other hand, the translation of housekeeping cytosolic mRNAs stops upon stress. These mRNAs accumulate with the associated proteins to form granular structures (Fig. 4). They were first identified in the cytosol of tomato cells after HS as HS granules enriched in low molecular weight HSPs (Nover et al., 1983). The granulation was later observed in the cytosol of mammalian cells as well (Arrigo et al., 1988). The granules in tomato cell lines contained non-translated mRNAs and excluded HS-induced mRNAs, which were found in polysomal fractions (Nover et al., 1989). These granules are considered as a storage form for non HS-induced mRNAs.

Later investigations identified additional types of membrane-less protein-RNA assemblies, such as the nucleolus or Cajal bodies in the nucleus, and Processing bodies (P-bodies) in the cytosol. They form under various stimuli and differ in their content which confers them specific functions. For example, stress granules (SGs) contain mRNAs coding for housekeeping proteins, but also translation factors, the small ribosomal subunit as well as RNA-Binding Proteins (RBPs) (Anderson and Kedersha, 2002) and play a role in gene regulation during stress response (Van

Treeck et al., 2018). On the other hand, P-bodies are enriched in untranslated mRNAs associated with components of the mRNA decay machinery and translational repressors and are thus involved in mRNA degradation (Anderson and Kedersha, 2006; Bashkirov et al., 1997; van Dijk et al., 2003; Van Dijk et al., 2002; Eystathioy et al., 2002, 2003; Ingelfinger et al., 2002).

I. B. Composition of stress granules

SGs consist in a compact core surrounded by a soft shell (Fig. 4). Whether the core or the shell is formed first is unclear, but it appears that the shell is dynamic while the core is dense and very stable (Protter and Parker, 2016). SGs contain untranslated mRNAs and proteins which have been comprehensively identified recently.

I. B. 1. Untranslated mRNAs

The mRNA composition of SGs has been uncovered in yeast and mammalian cells. About 10-15 % of bulk mRNA molecules are enriched in SGs (Khong et al., 2017; Van Treeck et al., 2018) and differences with the total transcriptome can be pointed out. Even though most mRNAs can be found in SGs, they are recruited with different efficiencies ranging from 1 to 95 %. For example, while 80 % of AHNAK mRNA is found in SGs, only 4 % of GAPDH mRNA can be detected in these assemblies (Khong et al., 2017). It also appears that no mRNA is over-represented in SGs, since actin mRNA, the most abundant species in SGs, represents only about 0.5 % of total SGs mRNAs (Khong et al., 2017). The mRNA composition of SGs seems to differ depending on the type of stress that stimulates their formation, which might be a result of different mechanisms of translation repression (Khong et al., 2017).

The efficiency of recruitment of mRNAs to SGs depends on several criteria. SGs mRNAs are usually very long with an average of 7.1 kb, while mRNAs depleted from SGs are in average only 2.5 kb-long. The coding region and the 3' UTR are significantly longer in mRNAs enriched in SGs. SGs also contain non-coding RNAs (ncRNAs) but at lower levels compared to mRNAs (about 20 % in mammalian cells, only 5 % in *Saccharomyces cerevisiae*). These ncRNAs enriched in SGs are also longer compared to the ones depleted from granules (Khong et al., 2017).

I. B. 2. Proteins

TIA-1 and TIA-1-Related protein (TIAR) were established as markers specific to RNA granules (Kedersha et al., 1999). These two proteins contain RNA recognition motifs in their N-terminal part (Kawakami et al., 1992; Tian et al., 1991) and could be involved in FAS-induced apoptosis via induction of DNA fragmentation (Taupin et al., 1995; Tian et al., 1995, 1991). They have also been shown to be involved in post-transcriptional regulation of mRNAs (Gueydan et al., 1999; Piecyk et al., 2000) and are key players of SGs assembly (Kedersha et al., 2000, 1999). For example, TIA-1 mutants lacking RNA-binding domains inhibit SGs assembly (Kedersha et al., 1999). However, the exact mechanism of TIA-1 and TIAR involvement in the recruitment of mRNAs to SGs remains to be clarified. Other components of SGs have further been identified. Most of the proteins from the 48S pre-initiation complex have been demonstrated to be part of SGs, including the small ribosomal subunit, and translation initiation factors, like eIF4E, eIF3, eIF4A, eIF4G as well as PolyA Binding Protein (PABP) (Kedersha et al., 2002). Some RNA-binding proteins which regulate mRNA structure and function, like HuR (Gallouzi et al., 2000), SMN (Hua and Zhou, 2004) or G3BP1 (Tourrière et al., 2003), are also part of SGs, as well as some proteins involved in cellular signaling pathways, such as TRAF-2 (Kim et al., 2005).

The instability of SGs has made their isolation difficult, but the recent proteomic analysis of SGs stable cores provided a more complete list of granules proteins (Jain et al., 2016). The analysis revealed that SGs cores form a very dense network of proteins. In average, a SG protein interacts with 8.32 other SG proteins in mammals. About 50 % of SG proteins are RBPs, most of them being proteins with predicted prion-like domains (PrLD). Among RBPs, many proteins enriched in SGs are translation factors. Several proteins detected in SGs cores demonstrate ATP-dependent activity, and indeed, it was shown that SGs dynamics, including assembly, movement and fusion, require ATP (Jain et al., 2016). Interestingly, many aggregation prone proteins involved in diseases such as neurological disorders or myopathies, have been identified in SGs, thus connecting protein aggregation pathologies with stress granules (Jain et al., 2016).

I. C. Proposed functions of RNA granules

I. C. 1. Stress-induced granules

By sequestration of specific proteins in SGs, their local concentration increases while their cytosolic concentration drops. This could be a way for the cell to block the action of some proteins in the cytosol, or to promote new interactions in the granules. Below, a summary of the various hypotheses that were made concerning the function of stress granules is presented. However, it has to be kept in mind that this question is still not fully resolved and remains under investigation.

I. C. 1. a. Promotion of cell survival

SGs are thought to be involved in many processes related to stress response. Their first potential role is to promote cell survival during stress. Several groups used cells with no or reduced expression of proteins known to participate in SGs assembly to test this hypothesis. HDAC6, a histone deacetylase also involved in the degradation of misfolded proteins, is required for SGs assembly. HDAC6 knock-out (KO) cell lines were prepared and demonstrated an increased percentage of apoptotic cells following arsenite treatment compared to wild-type (WT) cells (Kwon et al., 2007). Similar results were observed with knock-downs (KDs) of RSK2, a SG protein thought to serve as a scaffold for SGs assembly, and KOs of USP10, a deubiquitinase required for SGs assembly via its interaction with the stress granules marker G3BP1 (Eisinger-Mathason et al., 2008; Takahashi et al., 2013). In addition, the translation regulator in germ cells DAZL was knocked out in male mice which resulted in impaired SGs assembly and increased apoptosis upon heat stress (Takahashi et al., 2013). However, these experiments do not provide direct evidence of SGs role in cell survival during stress and the increased apoptosis could also be the result of non-SGs dependent side effects.

Another study established a more direct link between SGs formation and inhibition of apoptosis via the signaling scaffold protein RACK1. It was discovered that MTK1, a kinase involved in the activation of p38 and JNK triggering apoptosis, interacted with the receptor of activated protein C kinase 1, RACK1 (Arimoto et al., 2008). This protein has been shown to localize to SGs in mammalian cells upon arsenite treatment. In addition, the study showed that RACK1 sequestration into SGs inhibited the activation of MTK1 and blocked apoptosis induction.

Another approach consisted in verifying the effect of stress on cells that cannot assemble SGs upon treatment with chemicals, such as cyclohexamide or emetine, which both stabilize polysomes. A study focusing on TORC1, a kinase that couples nutrient availability and protein synthesis and which is recruited to SGs upon heat stress, established a link between SGs formation and protection from stress-induced DNA damage (Takahara and Maeda, 2012). Cells were treated with cyclohexamide and exposed to HS, and demonstrated an increased mutation rate compared to untreated cells. When the cells were at the same time treated with an inhibitor of TORC1, the mutation rate was similar whether SGs formation was inhibited or not, which suggested that TORC1 sequestration into SGs protected the cells from HS-induced DNA damage. (Takahara and Maeda, 2012).

Although these approaches do not exclude the involvement of non-SGs dependent effects, they support the hypothesis of a cytoprotective role of SGs.

I. C. 1. b. Translation regulation

Many translation factors and untranslated mRNAs have been found to be sequestered into SGs. Consequentially, one of the first hypotheses made about the function of SGs was that the sequestration of translation factors participated in the inhibition of translation during stress (Anderson and Kedersha, 2008; Kedersha and Anderson, 2002). However, it has been demonstrated later that SGs are not necessary for translation shutdown during stress response. Both in mammalian cells and yeast, the use of mutants cells which are unable to assemble SGs revealed that translation was still repressed upon stress (Buchan et al., 2008; Kwon et al., 2007). Several studies confirmed this result and suggested that SGs formation and translation repression upon stress are uncoupled (Loschi et al., 2009; Mokas et al., 2009). Yet, because of the high local concentration of mRNAs and translation factors in SGs, their interaction is facilitated and could promote the assembly of translation initiation complexes (Protter and Parker, 2016). This assembly could promote a faster return to translation when the stress is over.

I. C. 1. c. mRNA stabilization

Various stresses such as HS, exposure to UV, hyperosmolarity or glucose deprivation inhibit deadenylation and degradation of many mRNAs in yeast or in human cell lines (Gowrishankar et al., 2006; Hilgers et al., 2006). It was thought that this phenomenon could be due to the targeting

of mRNAs to SGs and several studies supported this possibility. The zipcode binding protein 1 (ZBP1), which regulates mRNA fate in cells, was shown to associate with some mRNAs in SGs in mammalian cells (Stöhr et al., 2006). This association was not necessary for directing mRNAs to SGs but was proven to increase their stability. However, the use of mutant *Saccharomyces cerevisiae* strains which were unable to assemble SGs demonstrated that mRNA stability was unaffected (Buchan et al., 2008). Similar results were obtained in mammalian cells where SGs formation was inhibited via KD of TIA-1, TIAR and G3BP1 with no changes in the stability of the tested mRNAs (Bley et al., 2015).

I. C. 1. d. mRNA triage

It was suggested that SGs could constitute sites of triage upon stress where mRNAs would be targeted either for degradation or for translation initiation (Kedersha et al., 2000). Preserving mRNAs and the associated pre-initiation complexes could make recovery faster by allowing a rapid return to active translation upon stress release. It was demonstrated that SGs and P-Bodies interact and share protein and RNA components (Kedersha et al., 2005) (Fig. 4). It could be shown that this interaction was promoted by the mRNA decay activator protein ZFP36, which suggested a role in mRNA remodeling and the targeting of some transcripts to P-Bodies for degradation. Depending on the mRNA transcript and on its interacting proteins, mRNAs could be targeted either for degradation via interaction with P-bodies, or sequestered for the duration of the stress.

I. C. 2. RNA granules formed under physiological conditions

RNA-protein assemblies can also be found at physiological conditions in neurons where they allow the rapid transport of specific mRNAs along the axon, via an active process (Ainger et al., 1993; Ferrandon et al., 1994; Knowles et al., 1996; Rook et al., 2000). These neuronal granules contain mRNAs, small and large ribosomal subunits as well as translation initiation factors and RBPs (Atlas et al., 2004; Barbarese et al., 1995; Knowles et al., 1996; Kohrmann et al., 1999; Krichevsky and Kosik, 2001; Smart et al., 2003). Although containing the translation machinery, the neuronal granules are translationally inactive (Krichevsky and Kosik, 2001) and are thought to be transported to the dendrites via association with microtubules (Ferrandon et al., 1994; Knowles et al., 1996). The content of these granules is released in response to an activation stimuli, either physiological, local or developmental (Ashraf et al., 2006; Hüttelmaier et al., 2005; Krichevsky

and Kosik, 2001; Schratt et al., 2006). RNA granules in neurons are thought to be tightly related to translational regulation (Kiebler and Bassell, 2006). Cell polarity and neuronal plasticity are the results of local translation of mRNAs and transportation of these mRNAs to dendrites may occur via neuronal granules.

Neuronal granules share many components with SGs (Anderson & Kedersha, 2006) and some neuronal granules proteins, such as Staufen can be transferred to SGs upon stress (Thomas et al., 2005). RNA granules are thus not only involved in stress response but can also play a role under physiological conditions in neurons.

I. C. 3. RNA granules and disease

In the 2000s, links between SGs and neurodegenerative disorders were established. Tar DNA Binding Protein 43 (TDP-43), when mutated, is one of the major aggregators which forms toxic inclusions in amyotrophic lateral sclerosis (ALS) and frontotemporal dementia (FTD). TDP-43 co-localizes with the SGs marker TIA-1 (Liu-Yesucevitz et al., 2010). Further studies reported the SGs localization of other RBPs involved in neurodegenerative diseases like FUS and huntingtin (Bosco et al., 2010; Waelter et al., 2001). Inversely, some SGs markers, like TIA-1 or PABP-1, have been identified as components of pathological inclusions of TDP-43, Tau, FUS or huntingtin (reviewed in Bentmann, Haass, & Dormann, 2013). Another indication of SGs involvement in neurodegenerative diseases was the discovery that brains from Alzheimer's patients demonstrate increased amounts of SGs (Vanderweyde et al., 2012).

The common feature between SGs and neurodegenerative diseases is that they both involve many RBPs. Under normal conditions, most of these RBPs are located in the nucleus where they participate in RNA processing, and are only exported to the cytosol upon stress. They usually have a strong tendency for aggregation, and the equilibrium between aggregating and non-aggregating species gets shifted towards the aggregated state in the cytosol upon stress (Han et al., 2012; Wolozin, 2014). The aggregation can increase and promote the formation of SGs if an additional factor able to shift this equilibrium is involved. It can be mutations in RBPs which promote their aggregation or the accumulation of another aggregating species, like Aβ in the case of Alzheimer disease, or aging (Wolozin, 2014). SGs could be precursors of pathological inclusions, via the sequestration of misfolded mutated RBPs leading to their conversion into pathological inclusions

(Molliex et al., 2015). However, this mechanism remains unclear and further studies are needed for its better understanding.

I. D. Dynamics of stress granules

SGs are dynamic structures whose composition is constantly changing. Both proteins and mRNAs are being exchanged with the surrounding cytosol, polysomes and other RNA-protein assemblies.

I. D. 1. Dynamics of stress granules composition

Dynamics of SGs composition was first observed with Fluorescence Recovery After Photobleaching (FRAP) experiments which revealed that TIA-1 and PABP-1 are not stable components of SGs and rather shuttle in and out (Kedersha et al., 2000). In addition, the average residence time of mRNA molecules in SGs calculated using MS2-GFP-tagged mRNAs, is less than a minute, suggesting a very dynamic exchange between granules and their environment (Mollet et al., 2008). Dynamic exchange between SGs and polysomes was observed, as well. While treatment of cells with puromycin (which disassembles polysomes) promotes SGs formation, emetine treatment (which fixes polysomes on mRNA) impairs their formation. However, when emetine is added to cells that were already exposed to arsenite, polysomes assembly is promoted and SGs disassemble, even though eIF2α is phosphorylated due to arsenite treatment. These results suggested that mRNAs can go back and forth between SGs and polysomes (Kedersha et al., 2000).

Another aspect of SGs dynamics consists in the exchange of content with other types of granules, like P-bodies. Several studies revealed interactions between SGs and P-bodies. It was observed that P-bodies could be recruited to SGs as a way to target mRNAs for degradation (Fig. 4) (Kedersha et al., 2005; Wilczynska et al., 2005). Contacts between SGs and P-bodies occur during SGs assembly and not between already assembled RNA granules, and depend on the cellular protein content (Mollet et al., 2008), suggesting their functional role in the process of SGs maturation.

I. D. 2. Liquid-like properties of stress granules

Live cell imaging revealed that SGs display liquid-like properties which include movement, fusion and fission (Kedersha et al., 2005). The first step of SGs assembly consists in the formation of small structures which evolve by interacting and fusing with each other to form mature SGs (Fig. 4). The movement of SGs in the cytosol persists even after their formation. SGs are reversible

structures which form within 15 min of arsenite treatment and disassemble 2 to 3 h after arsenite removal (Kedersha et al., 2000). It was revealed that SGs disassembly happens in three distinct steps (Wheeler et al., 2016). First, large SGs disassemble into small heterogenous foci. Second, the shell of these foci dissolves while small and stable structures, which could correspond to the cores of SGs, appear. Finally, these small core structures are either dissolved or degraded by autophagy (Nadezhdina et al., 2010; Wheeler et al., 2016) (Fig. 4). ATP is essential for SGs dynamics and its depletion not only prevents SGs formation, but also dramatically impairs their fusion and movement in cells with already formed granules. This suggests an involvement of ATPases such as chaperones and helicases (Jain et al., 2016). While the overexpression of HSP70 in HeLa cells prevented SGs formation, depletion of HSP70 impaired SGs disassembly (Mazroui et al., 2007). This was also verified in yeast where HSP104, a central disaggregase in *Saccharomyces cerevisiae*, participates in SGs disassembly by promoting the release of the translation machinery from the granules (Cherkasov et al., 2013; Walters et al., 2015).

Another key player of SGs dynamics are microtubules of the cytoskeleton. Disruption of microtubules impairs SGs assembly, movement and disassembly (Nadezhdina et al., 2010). The association of granules with microtubules has been demonstrated and is thought to direct their movement and fusion by coalescence in the maturation phase (Chernov et al., 2009; Nadezhdina et al., 2010). This association could take place via interaction with cytoskeleton motor proteins. While KD of dynein, the motor protein responsible for retrograde transport, inhibited SGs formation, KD of kinesin, responsible for anterograde transport, delayed both SGs formation and dissolution in mammalian cells (Loschi et al., 2009).

I. D. 3. Maturation of stress granules into amyloid-like assemblies

It has recently been proposed that SGs could mature under certain conditions into amyloid-like fibers (Fig. 4). Biotinylated isoxazole (b-isox), an agent triggering the precipitation of many RBPs, allowed *in vitro* investigation of the aggregation of the RBP FUS. Addition of b-isox to recombinant FUS protein *in vitro* generated hydrogels which, according to X-ray and microscopic analyses are composed of amyloid-like fibers (Han et al., 2012; Kato et al., 2012). Furthermore, it was shown that some RBPs with Intrinsically Disordered Regions (IDRs), like hnRNPA1, eIF4GII and FUS, could form liquid-like droplets *in vivo* and *in vitro*. Over time, these droplets can transition to a more stable state by forming amyloid-like fibers. This event is quite unlikely at

physiological concentrations, but ALS-related mutations in FUS or hnRNPA1 increase its likelihood dramatically. A possible mechanism is that the formation of SGs increases the local concentration of these RBPs, such that, in the case of mutations, aggregation is promoted and could lead to the formation of fibers on a longer timescale. The aggregation, which is first limited to SGs, could expand outside of this subcellular compartment and form toxic amyloid-like fibers (Lin et al., 2015; Molliex et al., 2015; Murakami et al., 2015; Patel et al., 2015).

I. E. Molecular aspects of stress granules assembly

I. E. 1. Liquid-liquid phase separation

A first big advance concerning the mechanism of SGs formation was the discovery that ribonucleoproteins (RNPs) granules found in embryos of *Caenorhabditis elegans*, P-bodies, display liquid-like properties (Brangwynne et al., 2009). It could be shown that these granules are formed by phase separation. This process, referred to as Liquid-Liquid Phase Separation (LLPS), consists in the spontaneous formation of two phases in a solution (Boeynaems et al., 2018; Brangwynne et al., 2009; Elbaum-Garfinkle et al., 2015; Weber and Brangwynne, 2012). These RNP assemblies are formed by a combination of specific interactions between folded proteins and peptides and of nonspecific interactions involving IDRs. The sum of these interactions triggers the LLPS by increasing the local concentration of RNA and/or proteins (Protter et al., 2018). Importantly, many RNAs and proteins in RNPs demonstrate multivalent interactions (Li et al., 2012).

I. E. 2. Major role of RNA-binding proteins

For long, proteins were thought to be the key drivers of SGs assembly. mRNAs were simply thought to serve as a scaffold to bring RBPs together and increase their local concentration. The observation that some RBPs could self-assemble to form liquid-like droplets *in vitro*, without the need for RNAs, supported this hypothesis, as demonstrated for hnRNAP1, eIF4GII, FUS or Whi3 (Lin et al., 2015; Molliex et al., 2015; Patel et al., 2015; Zhang et al., 2015). It was hypothesized that RBPs interacted with mRNAs via their RNA-binding domain (RBD) and that phase separation was driven by interaction between the low-complexity sequences of these RBPs brought together (Han et al., 2012). Additionally, SGs cores have been shown to be largely resistant to RNase treatment which suggested an RNA-independent mechanism for the maintenance of SGs (Jain et

al., 2016). However, recent evidence highlighted the role of mRNAs in the process of SGs formation and suggested that it was not limited to bringing RBPs together.

I. E. 3. Emerging role of RNA

I. E. 3. a. Self-assembly of RNA

The involvement of RNA-RNA interactions in the process of RNPs formation has been uncovered recently. Several studies reported the ability of RNA to self-assemble under certain conditions. It was reported that some mRNAs containing ALREX-promoting signal sequences accumulated in TIA-1 positive aggregates when injected into the cytoplasm of COS-7 cells (Mahadevan et al., 2013). It was observed in NRK cells treated with puromycin that transfection with α-Globin and Luciferase mRNAs triggered SGs formation (Bounedjah et al., 2014). Very recently, a study reported that total yeast RNA self-assembled *in vitro* under close-to-physiological conditions. Strikingly, the formed aggregates showed a large overlap with SGs transcriptome (Van Treeck et al., 2018). Altogether, these studies suggested that RNA-RNA interactions could be important in the process of SGs assembly.

I. E. 3. b. Influence of RNA on biophysical properties of RNA granules

Like in the case of neuronal granules, RNA-proteins assemblies can influence the spatial organization of transcripts. This is the case in *Ashbya gossypii*, a fungus closely related to *Saccharomyces Cerevisiae*, where the cyclin (CLN3) and formin (BNI1) transcripts associate with the protein Whi3 in large assemblies (Zhang et al., 2015). Whi3 phase separates both *in vivo* and *in vitro* to form either chains at low concentration, or droplets above a protein concentration threshold. However, in the presence of *in vitro* transcribed CLN3 mRNA, the phase separation was facilitated and could take place at lower protein concentrations.

I. E. 3. c.Importance of RNA secondary structure

Another important recent progress is the discovery of the importance of RNA secondary structure in RNPs formation. Protein Whi3 forms different types of droplets in the filamentous fungus *Ashbya gossypii*: perinuclear droplets containing cyclin (CLN3) mRNA and droplets at cell tips which incorporate formin (BNI1) transcript (Langdon et al., 2018). It turned out that Whi3 could

influence mRNA structure depending on RNA sequence and secondary structure. Thus mRNA structure could then be a key parameter defining the composition of Whi3 granules.

I. E. 3. d. RNA-seeded amyloid granules

Amyloid nuclear bodies (A-bodies) were recently discovered in cells exposed to acidosis or HS (Audas et al., 2016). They play a role in promoting the entrance of cells in a dormant state as a response to stress. These assemblies contain immobile proteins containing amyloid converting motifs (ACMs) and are reversible in a mechanism involving HSP70 and HSP90. It was discovered that a ribosomal intergenic non coding RNA (rIGSRNA) is needed for the formation of the A-bodies and that it increases the local concentration of ACM-containing proteins thus allowing the initial step of fibrillization. Amyloid formation would be further driven by polymerization of amyloid-prone proteins (Audas et al., 2016).

I. E. 3. e. Free mRNA

During stress response, polysome disassembly allows an increase in protein-free mRNAs concentration in the cytosol, and it was estimated to reach 180 µg/mL in U-2 OS mammalian cell line and 170-800 µg/mL in *Saccharomyces cerevisae* (Van Treeck et al., 2018). The same study showed that purified protein-free RNA of yeast formed assemblies at a concentration close to the *in vivo* concentration during stress response. Additionally, when IDRs-containing proteins were added to the RNA solution, they were found to be recruited to the RNA assemblies. Finally, sequencing of the mRNAs forming these assemblies revealed a strong overlap with mRNA enriched in SGs formed *in vivo*. This report strongly supported the importance of RNA-RNA interactions in the process of RNPs assembly.

It has been assumed that the formation of RNA-protein granules is one of the defense mechanisms in response to stress but the mechanism of their assembly is still largely unclear. Under normal conditions, before translation, mRNAs are covered with RNA-binding proteins involved in mRNA maturation, splicing, stabilization, or localization. They lose these associated proteins during translation but become densely coated with ribosomes, which limits the exposure of stripped mRNAs to the cytosol (Brandt et al., 2010). Under stress, cytosolic mRNAs can be released from polyribosomes and be exposed to the cytosolic content as free mRNA. It has been suggested that a fraction of free mRNA interacts with RNA stabilizing proteins, such as YB-1. The remaining free

mRNA molecules would then become exposed to misfolded and aggregation-prone proteins and trigger SGs formation (Bounedjah et al., 2014) (Fig. 3).

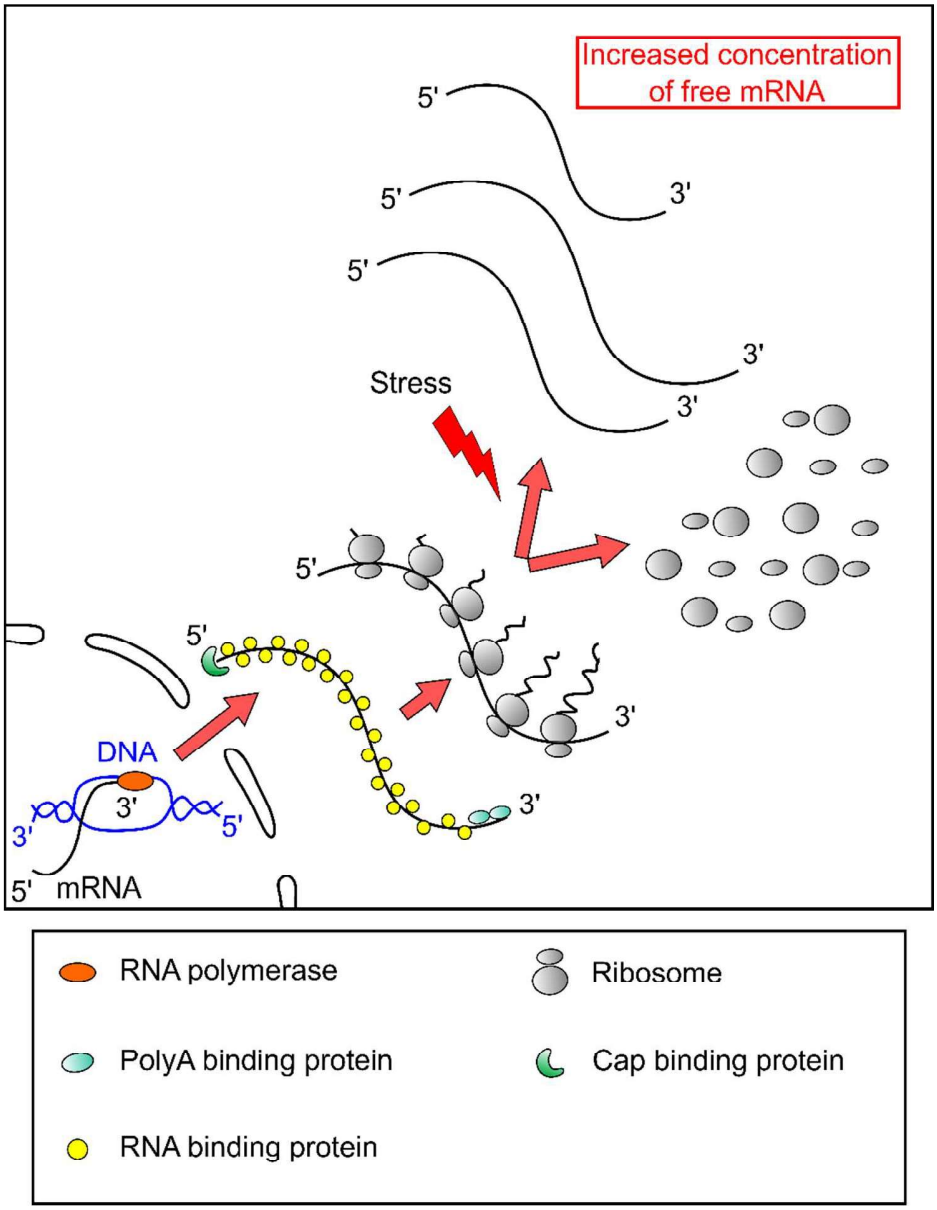

Figure 3. Polysome dissociation upon stress and release of protein-free mRNA in the cytosol.
mRNAs are covered with proteins involved in mRNA splicing, maturation, stabilization or localization. They lose their associated proteins when translation starts but they become densely coated with ribosomes. Upon stress, polysomes dissociation generates protein-free mRNAs which are exposed to the cytosolic content.

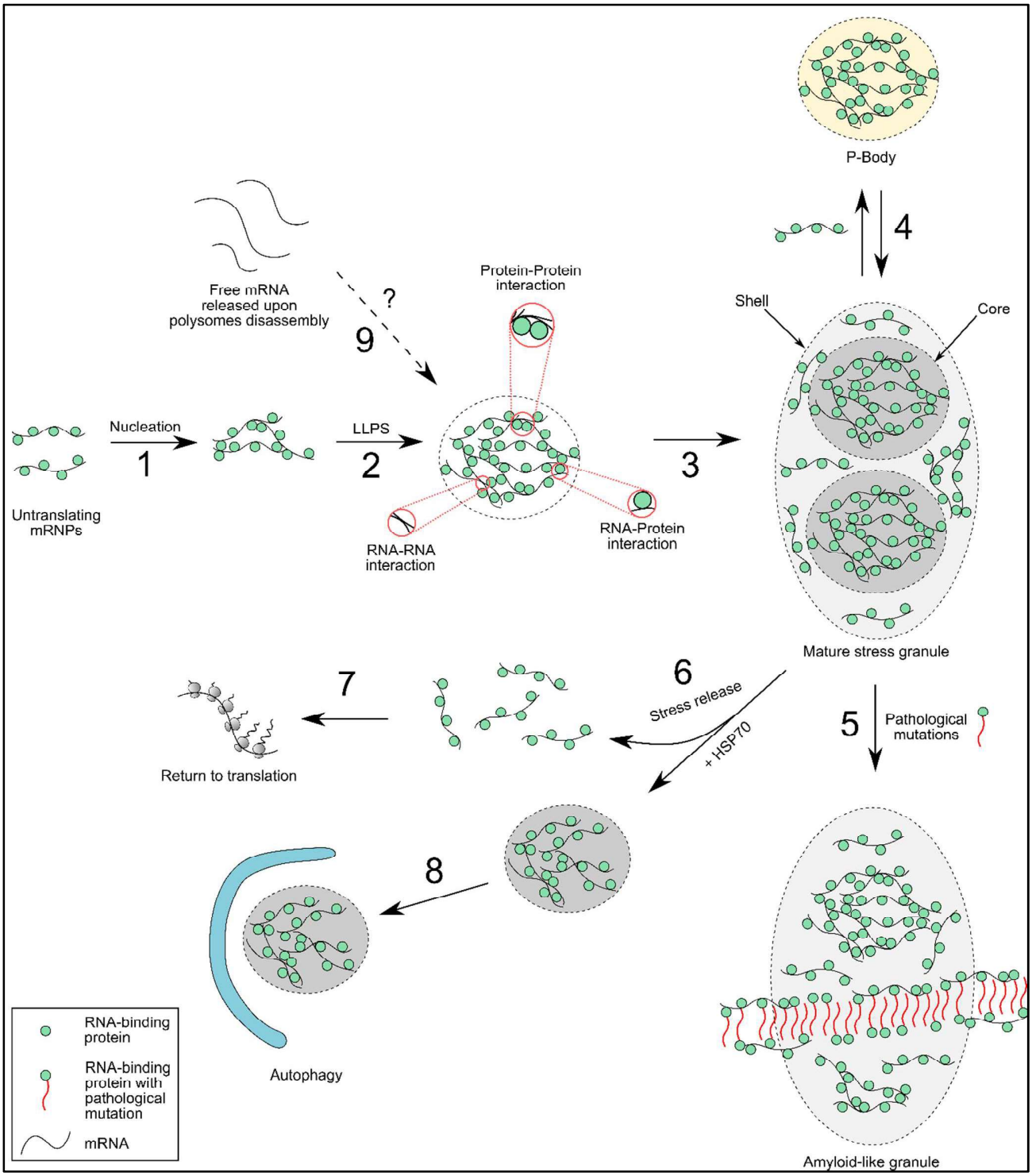

Figure 4. Life-cycle of stress granules, adapted from (Lin et al., 2015; Wheeler et al., 2016).
Upon translation arrest and polysome dissociation, untranslating mRNPs accumulate in the cytosol and mRNAs bring RNA-binding proteins together (1). The locally high concentration of mRNPs triggers Liquid-Liquid Phase Separation (LLPS) via protein-protein, RNA-protein and RNA-RNA interactions (2). These

RNA-protein assemblies grow by recruitment of other mRNPs to form mature SGs, with solid cores and soft shells (3). Exchange of proteins and of mRNAs takes place with P-bodies, potentially participating in the degradation of some mRNAs (4). In the case of pathogenic mutations of RNA-binding proteins (like FUS or hnRNPA1) leading to an increased aggregation propensity, amyloid fibers can form in granules (5). Upon stress release, HSP70 and other ATPases participate in SGs disassembly (6). SGs are partially dissolved with a return to translation for some mRNAs (7) while solid cores are degraded by autophagy (8). Free mRNA released in the cytosol upon polysome disassembly could play a role in SGs assembly and in LLPS (9) as recently proposed (Bounedjah et al., 2014).

II. mRNA modifications upon stress

It has been shown that different stressors, including HS, induce modifications of RNA molecules. The stress-induced modifications could influence mRNA behavior, interactions and granulation. Here we will focus on two stress-inducible modifications, namely the methylation of adenosines on the position N6 (m^6A) and on the position N1 (m^1A) (Fig. 5).

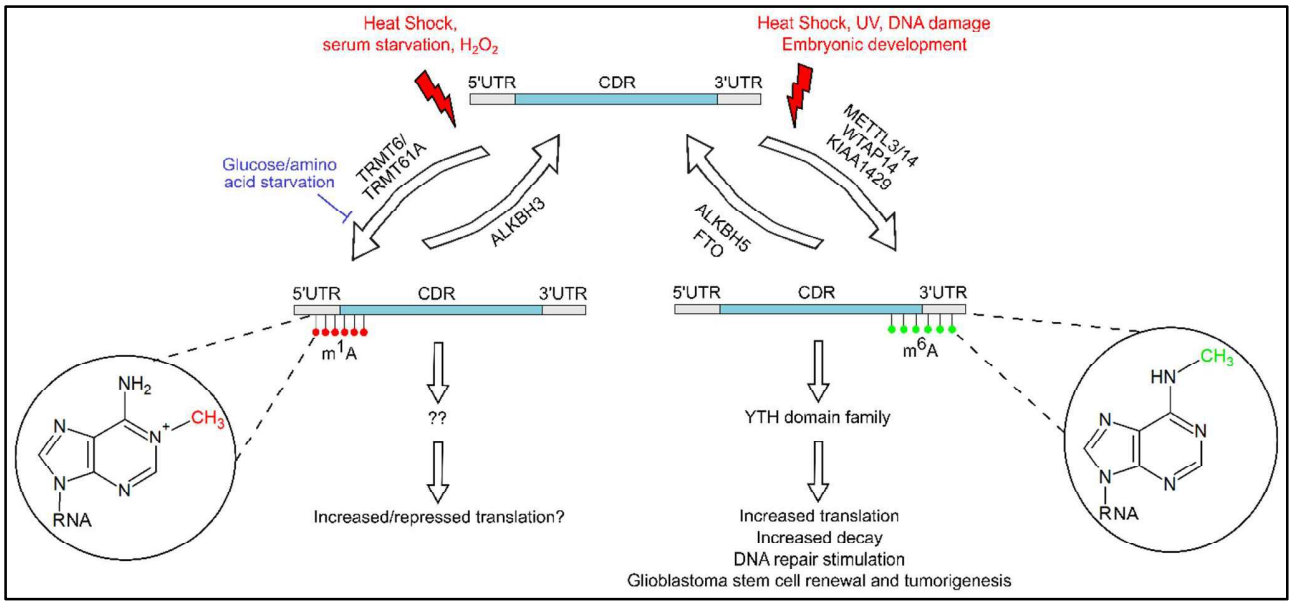

Figure 5. Example of two mRNA modifications stimulated upon stress.
m^6A is a well-characterized modification and its writers (METTL3/14, WTAP14, KIAA1429), erasers (ALKBH5, FTO) and readers (proteins from the YTH domain family) have been identified. Several functions for this modification have been discovered. On the other hand, less is known about m^1A modification and its role remains to be clarified.

II. A. m^6A

In the early 50s, modifications of RNA nucleotides were discovered (Cohn and Volkin, 1951). One of the most common and conserved of these modifications is the methylation of adenosine at the position N6 (m^6A), first identified in rRNA and tRNA (Iwanami and Brown, 1968; Saneyoshi et al., 1969). This modification was later found in mRNAs as well (Desrosiers et al., 1974). m^6A represents about 0.1-0.4 % of total adenosine content in mammals, which corresponds to several sites per mRNA and it makes it one of the most abundant mRNA modifications (Meyer et al., 2012). Methylated adenosines at this position (m^6A) were shown to be specifically enriched in the 3'-UTR of mRNA and near stop codons in mammals (Meyer et al., 2012). They are induced upon stress, such as HS, exposure to UV light (Meyer et al., 2015) but are also generated in normal conditions during embryonic development (Wang et al., 2014b).

A protein complex containing the methyltransferase METTL3/METTL14 was identified as a "writer" for m^6A methylation of mRNAs (Bokar et al., 1997). The heterodimer METTL3/METTL14 catalyzes the methylation of mRNAs; WTAP associates with the complex and regulates its activity (Liu et al., 2014; Ping et al., 2014; Schwartz et al., 2014; Wang et al., 2016). This structural modification allows the m^6A-specific recognition of the modified mRNAs by specialized proteins, so-called "readers", either via direct interaction with the deposited methyl group, or indirectly via a conformational switch generated by the methylation. Some of these proteins belong to the YTH domain family. These interactions play a role in pre-mRNA processing, translation initiation and mRNA degradation (Dominissini et al., 2012). The N6-methylation is reversible and demethylases (or "erasers") which can remove delete the modification upon certain conditions, such as FTO and ALKBH5, have been identified (Jia et al., 2011; Zheng et al., 2013).

Although base pairing is not impaired, this form of methylation favors single-stranded structures by destabilizing double-stranded structures (Roost et al., 2015). Interaction between RNA and RBPs could also be affected (Zhao et al., 2017). However, m^6A seems to enhance translation efficiency. In 3'-UTRs and near stop codons, this takes place via YTHDF1 (Wang et al., 2015) which binds components of the translation initiation complex, like eIF3. In 5'-UTRs, although the modification is less abundant, it was shown to enhance cap-independent translation in a mechanism that is different from IRES, and involves direct recruitment of eIF3 (Meyer et al., 2015). On the other hand, a recent publication provided evidence that this modification decreases translation

efficiency (Slobodin et al., 2017). m^6A has also been involved in the regulation of other processes like mRNA splicing (Xiao et al., 2016) and mRNA degradation (Wang et al., 2014a).

Defects in m^6A methylation have been linked to several diseases (Zhao et al., 2017). While Mettl3 -/- mice are not viable, Mettl3 KOs in mammalian cells demonstrate an increased mRNA lifetime. m^6A could be involved in mRNA turnover in cells, especially during embryonic development and cell differenciation. In addition, altered levels of the demethylases FTO and ALKBH5 are detected in some cancers. Their inhibition in some cases reduced cancer progression (Roundtree et al., 2017) (Fig. 5).

II. B. m^1A

Another type of methylation of adenosines in mRNAs is at the N1 position (m^1A). It was first discovered in yeast tRNAs and rRNAs but is conserved in humans and has been shown to play a role in their structure and stability (Dominissini et al., 2016; Motorin and Helm, 2010; Peifer et al., 2013; Sharma et al., 2013, 2018; Yang et al., 2016). N1-methylation of adenosine was more recently discovered on mRNAs as well. m^1A sites are enriched in 5' UTRs and in coding sequences around the start codon and the first splice site (Dominissini et al., 2016). To a lesser extend they can also be found in 3' UTRs. m^1A can be converted into m^6A by Dimroth rearrangement in alkaline conditions (Dominissini et al., 2016) (Fig. 6). They are also reversible *in vivo* and ALKBH3 has been identified as one of the demethylases responsible (Dominissini et al., 2016). This form of methylation is less abundant than m^6A, with an average frequency of one site per mRNA. m^1A is however frequent on tRNAs at the position A58, where it is deposited by the methyl transferase TRMT6/TRMT61A composed of two subunits in human, and by TrmI, composed of a single subunit, in bacteria and archaea. The crystal structure of TrmI has been solved and revealed that the methyltransferase forms homotetramers and can bind up to two tRNA molecules at the same time (Barraud et al., 2008; Guelorget et al., 2010; Gupta et al., 2001; Kuratani et al., 2014). In human, the large subunit, TRMT6, specifically binds the substrate while TRMT61A is a catalytic subunit. The crystal structure of the human methyltransferase showed that tRNA molecule interacts with TRMT6 from one heterodimer and with TRMT61A from the opposite heterodimer (Finer-Moore et al., 2015). It is believed that the binding of the tRNA allows a large conformation change that makes the position A58 accessible for methylation (Finer-Moore et al., 2015). It has recently been shown that TRMT6/TRMT61A is at least partially responsible for m^1A methylation of

cytosolic mRNAs (Li et al., 2017; Safra et al., 2017). RNA sequencing data revealed the motif recognized by the methyltransferase and it appears to be very similar to the tRNA motif consisting in a seven-bases-loop stabilized by a stem of variable length (Fig. 7) (Li et al., 2017; Safra et al., 2017).

The role of this type of methylation is not well understood. A potential effect on translation was hypothesized since the methylation disrupts A:U base pairing: the methylation occurs at the Watson-Crick interface and generates a positively charged base, which disrupts complementarity. The positive charge can strongly influence the secondary structure of RNA and thus have an effect on proteins-RNA interactions (Roundtree et al., 2017). Safra *et al* observed a repression of translation based on polysome profiling analysis of mRNAs containing m^1A (Safra et al., 2017). A different effect on translation was suggested depending on the subcellular localization of the methylated mRNA (Li et al., 2017). High rates of m^1A methylation were reported in mitochondrial mRNAs, but the methylation sites followed a different pattern than in cytosolic mRNAs and were mostly detected in the coding sequence (CDS). The methyl group deposited by the mitochondrial methyl transferase TRMT61B impaired translation. It was suggested that m^1A methylation of mitochondrial mRNAs could play an important role in embryonic development (Safra et al., 2017). The example of the mitochondrial ND5 mRNA supports this hypothesis since it is m^1A methylated only until the 8-cells-stage of development, which corresponds to the stage of zygotic transcriptome activation (Safra et al., 2017). Importantly, m^1A methylation of mRNA is induced upon several stimuli, like HS, serum starvation and H_2O_2 treatment. It is however reduced upon glucose or amino acid starvation (Dominissini et al., 2016, Fig. 5).

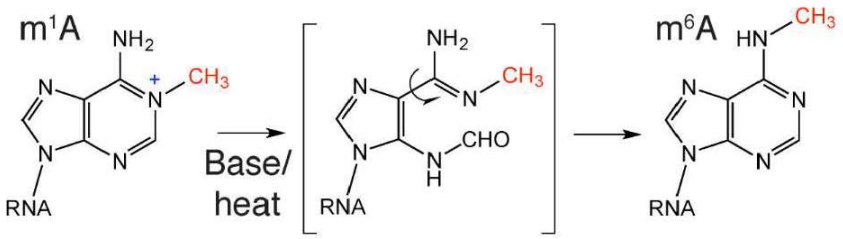

Figure 6. The Dimroth rearrangement (Dominissini et al., 2016).
m^1A can be re-arranged into m^6A upon alkaline treatment or heating.

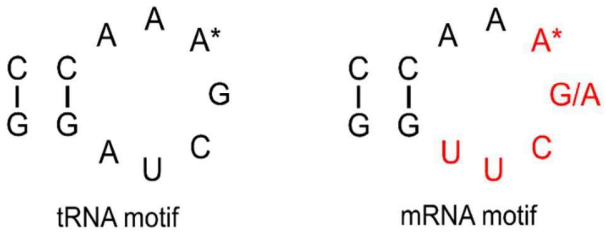

Figure 7. tRNA and mRNA motifs recognized by TRMT6/61A.
The motives show high similarity. They are both composed of a 7 bases loop which is stabilized by a stem. The stem is 5 bases long in tRNA but its length varies in mRNA, with longer stems increasing methylation efficiency.

III. Research project

III. A. Questions

In this project, we aimed at a molecular understanding of protein-free mRNA involvement in stress response in mammalian cells. Exposure of free mRNA to the cytosolic content inevitably leads to new interactions with cytosolic proteins. What is the interactome of free mRNA upon stress? What happens to free mRNA released in the cytosol in the early phase of stress response? Does the release of free mRNAs upon stress initiate SGs formation? What is the molecular mechanism of this process? Could stress-inducible mRNA modifications, such as m^1A or m^6A, play a role in this granulation?

III. B. Strategy

III. B. 1. Stress conditions to study stress granules formation

III. B. 1. a. Heat shock

The aim of this project was to study the early phase of stress response and the process of SGs formation. It was important to use a stress which was known to induce SGs in mammalian cells but which was also easy to manipulate in order to adjust the timeframe needed to study the very beginning of stress response. We decided to use HS. As it was first observed in Peruvian tomato cells in 1983 (Nover et al., 1983), and a few years later in mammalian cells (Arrigo et al., 1988), HS induces the formation of cytosolic SGs. HS was shown to promote the activation of the eIF2α kinase HRI. Once eIF2α is phosphorylated by HRI, translation is stopped, polysomes disassemble and SGs form (Lu et al., 2001). By manipulating the duration and/or the temperature of HS, we

could access the early phase of stress response and the moment when SGs are not formed yet but are being assembled.

III. B. 1. b. Arsenite treatment

Arsenic is a chemical element, often qualified of semi-metal due to its chemical and physical properties. It is highly toxic and exposure of living organisms to arsenic has been connected to increased risks of cancer development. It can mostly be found in four oxidation states: -3, 0, +3 and +5, the latter two being predominant (International Agency for Research on Cancer, 2012). Arsenite is a well-known strong inducer of SGs assembly, and we decided to use it as a positive control for SGs assembly. Trivalent arsenicals, such as arsenite, bind with high affinity to sulfhydryl groups (or thiols). They can thus bind to peptides and proteins via their reduced cysteines. It was estimated that about 200 enzymes could be inhibited by arsenic, including critical antioxidant proteins such as glutathione reductase, glutathione peroxidase, thioredoxin reductase or thioredoxin peroxidase (Shen, Li, Cullen, Weinfeld, & Le, 2013). It is thought that exposure of cells to arsenite increases the concentration of reactive oxygen species (ROS) as a consequence of the inactivation of these antioxidant enzymes (Anderson et al., 2015). This accumulation of ROS induces the eIF2α kinase HRI in an unclear mechanism involving HSC70 and HSP90 chaperones. eIF2α is then phosphorylated by the activated kinase HRI, which triggers translation arrest, polysomes disassembly and SGs formation (Lu et al., 2001; Mcewen et al., 2005).

III. B. 2. Study of free mRNA interactome

Contrary to the role of proteins during stress response, RNA role in stress response and phase transition remains less clear. We decided to investigate the role of free mRNAs by identifying their interactomes during the early phase of stress response in mammalian cells. We used free mRNA baits and identified interacting proteins from heat shocked HeLa cell lysate by means of quantitative mass spectrometry. mRNA baits which were biotinylated so that they could be pulled down using streptavidin beads. Mass spectrometry analysis allowed us to identify a set of highly significant interactors. Some interactions were selected for biochemical verification and functional analysis.

CHAPTER 2: MATERIAL AND METHODS

A list of chemicals and reagents can be found in the Appendix 5 while a list of antibodies used is provided in the Appendix 6. The composition of all the buffers mentioned is given at the end of this section.

I. Cell culture and transfections

I. A. Cell culture

I. A. 1. Cell lines

HeLa: human epithelial adenocarcinoma cells, ATCC, CCL-2.
B16F10: murine melanoma cells, ATCC, CRL-6475.

I. A. 2. Cell culture

Cells were cultured in Dulbecco's modified Eagle's medium supplemented with 10 % (vol/vol) Fetal Bovine Serum, 2mM L-Glutamine, 100 IU/mL penicillin G, 100 µg/mL streptomycin sulphate and non-essential amino acids at 37 °C and 5 % CO_2 in a humidified incubator (Heracell 150i CO_2 incubator, ThermoFisher Scientific). Cells were manipulated in a sterile environment in a safety cabinet (Maxisafe 2020, ThermoFisher Scientific). Cells were splitted using Trypsin-EDTA solution.

I. A. 3. Generation of TRMT61A KD cell lines

HeLa cell lines with low levels of TRMT61A were established by PEI transfection (6:1 PEI to DNA ratio) of 2 x 10^5 cells in one well of a 6-well plate with 1 µg TRM61 Double Nickase Plasmids (h) mix. The transfected cells were then selected with Puromycin. After most of the cells died, single colonies deriving from a single cell were isolated, grown and tested for TRMT61A expression. Clones with reduced expression of TRMT61A were selected and expanded for experimentation.

I. B. Transfections

I. B. 1. PEI transfections

Polyethylenimine (PEI) was dissolved at 1 mg/mL in hot ddH_2O and HCl was added until pH reached 2-3. The solution was stirred for approximately 3 h until PEI was completely dissolved. NaOH was added until pH 7 and the solution was sterilized using a 0.22 µm filter. Aliquotes were stored at -20 °C, thawed before transfection and kept at 4 °C for 2 weeks. For transfection, cells were seeded the day before so that they reached about 70 % confluency next day. DMEM was refreshed. Plasmid DNA was mixed with Opti-MEM so that the final volume of the mixture represented 10 % of the total volume of medium in the culture vessel. PEI was added to the mix at the appropriate ratio depending on the cell line (DNA: PEI ratio of 1:6 for HeLa and B16F10). The solution was vortexed gently and incubated at room temperature (RT) for 15 min. The transfection mix was then added to the cells dropwise. If the cells had to be treated, medium exchange could be done from 6 h after transfection.

I. B. 2. Electroporations

Cells were trypsinized, counted and washed with PBS. 4 x 10^6 to 8 x 10^6 cells were used per transfection with up to 60 µg DNA. The cells were resuspended in ice-cold intracellular buffer supplemented with 2 mM ATP and mixed with the plasmid DNA to transfect in a final volume of 400 µL. The cells were transferred to a Gene Pulser/MicroPulser electroporation cuvette (0.4 cm gap, Bio-Rad, 1652088) and kept on ice until transfection. The cells were electroporated using a Gene Pulser X Cell electroporation system from Bio-Rad (exponential pulse, voltage of 310 V for HeLa cells, capacitance of 950 µF, infinite resistance). The cells were then washed with fresh DMEM and replated in the desired format. Medium was refreshed 6 h after transfection.

I. B. 3. Transfection with TRMT6/61A for co-immunoprecipitation

2 x 10^6 HeLa cells were seeded in 10 cm-dishes and transfected next day using 1 mg/mL PEI solution and 5 µg 3xFlag-TRMT61A and 5 µg Flag-TRMT6 or 10 µg pcDNA3.1-Hygro (1:6 DNA to PEI ratio). The cells were then collected 24 h after transfection for co-immunoprecipitation.

I. B. 4. Transfections with Aβ

For study of Aβ aggregation, 4-8 x 10^6 HeLa WT and/or TRMT61A KD cells were transfected by electroporation with 30 µg Aβ-EGFP or 10-30 µg EGFP expression vectors. In the case of the reconstitution of TRMT61A KD, cells were transfected with 10 µg Aβ-EGFP, 20 µg Flag-TRMT6 and 20 µg 3xFlag-TRMT61A. After electroporation, cells were washed and seeded in a 12-well plate at 5 x 10^5 cells/well for study of Aβ accumulation studies, or seeded in 10 cm dishes at 4 x 10^6 cells per dish for Aβ or polyA mRNA pulldowns. The cells were collected 48 h after transfection for accumulation studies or 24 h after transfection for Aβ or polyA mRNA pulldowns. For western blot analysis, the cells were washed with ice-cold PBS and lysed with SDS-sample buffer. Samples were analyzed using anti-GFP and anti-GAPDH antibodies.

I. B. 5. Transfections with mRNA

4 x 10^6 HeLa cells were transfected with 4 µg Cy5-HSP70 mRNA or the molar equivalent of Cy5-55mer oligo (5'-GGG ACU GCA AAA GAA GCG GCU UCG GUC GCG AUA CUA CGG UCC CAA GAG CAA UCC U-3') by electroporation in 400 µL intracellular buffer freshly supplemented with 2 mM ATP. After electroporation, the cells were washed and plated in a 12-well plate with Poly-L-lysine cover slides at 1 x 10^6 cells/well. They were left for recovery at 37°C for 6 h and further processed for microscopy.

II. Basic biochemical and biomolecular techniques

II. A. Protein analysis

II. A. 1. Sodium Dodecyl Sulfate-Polyacrylamide Gel Electrophoresis (SDS-PAGE)

Solutions for stacking and resolving gels were poured between glass plates using a Mini-PROTEAN Tetra Handcast system (Bio-Rad) with the desired comb. Reducing SDS sample buffer was added to the samples which were boiled and loaded in the wells of the gel. Electrophoresis was run using a Mini-PROTEAN Tetra Vertical Electrophoresis Cell (Bio-Rad) at 200 V at RT for about 1 h.

II. A. 2. Western blot

After electrophoresis, the washed gel was soaked in transfer buffer and put on chromatography paper (3MM CHR, GE Healthcare, 3030-672) soaked in the same buffer. A Nitrocellulose blotting membrane (Amersham Protran 0.45 µm NC, GE Heathcare, 10600007) was put on the gel, and chromatography paper soaked in transfer buffer was added on top. A roller was then used to remove air bubbles. The sandwich was placed between two foam pads, transferred to a gel holder cassette, and into the tank filled with cold transfer buffer. An ice block was added to the tank and transfer was run at 100 V, at RT, for 30 min using a Criterion Blotter (wet system, Bio-Rad). The membrane was then blocked with blocking buffer, for 1 h at RT and incubated overnight at 4°C with the primary antibody at the appropriate dilution in blocking buffer with gentle shaking. Next day, the membrane was washed three times with TBS for 5 min. Incubation with the appropriate secondary antibody at the dilution recommended by the provider, was done in blocking buffer for 1 h at RT. After being washed three times with TBST for 5 min, the membrane was developped using the SuperSignal West Pico PLUS Chemiluminescent Substrate. Chemiluminescence images were acquired with the Chemidoc MP imaging system (Bio-Rad) and bands quantified using the Image Lab 5.0 software (both from Bio-Rad).

II. A. 3. Coomassie staining of protein gels

After electrophoresis, the washed gel was incubated in the Coomassie Brilliant Blue G250 staining solution overnight at RT. Next morning, the gel was transferred into destaining solution and incubated at RT for at least 2 h, the destaining solution being occasionally refreshed. Images were acquired with the Chemidoc MP imaging system and bands quantified using the Image Lab 5.0 software (Bio-Rad).

II. B. Cloning

The list of plasmids that were prepared and/or used in this thesis is given in the appendix 4.

II. B. 1. Fast cloning

For cloning, the method of fast cloning was used (Li et al., 2011). This simple methods consists in the separate amplification of the insert and the backbone using a high fidelity polymerase. The ends of the insert had 16-bases overlap with the ends of the backbone. The insert and the backbone were

mixed (different ratios can be tested) in the presence of the restriction enzyme DpnI which specifically digests methylated DNA (ie the template used for PCR and purified from bacteria). After digestion, the mixture was transformed in *Escherichia Coli* (DH5α strain) to obtain the desired clone. This method was adapted for deletions using only one pair of primers with overhangs, or for small insertions where the fragment to be inserted can be directly introduced in primers for amplification of the vector.

II. B. 2. PCR

PCR was run according to the DNA polymerase provider's instructions for 30 cycles (Phusion High fidelity DNA polymerase, Herculase II Fusion DNA polymerase, ALLin HiFi DNA polymerase) using a PeqStar 2x Gradient thermocycler (Peqlab). Amplification was verified by running a small aliquote of the PCR product supplemented with DNA Gel loading dye on an agarose gel stained with SYBR Safe in TAE buffer using the PerfectBlue Gel system Mini S (Peqlab). Images were acquired with the Chemidoc MP imaging system.

II. B. 3. List of primers used for cloning

Table 1. List of primers used for cloning.

Primer name	**Primer sequence (5'-3')**	**Plasmid cloned**
pF-NQO1-2x-FLAG-fw	CATGACGGTGATTATAAAGATCATGACA TCGATTACAAGGATGACGACGATAAG	1-874 (cloned by Adrian Martinez Limon)
pF-NQO1-2x-FLAG-rev	ATAATCACCGTCATGGTCTTTATAGTCCA TGGTGGCAAGCTTAAGT	1-874 (cloned by Adrian Martinez Limon)
F-BRAF-fw	CATGACGGTGATTATAAAGATCATGACA TCGATTACAAGGATGACGATGACAA	1-894
F-BRAF-rev	ATAATCACCGTCATGGTCTTTATAGTCCA TGGATCCGAGCTCGGT	1-894

Primer name	Primer sequence (5'-3')	Plasmid cloned
pcDNA3-RBS-fw	AAACTTAAGCTTGGTAAGGAGGGATCCA TGGACTATAAAGACC	1-894
pcDNA3-RBS-rev	TTTATAGTCCATGGATCCGAGCTCCTTAC CAAGCTTAAGTTT	1-894
FLAG-TRMT6/61A-fw	CATGACGGTGATTATAAAGATCATGACA TCGATTACAAGGATGACGACGATA	1-967
FLAG-TRMT61A-rev	ATAATCACCGTCATGGTCTTTATAGTCGC CTGGGGTCTTGGTG	1-967
m1A-1-383-fw	GCGGGTTCGAGTCCCGCCAAGCTTCCACC ATGCAG	1-1008
m1A-1-383-rev	GCGGGTTCGTGTCCCGCCAAGCTTCCACC ATGCAG	1-1008
m1A-1-383-fw-CTRL	GCGGGACTCGAACCCGCCTCGAGATCTG AGTCCGG	1-1009
m1A-1-383-rev-CTRL	GCGGGACACGAACCCGCCTCGAGATCTG AGTCCGG	1-1009
m1A-1-874-fw	GGCGGGTTCGAGTCCCGCCAAGCTTGCC ACCATGGAC	1-1010
m1A-1-874-rev	GGCGGGACTCGAACCCGCCAAGTTTAAA CGCTAGCCAGCTT	1-1010
m1A-CTRL-1-874-fw	GGCGGGTTCGTGTCCCGCCAAGCTTGCCA CCATGGAC	1-1011
m1A-CTRL-1-874-rev	GGCGGGACACGAACCCGCCAAGTTTAAA CGCTAGCCAGCTT	1-1011

II. B. 4. Preparation of competent cells

Escherichia Coli (DH5α strain) cells were spread on an LB-agar plate and let grown overnight. A single colony was used to inoculate 250 mL of LB-medium supplemented with 20 mM $MgSO_4$.

The cells were grown until OD_{600} reached 0.4-0.6. The cells were pelleted by centrifugation at 5000 rpm for 5 min at 4°C and the supernatant was discarded. The cells were gently resuspended in 100 mL ice-cold TFBI and kept on ice for 5 min. They were centrifuged at 5000 rpm for 5 min at 4°C and the supernatant was discarded. The pellet was resuspended in 10 mL ice-cold TFBII and incubated on ice for 15 to 60 min. The cells were aliquoted, frozen with liquid nitrogen and stored at -80 °C.

II. B. 5. Bacterial transformation

For plasmid DNA preparation, the *Escherichia Coli* DH5α strain was used while the BL21 strain was used for protein purification purposes. For transformation, about 200 ng of plasmid DNA were mixed with chemically competent cells and incubated on ice for 30 min. The mixture was heated at 42 °C for 60 sec and put back on ice for 5 min. 200 µL LB-medium was added to the cells and they were incubated at 37 °C with gentle shaking for 1 h. The cells were then plated on agar LB agar plates supplemented with the appropriate antibiotic (Ampicillin sodium salt, Kanamycin sulfate from *Streptomyces kanamyceticus*). The plates were incubated at 37 °C overnight.

II. B. 6. Plasmid preparation

For small volumes of bacterial culture (2 to 10 mL), DNA was purified using GeneJET Plasmid Miniprep kit according to the provider's instructions. For larger volumes (100-200 mL), the GenElute HP Endotoxin-Free Plasmid Maxiprep kit was used according to the provider's instructions.

II. C. Real time PCR

II. C. 1.2 $^{-ddCt}$ method

The results of the qPCR are given as Ct values for each gene and each sample. The method of 2^{-ddCt} was used for the estimation of gene expression. This method is based on the assumption that the amplification was 100 % efficient for all the samples (Arocho et al., 2006; Livak and Schmittgen, 2001). The first step is to average the Ct values for the triplicates in each sample. The results are normalized to the housekeeping gene values. In the next step, a reference sample is chosen. The other samples will be normalized to this reference sample in order to compare gene

expressions. Finally, the ratio of expression compared to the reference sample is calculated by using the exponential function with base 2.

$$dCt = Ct(test\ gene) - Ct(housekeeping\ gene)$$

$$ddCt = dCt(test\ sample) - dCt(reference\ sample)$$

$$Relative\ expression = 2^{-ddCt}$$

II. C. 2.qPCR method

Total RNAs were purified by addition of TRIzol reagent extraction according to the provider's instructions. cDNAs were prepared using RevertAid RT Reverse Transcription kit according to the manufacturer's instructions. The synthesized cDNAs were diluted about 10x for qPCR and were amplified using pre-designed KiCqStart SYBR Green Primers or self-designed primers (both from Sigma-Aldrich, sequences detailed in the "Primers" section), and KiCqStart SYBR Green qPCR ReadyMix according to the provider's instructions. Real time PCR was performed using the CFX96 Touch Real-Time PCR Detection System (Bio-Rad). The cycling conditions used were the following: 3 min at 95 °C ; [15 sec at 95 °C-30 sec at 58 °C-15 sec at 72 °C] x39. Each reaction was performed in triplicates, Cq values were averaged from the triplicates and results were analyzed using the 2^{-ddCt} method, GAPDH being used as the housekeeping gene. Analysis was performed using the CFX Manager Software (Bio-Rad).

II. C. 3.List of primers used for qPCR

Table 2. List of primers used for qPCR.

Primer name	**Primer sequence (5'-3')**	**Gene amplified**
FH1_HSPA1A	AATTTCCTGTGTTTGCAATG	*hspa1a*
RH1_HSPA1A	AAAATGGCCTGAGTTAAGTG	*hspa1a*
FH1_HSPA8	CTATCACTAATGACAAGGGC	*hspa8*
RH1_HSPA8	GAATTCTTGGATGACACCTTG	*hspa8*
FH1_GAPDH	ACAGTTGCCATGTAGACC	*gapdh*
RH1_GAPDH	TTTTTGGTTGAGCACAGG	*gapdh*

Primer name	Primer sequence (5'-3')	Gene amplified
NQO1-qPCR2-fw	TTTGACCTAAACTTCCAG	*nqo1* from 1-1010 and 1-1011
NQO1-qPCR2-rev	GGATATCTGCAGAATTCT	*nqo1* from 1-1010 and 1-1011
qPCR-Ub-EGFP-fw	ATCAAGGTGAACTTCAAGAT	*egfp*
qPCR-Ub-EGFP-rev	TTCTCGTTGGGGTCTTTGCT	*egfp*

II. D.RNA preparation

II. D. 1. mRNA *in vitro* transcription

II. D. 1. a. Template preparation and purification

The plasmids used for transcription include 1-894 and 2-67. The plasmids were linearized with XbaI and XhoI respectively. The linearized template was further purified by Phenol/Chloroform/Isoamylalcohol extraction and ethanol precipitation as following. The volume of the DNA template was adjusted to 100 µL with water. One volume of Phenol/Chlorofom/Isoamylalcohol pH 8 (25:24:1) was added to the solution with was vortexed for 30 sec and centrifuged at 21000 g for 2 min at 4 °C. The upper aqueous phase containing the DNA was collected and transferred to a clean tube. The Phenol/Chloroform/Isoamylalcohol extraction was repeated one more time. 1/10 volume of 3 M Sodium Acetate pH 5.2 and 3 volumes of cold 100 % Ethanol were added to the aqueous phase. After 30 min at -80 °C, the solution was centrifuged at 21000 g for 20 min at 4 °C. The supernatant was discarded, the pellet was washed with 70 % Ethanol before being air dried. The DNA pellet was then resuspended in DEPC treated water.

II. D. 1. b. *In vitro* transcription

A 20 µL reaction was assembled as described in Table 3, using Ampliscribe T7 High Yield Transcription kit.

Table 3. *In vitro* transcription reaction.

Description	Volume
DEPC-treated H2O	7.5 µL – x µL DNA
Linearized DNA template (1 µg)	x µL DNA
10x AmpliScribe T7 Reaction Buffer	2 µL
100 mM ATP	1.5 µL
100 mM CTP	1.5 µL
100 mM GTP	1.5 µL
100 mM UTP	1.5 µL
100 mM DTT	2 µL
RiboGuard RNase Inhibitor	0.5 µL
AmpliScribe T7 enzyme solution	2 µL

The reaction was incubated at 37 °C for 4 h. DNA was digested by adding 1 µL DNase I and the reaction was incubated for 15 more min at 37 °C before proceeding to purification.

II. D. 1. c. mRNA purification

Several purifications methods were used. The fastest way is to use purification kits (MegaCLEAR transcription clean up kit or RNeasy Mini kit) . These involve columns silica columns and allow recovery of mRNA free of single nucleotides. The downside of this method is that elution has to be performed in a relatively large volume (20 to 30 µL minimum) which considerably dilutes the sample. This method was used if this purification step was the final one before mRNA was used for experiments. A cheaper alternative that allows a good recovery of the mRNA but presents a risk of free nucleotides contamination, is the Phenol/Chloroform/Isoamylalcohol extraction followed by ethanol precipitation. The protocol is similar to the plasmid DNA purification method described for preparation of the template for *in vitro* transcription, but the pH of the

Phenol/Chloroform/Isoamylalcohol (125:24:1) is of 4.5, which allows the specific isolation of RNA. The mRNA being collected as a pellet, it can be resuspended in a volume of water as small as desired. This technique was used when further processing of mRNA required a high mRNA concentration, like for mRNA biotinylation.

II. D. 1. d. Assessment of mRNA quality

After *in vitro* transcription or biotinylation, mRNA quality was assessed by running a small fraction of product on an agarose gel prestained with SYBR Safe in the presence of formaldehyde (FA), which denatures mRNA by removing secondary structures. 5x FA Loading Dye was added to 1 µg of product and the mixture was heated at 65 °C for 3-5 min. It was then chilled on ice for 5 min and loaded on the equilibrated 0.6 % agarose FA Gel pre-stained with SYBR Safe. Electrophoresis was performed at 5-7 V/cm in 1x FA Gel buffer. Images were acquired with the Chemidoc MP imaging system.

II. D. 2. mRNA biotinylation

For this purpose, the mRNA was purified by Phenol/Chloroform/Isoamylalcohol extraction and ethanol precipitation. *In vitro* transcribed mRNA was then biotinylated using RNA 3' End biotinylation Kit and the reaction was performed with 50 pmol mRNA and was incubated at 16 °C overnight. Purification of the biotinylated mRNA was performed using silica colums-based purification (MegaCLEAR transcription clean up kit or RNeasy Mini kit). Biotinylated mRNA quality was assessed as described previously.

II. D. 3. Cy5 labeling of mRNA

II. D. 3. a. *In vitro* transcription of mRNA

This method involves the incorporation of GMP during a classic *in vitro* transcription. DNA templates were prepared as described previously. GMP was added in excess at 15 mM to an *in vitro* transcription reaction, and was then incorporated in most mRNA molecules synthesized and only at the position +1. Purification of the product was performed using RNeasy Mini kit and mRNA quality was assessed as described previously.

II. D. 3. b. Cy5-labeling

EDC coupling: The RNA was dissolved in 75 µL 1x Reaction Buffer (150 mM NaCl, 10 mM EDTA, 10 mM Potassium phosphate, pH 7). The prepared RNA solution was added to a tube containing 12.5 mg EDC (1-Ethyl-3-(3-dimethylaminopropyl)carbodiimid*hydrochloride) and 50 µL of 0.25 M ethylene diamine + 0.1 M imidazole in ddH_2O were immediately added to the reaction. The tube was vortexed and briefly centrifuged, then 200 µL of 0.1 M imidazole (pH 6) solution were added. The reaction mixture was heated to 37 °C for 2.5-3 h. The RNA was ethanol precipitated twice in 0.3 M NaOAc (pH 5.5).

Dye labeling: One Amersham Cy5 Mono-Reactive Dye Pack was used for up to three labeling reactions. The dye was dissolved in 60 µL DMSO (RNase free) and aliquoted to 20 µL. The mRNA was dissolved in 20 µL of a freshly prepared 0.1 M $NaHCO_3$ solution. One 20 µL aliquot was added to the mRNA and the mixture was incubated for 90 min at RT in the dark. The mRNA was ethanol precipitated twice in 0.3 M NaOAc (pH 5.5), resuspended in ddH_2O and stored at -20 °C.

II. D. 4. *In vitro* transcription of initiator tRNA

II. D. 4. a. *In vitro* transcription

Human tRNA-iMet was synthesized *in vitro* using Ampliscribe T7 High Yield transcription kit. Two oligonucleotides were used for this purpose. One oligonucleotide (iMet-tRNA) was used as a template. It contained the complementary sequence of T7 RNA polymerase promoter followed by the complementary sequence of tRNA iMet with two modifications. The first modification was the modification of the first base of the tRNA (A in the original sequence) into a G since T7 polymerase always starts polymerizing from G after the promoter. The complementary base in the acceptor stem was accordingly exchanged into C. A second oligonucleotide (tRNA-prime) was used to prime the T7 RNA polymerase. These two primers annealed and tRNA-prime constituted a starting point for transcription while iMet-tRNA was the template for polymerization. The sequence of the two oligonucleotides is given below and the modifications are underlined. For the transcription, the reaction was assembled as described in the protocol for *in vitro* transcription but the linear DNA template was replaced by the two oligonucleotides, both at 1 µM final. The reaction was incubated at 37 °C for 4 h 30. The final product was purified by Phenol/Chloroform/Isoamylalcohol

extraction followed by Ethanol precipitation. Before performing experiments, tRNA was refolded by being heated at 85 °C for 3 min and then refolded in Refolding Buffer at 30 °C for 15 min.

iMet-tRNA: 3'-T-TCG-AAT-TAT-GCT-GAG-TGA-TAT-CCG-TCT-CAC-CGC-GTC-GCC-TTC-GCA-CGA-CCC-GGG-TAT-TGG-GTC-TCC-AGC-TAC-CTA-GCT-TTG-GTA-GGA-GAC-GGT-GGT-5'

tRNA-prime: 5'-A-AGC-TTA-ATA-CGA-CTC-ACT-ATA-3'

II. D. 4. b. Assessment of tRNA quality

A TBE-Urea gel solution was poured between glass plates using the Mini-PROTEAN Tetra Handcast system with the desired comb. Short RNAs were supplemented with 2x RNA loading dye and heated at 95 °C for 5 min before being incubated on ice for 5 min. The RNAs were loaded on a 6-15 % TBE-Urea-PAGE along with low range ssRNA ladder. A voltage of 200 V was applied to the gel for about 20 min in a Mini-PROTEAN Tetra Vertical Electrophoresis Cell. The gel was then incubated in a 1x GelRed solution in water for about 20 min. Images were acquired with the Chemidoc MP imaging system.

II. E. RNA extraction from mammalian cells

II. E. 1. Extraction of total RNA

DMEM was removed from the cell culture container and TRIzol reagent was directly added to the cells. Total RNA extraction was performed according to the provider's instructions, RNA was precipitated and resuspended in DEPC-treated water.

II. E. 2. Extraction of polyA mRNA

2 x 10^6 cells were washed with PBS and resuspended in 500 µL PolyA Lysis Buffer. They were kept at RT for 5 min and passed 5 times through a 20 G needle (Braun, C721.1). 500 µL lysate was added to 100 µL Oligo $d(T)_{25}$ Magnetic Beads pre-washed twice with lysis buffer, and incubated at RT for 10 min. As a control, beads were incubated with PolyA Lysis Buffer only. The beads were washed 2 x with Wash Buffer I, 2 x with Wash Buffer II and 1 x with Low Salt Buffer. The beads were resuspended in 100 µL Elution Buffer, heated at 50 °C for 2 min and the supernatant containing the eluted polyA RNA was collected.

II. E. 3. Extraction of total tRNAs

2 x 10^6 cells were collected and RNAs shorter than 200 nucleotides were extracted using mirVana miRNA isolation kit according to the provided protocol (enrichment procedure for small RNAs). Small RNAs were supplemented with RNA loading dye and run on an 8 % Urea-TBE PAGE as described previously. The band corresponding to tRNAs was identified by UV shadowing using a Pre-coated TLC-sheets ALUGRAM SIL G/UV_{254} (Macherey-Nagel, 818133) and a UV lamp (3UV-38, UVP), and was cut out of the gel. The gel pieces were cut in smaller pieces using a scalpel and were incubated overnight at 21 °C at 600 rpm in 0.5 M Ammonium Acetate. Next day, the solution was collected and 1 mL 100 % Ethanol was added per 400 µL Ammonium Acetate solution. After 60 min at -80 °C, the samples were centrifuged at 17000 g at 4 °C for 30 min. Pellets were washed with 70 % Ethanol, air dried and frozen directly or after resuspention in DEPC-treated water. The tRNAs were refolded as described previously with *in vitro* transcribed tRNA-iMet.

III. *In vitro* assays

III. A. Purification of recombinant TRMT6/61A

Human his-tagged TRMT6/61A dimer was purified from *Escherichia coli* BL21 cells using 1 mL HisTrap HP histidine-tagged protein purification columns (GE Healthcare, 17524705). Eluted fractions containing the recombinant proteins were pooled and incubated overnight with HisGST-PreScission protease at 4 °C. Protein solution was then subjected to size-exclusion chromatography using a HiLoad Superdex 200 column (GE Healthcare, 17517601) in 50 mM HEPES NaOH pH 7.5, 150 mM NaCl and 1 mM DTT.

III. B. Melting analysis of TRMT6/61A

This method uses the ability of the SYPRO Orange dye to bind to hydrophobic surfaces (Steinberg et al., 1996). When proteins unfold at higher temperature, they expose their hydrophobic regions which become available for SYPRO Orange binding. This results in an increase in fluorescence which can be detected by a qPCR machine and allows the measurement of the melting temperature of proteins (Lo et al., 2004). 10 µM of purified recombinant heterodimer TRMT6/61A were mixed with or without 10 µM tRNA and with SYPRO Orange dye 1:5000 in 100 mM Tris HCl pH 7.6, 100 mM NH_4Cl, 10 mM $MgCl_2$, 0.1 mM EDTA, and 1 mM DTT (added fresh). Fluorescence change was recorded with a CFX96 Real-Time PCR detection system while gradually increasing

the temperature from 20 ºC to 80 ºC in 0.5 ºC/15 sec steps (excitation at 450-490 nm, detection at 510-530 nm). Background fluorescence from the buffer as well as from the tRNA were subtracted before further analysis. The apparent melting temperature values were obtained by calculating the first derivative of the fluorescence change.

III. C. CD Spectroscopy

Circular Dichroism (CD) Spectroscopy uses polymerized light and measures the difference of absorbance of a molecule in right-handed and left-handed circularly polarized light. Proteins secondary structures such as α-helixes (Holzwarth and Doty, 1965) or β-sheets (Greenfield and Fasman, 1969) give specific signals, and the fraction of the different conformations in a molecule can be identified. CD spectra of proteins were recorded using a Jasco J-810 spectropolarimeter at 37 ºC and 45 ºC in 50 mM HEPES NaOH pH 7.5 and 150 mM NaCl. Proteins at 5 µM were placed in a 1-mm path absorption cells (Hellma Analytics) and samples were scanned three times from 260 nm to 200 nm in 0.5 nm steps at 50 nm/min. The values from the buffer were subtracted.

III. D. Protease sensitivity assay

Recombinant protein was diluted at 1.5 µM in 25 mM Hepes KOH pH 7.5, 150 mM NaCl, 5 mM $CaCl_2$ and 2 mM DTT and incubated at 37 °C or 45 °C for 20 min. Proteinase K was added at 0.1 ng/µL and the tubes were kept at the same temperature. Samples were collected after 0, 3, 6 and 9 min and digestion was immediately stopped by addition of saturated PMSF. The samples were analyzed by SDS-PAGE and Coomassie staining. Images were acquired with the Chemidoc MP imaging system and bands quantified using Image Lab 5.0 software.

III. E. TRMT6/61A binding to mRNA *in vitro*

In vitro transcribed tRNA was refolded as described previously. Recombinant TRMT6/61A was diluted to 10 nM in HLB supplemented with RNAsin 1:100 and Phosphatase Inhibitor Cocktail 2 1:100 and incubated at indicated temperature for 20 min. tRNA was added at a final concentration of 1 µM and the mixture was further incubated at room temperature for 20 min with 20 µL Dynabeads M-280 Streptavidin coated with biotinylated mRNA. The beads were washed and eluted as described for RNA pulldowns.

III. F. TRMT6/61A binding to tRNA *in vitro*

An infinite M200 Pro Microplate Reader (Tecan) was used to record the change in tRNA UV light absorbance upon binding to the TRMT6/61A heterodimer. tRNA (1 µM) and protein solutions (at the indicated concentration) were prepared in 100 mM Tris HCl pH 7.6, 100 mM NH_4Cl, 10 mM $MgCl_2$, 0.1 mM EDTA, and 1 mM DTT (freshly added). The mix was pre-incubated for 10 min at 25 ºC in a UV-transparent 96-well plates (Corning). Temperature was raised to 37 ºC or 42 ºC for another 10 min before measuring the absorbance between 230 nm and 350 nm in 2-nm steps. The formula $(\lambda_{max} - \lambda_{260})/\lambda_{max}$ was used to determine the binding of the tRNA to the protein, where λ_{max} is the 260 nm absorbance of the pure tRNA and λ_{260} is the 260 nm absorbance from the tRNA/protein mix. The background absorbance from the buffer as well as from the protein only solution was subtracted before calculations.

IV. Cell-based assays

IV. A. Characterization of stress conditions

IV. A. 1. Kinetics of eIF2α phosphorylation status

30 x 10^6 HeLa cells were collected and resuspended in 3.5 mL DMEM. The cells were incubated at 45 °C and 500 µL of cell suspension were collected after 0, 30, 60 or 120 min. The collected cells were washed twice with ice-cold PBS, resuspended in 100 µL HLB supplemented with RNAsin and Phosphatase Inhibitor Cocktail 2 and kept on ice for 10 min. The lysate was passed through a 20 G needle 20 times and centrifuged at 640 g at 4 °C for 5 min. The supernatant was collected, supplemented with 1/10 volume of 1 M Potassium Acetate and centrifuged at 10400 g at 4 °C for 20 min. Protein concentration was measured using Bradford reagent and BSA standards, and normalized. Samples were analyzed by western blotting using antibodies against total eIF2α or against the phosphorylated form (Ser51) of eIF2α.

IV. A. 2. Study of HSP70 induction

2 x 10^6 HeLa cells were collected and resuspended in 2 x 1 mL DMEM. They were incubated at 37 °C or at 45 °C in suspension. 1.5 x 10^6 cells were collected after 0, 30, 60 and 120 min of incubation. Total RNAs were purified by TRIzol extraction and used for preparing cDNA and to run qPCR using primers specific to *hsp70*, *hsc70* and *gapdh* genes as previously described.

IV. A. 3. Polysomes profiling

HeLa cells were seeded at 5 x 10^6 per 10 cm-dish. Next day, DMEM was refreshed and supplemented with 25 mM Hepes NaOH pH 7.6. The dishes were incubated at 45 °C for 1 h or treated with 1 mM arsenite for 30 min at 37 °C. The cells were washed twice with ice-cold PBS supplemented with 100 µg/mL cycloheximide and resuspended in 600 µL Lysis Buffer supplemented with Phosphatase Inhibitor Cocktail 2 1:100, RNAsin 1:1000 and 100 µg/mL cycloheximide. After a 15 min incubation on ice, the lysates were centrifuged at 10000 g for 5 min at 4 °C. 550 µL of supernatant was loaded on a cold 10-50 % Sucrose gradient in an Open-top Polyclear 16.8 mL tube (Seton) and centrifuged in an Optima XPN-80 ultracentrifuge (Beckman Coulter) using a SW28.1 rotor, at 100000 g for 4 h at 4 °C. Gradient absorbance at 254 nm was measured on a gradient station (Biocomp) at a speed of 0.2 mm/sec. For monosome analysis, the 80S fraction was collected. Samples were normalized according to the absorbance at 260 nm and analyzed by western blotting using anti-S6 antibody.

IV. B. Cell viability assays

IV. B. 1. Heat sensitivity

HeLa WT and TRMT61A KD cells were seeded at 1.25 x 10^4 cells/well in duplicates in a 48 well plates in 200 µL DMEM supplemented with 25 mM Hepes NaOH pH 7.5. The plates were immediately placed in an incubator at 37 °C or 45 °C for 2 h and then placed back at 37 °C for overnight recovery. 14 h later, medium in each well was discarded and replaced by 200 µL 0.33 mg/mL XTT + 12.5 µg/mL PMS in DMEM. After 2 h of incubation at 37 °C, A_{475} and A_{600} were measured (12 measurements per well, 5 flashes) using the Infinite M200 Pro Microplate Reader. Duplicates were averaged and specific absorbance was calculated as following:

$$Specific\ Absorbance = A_{475nm}(Sample) - A_{475nm}(Blank) - A_{660nm}(Sample)$$

IV. B. 2. Arsenite sensitivity

HeLa cells WT and TRMT61A KD were seeded in two 48-well plates at 1.25 x 10^4 cells/well. Next day, the cells were treated with 0 or 0.5 or 1 or 2 mM arsenite for 1 h at 37 °C in triplicates. The cells were washed with PBS, then 200 µL 0.33 mg/mL XTT + 12.5 µg/mL PMS in DMEM was

added per well. After 4 h of incubation at 37 °C, A_{475} and A_{600} were measured and specific absorbance was calculated as described previously. Triplicates were averaged.

IV. C. Pulldowns

IV. C. 1. Free mRNA pulldowns

About 60 x 10^6 HeLa cells were trypsinized and collected. They were transferred to a 15 mL tube, resuspended in 2 mL fresh medium and kept in a water bath at 45 °C for 1 h. After two PBS washes, the cells were resuspended in 1.5 volume HLB and kept on ice for 10 min. The lysate was passed through a 20 G needle 20 times and centrifuged at 640 g at 4 °C for 5 min. The supernatant was collected, supplemented with 1/10 volume of 1 M Potassium Acetate and centrifuged at 10400 g at 4 °C for 20 min. Protein concentration was measured using Bradford reagent and BSA standards, and normalized to 5 µg/µL. For each sample, 20 µL of Dynabeads M-280 Streptavidin were washed one time with B&W, two times with Solution A, one time with Solution B and one last time with B&W. The beads were incubated with 2 µg biotinylated HSP70 mRNA (or DEPC H_2O) in B&W in a volume of 40 µL at RT for 30 min. The beads were then washed three times with B&W and one time with HLB. 100 µL of lysate was then added to the beads and incubated at 4 °C for 2 h with gentle shaking. The beads were washed six times with 50 µL Washing Buffer and three times with MS buffer. The beads were then frozen at -80 °C until further processing for mass spectrometry. For biochemical verifications of the interactions, the protocol was similar with a few modifications: non heat shocked cells were used as a control, HLB was supplemented with RNAsin 1:100 and Phosphatase Inhibitor Cocktail 2 1:50 and beads without biotinylated mRNA were used as a negative control. Finally, after the beads were washed with Washing Buffer, protein elution was performed with 250 u benzonase in 10 µL Washing Buffer at 37 °C for 15 min. The eluate was collected for Western Blot using the indicated antibodies.

IV. C. 2. TRMT6/61A and eIF2α co-immunoprecipitation

The cells were collected 24 h after transfection with Flag-TRMT6 and 3xFlag-TRMT61A, resuspended in fresh DMEM supplemented with Hepes NaOH pH 7.5 (1 mL per dish) and incubated at 37 °C or 45 °C for 1 h. Cells were washed twice with ice-cold PBS and resuspended in HLB supplemented with RNAsin 1:100 and Phosphatase Inhibitor Cocktail 2 1:50, kept on ice for 10 min, passed through a 20 G needle 20 times and centrifuged at 640 g at 4 °C for 5 min. The

supernatant was collected, and supplemented with 1/10 volume of 1 M potassium acetate. Half of the lysate was treated with 250 u benzonase at 37 °C for 15 minutes while the other half remained untreated. All the lysates were centrifuged at 10400 g at 4 °C for 20 minutes and the supernatants were collected. Protein concentration was normalized to 1.5 µg/µL using Bradford reagent. 10 µL washed Anti-Flag M2 affinity gel were blocked with 1 % BSA in HLB for 1 h on ice before being incubated with 200 µL lysate at 4 °C for 3 h. Beads were washed 4 times on columns with Washing Buffer. Elution was performed with 50 µL 3x Flag peptides solution at 100 µg/mL in TBS for 5 min at RT. The eluate was collected analyzed by SDS-PAGE and western blotting using anti-Flag and anti-eIF2α antibodies.

IV. C. 3. PolyA mRNA pulldown and detection of associated TRMT6

2 x 5 x 10^6 HeLa cells were counted, collected and resuspended in 2 x 1 mL DMEM supplemented with 25 mM Hepes NaOH pH7.5. The cells were transferred into 15 mL tubes and one tube was kept at 37 °C while the other one was incubated at 45 °C for 60 min in a water bath. The cells were then collected, washed twice with ice-cold PBS and resuspended in 300 µL LB supplemented with 2 mM DTT, Phosphatase Inhibitor Cocktail 2 1:100 and RNAsin 1:1000. They were kept incubated at RT for 5 min and passed 5 times through a 20 G needle. The protein concentration of the lysates was measured and normalized using Bradford reagent. 400 µL of lysate at the protein concentration of 1.5 µg/µL were added to 100 µL of washed Oligo $d(T)_{25}$ Magnetic Beads and incubated at RT for 30 min. 2/3 of the beads were washed 3x with LB and resuspended in 10 µL LB supplemented with 250 units of benzonase for protein elution. After 15 min at 37 °C, the supernatant was collected and analyzed by SDS-PAGE and western blotting using anti-TRMT6 antibody. The rest of the beads were processed for RNA elution as described in the "Extraction of polyA mRNA" part. After elution, RNA amounts were estimated using RiboGreen.

IV. C. 4. PolyA mRNA pulldown and detection of associated Aβ-EGFP

4 × 10^6 HeLa cells were electroporated with 30 µg Aβ-EGFP or 10 µg EGFP expression vectors and seeded in 10 cm dishes (one transfection per dish). 24 h after transfection, the cells were washed twice with ice-cold PBS and resuspended in 300 µL LB supplemented with 2 mM DTT, Phosphatase Inhibitor Cocktail 2 1:100 and RNAsin 1:1000. After a 15 min incubation on ice, the lysates were centrifuged at 10000 g for 5 min at 4 °C. The protein concentration of the supernatants

was measured and normalized using Bradford reagent. 350 µL lysate was added to 50 µL of washed Oligo $d(T)_{25}$ Magnetic Beads and incubated at RT for 30 min. The beads were washed 3x with LB and resuspended in 10 µL LB supplemented with 250 units of benzonase nuclease for elution. After 15 min at 37 °C, the supernatant was collected and analyzed by SDS-PAGE and western blotting using anti-GFP antibody.

IV. C. 5.Aβ pulldown

8 x 10^6 HeLa WT or TRMT61A KD cells were transfected by electroporation with 30 µg Aβ-EGFP or 10 µg EGFP. 24 h after transfection, the cells were washed two times with PBS and resuspended in 300 µL LB supplemented with Phosphatase Inhibitor Cocktail 2 1:100, RNAsin 1:1000 and 1x protease inhibitor. The cells were kept on ice for 20 min, then centrifuged at 10000 g at 4 °C for 5 min. Supernatants were collected and protein concentration was normalized to 1 µg/µL using Bradford reagent. 200 µL of each lysate were diluted with 300 µL LB supplemented with RNasin (1:1000) and 1 x protease inhibitor. For each sample, 10 µL GFP-Trap magnetic agarose were washed three times with LB. 450µL of each lysate were added to 10 µL washed GFP-Trap magnetic agarose and incubated at 4 °C for 1 h with gentle shaking. The agarose was washed three times with LB supplemented with RNasin (1:1000) and 1x Protease Inhibitor and three times with MS Buffer. The agarose was frozen at -80 °C until further processing for mass spectrometry.

IV. D. m^1A/m^6A sandwich assay

HeLa WT and TRMT61A KD cells (2 x 10^6) were resuspended in 1 mL DMEM supplemented with 25 mM Hepes NaOH pH 7.5 and incubated at 37 °C or 45 °C for 1 h. PolyA mRNAs were extracted as described previously until washing with Low Salt Buffer. The beads were resuspended in 425 µL Low Salt Buffer. 25 µL of the beads were eluted 20 µL Elution Buffer by heating the beads at 50 °C for 2 min and the amount of polyA mRNA in the different samples was compared using RiboGreen. The 2 x 200 µL beads left were pipetted into clean tubes, buffer was discarded and beads were resuspended in 200 µL PBST (PBS + 0.1 % Tween 20) with 2 µL anti-m^1A or 2 µL m^6A and incubated at 4 °C overnight. Next day, the beads were washed 3 x for 5 min with 500 µL PBST. Bound antibody was eluted by incubation at 37 °C for 15 min with 250 u benzonase nuclease in 10 µL 25 mM Tris HCl pH 7.5, 10 mM $MgCl_2$, 2 mM DTT. Supernatant was collected and analyzed by SDS-PAGE and western blotting using anti-Mouse (1:1000) or anti-Rabbit

(1:1000) directly as primary antibodies to detect the amount of anti-m^1A or anti-m^6A that bound polyA-mRNA. Bands were quantified and their intensity was normalized to the corresponding polyA mRNA amount detected by RiboGreen assay.

IV. E. HPLC analysis of total tRNAs

tRNA pellets were resuspended in 16 µl of MS grade water and digested to nucleosides by incubation with 0.1 U nuclease P1 and 0.1 U bacterial alkaline phosphatase BAP C75 in P1 buffer (25 mM NH_4OAc pH 5.0) at 37 °C for 1 h. Chromatographic separation was performed on an UltiMate 3000 HPLC (Thermo Fisher Scientific) equipped with a diode array detector (DAD). 5 µl of the nucleoside mixture were loaded on a Synergy Fusion RP column (4 mm particle size, 80Å pore size, 250 mm length, 2 mm inner diameter) from Phenomenex with 100 % buffer A (5 mM NH_4OAc pH 5.3) and separated at 35 °C with a flow rate of 0.35 ml/min using a linear gradient of buffer B (100 % acetonitril) to 20 % in 20 min, then to 40 % in 2 min. At the end of the gradient the column was washed with 95 % buffer B for 7 min and re-equilibrated with buffer A for 4 min. The nucleosides were monitored by recording the UV chromatogram at 254 nm.

IV. F. Reporter systems

IV. F. 1. Ub-EGFP reporter assay

12×10^6 HeLa cells were electroporated with 20 to 30 µg m^1A-Ub-EGFP or mut-Ub-EGFP expression vectors and seeded in 10 cm dishes (two dishes per transfection). 5 h after transfection, cells were collected by trypsinization and inactivation with 10 % FBS/DMEM. The cells were counted and the number of cells from each transfection was adjusted. The cells were then washed twice with 10 mL 0 % FBS/DMEM and resuspended in 800 µL 0 % FBS/DMEM supplemented with 25 mM Hepes NaOH pH 7.5 and with 10 µM Actinomycin D. The cells in suspension were incubated at 45 °C for 30 min and resuspended every 10 min. After 30 min, the cells were transferred to 37 °C and 300 µL of cell suspension was added to 300 µL pre-heated 0 % FBS/DMEM supplemented with 25 mM Hepes NaOH pH7.5 and with 10 µM Actinomycin D. 50 µL aliquots were collected after 0, 15 and 30 min at 37 °C, the cells being resuspended every 10 min. To immediately stop translation, the samples were directly added to SDS sample buffer pre-heated at 95 °C. After sonication, the samples were analyzed by SDS-PAGE and western blotting using anti-GFP and anti-GAPDH antibodies.

IV. F. 2. NQO1 reporter assay

HeLa cells, WT and TRMT61A KD were seeded in a 12-well plate at 1 x 10^5 cells per well. B16F10 cells were seeded in a 12-well plate at 1.5 x 10^5 cells/well. Next day, they were transfected with 250 ng reporter constructs and different amounts of Aβ-GFP construct (0 ng, 250 ng, 500 ng or 1000 ng for HeLa WT and B16F10 cells and 0 ng, 500 ng, 1000 ng and 2000 ng for HeLa TRMT61A KD cells) using PEI (the ratio DNA:PEI was 1:6 using a 1 mg/mL PEI solution). 24 h after transfection, cells were collected and analyzed by SDS-PAGE and western blotting using anti-GFP (1:1000) and anti-Flag (1:1000) antibodies. For analysis, the amounts of NQO1 were normalized to GAPDH signal, referred to "No Aβ-GFP" condition and multiplied by GFP signal (normalized to GAPDH) in order to take into account Aβ-GFP amounts. The values for the 3 different amounts of Aβ-GFP transfected were averaged. Finally, numbers were referred to the "WT motif" condition.

The same conditions were used for checking the mRNA levels of the reporters. The cells were collected 24 h after transfection and total RNAs were extracted and processed for qPCR as described previously. Primers for qPCR were designed so that the forward primer was at the end of the NQO1 gene while the reverse one was on the backbone of the plasmid, before the polyA sequence, such that endogenous NQO1 mRNA was not amplified.

IV. G. RiboGreen assays

For estimating the amount of RNA in a solution, RiboGreen was used. This reagent binds RNA which induces a strong increase in fluorescence emission at 500 nm. This dye is very sensitive and allows the precise quantification of RNA amounts in solution. For this assays, RNA in solution was diluted in TE buffer in a final volume of 100 µL. The volume of solution to add depends on its RNA concentration and should be titrated in order to be in the linear range of detection. 100 µL of a solution of RiboGreen diluted 2000 times in TE buffer was added to each sample. The M200 Pro Microplate Reader was used for measuring fluorescence (λ_{ex}=500 nm and λ_{em}=525 nm). A titration curve using known amounts of RNA was used to estimate RNA amounts in the samples.

IV. H. Stress granules isolation

Stress granules were prepared as described (Khong et al., 2018) omitting the affinity purification step. HeLa cells were treated with 0.5 mM arsenite at 37 °C for 60 min, washed, pelleted and flash-

frozen in liquid nitrogen. The pellets were thawed, resuspended in 500 µL SG Lysis Buffer, passed seven times through a 26 G needle and centrifuged at 1000 g for 5 min at 4 °C. The lysate was transferred to a new tube and centrifuged at 17000 g for 20 min at 4 °C. The resulting supernatant was called 'Soluble 1'. The pellet was resuspended in 500 µL SG Lysis Buffer and centrifuged again at 17000 g for 20 min at 4 °C. The resulting supernatant was called 'Soluble 2'. The pellet was resuspended in 150 µL SG Lysis Buffer, spinned at 850 g for 2 min at 4 °C. The supernatant was called 'SG fraction' and constituted the stress granule core enriched fraction. Total RNA was extracted from the SG pellet by Trizol extraction and RNA precipitation and stored at -80 °C until MS analysis. PolyA mRNA for comparison was prepared from HeLa cells heated at 45 °C for 60 min as described previously. The eluted mRNAs were precipitated and stored at -80 °C until MS analysis. The collected samples were analyzed by western blotting using anti-TIAR and anti-GAPDH antibodies.

V. Microscopy and immunofluorescence

V. A. Cy5-labeled RNA microscopy

6 h after transfection with RNA, the cells were washed with PBS and fixed with 4 % paraformaldehyde in PBS at RT for 10 min. One slide was then treated with 250 units benzonase nuclease in PBS supplemented with 2 mM $MgCl_2$ at 37 °C for 20 min. All the slides were washed with PBS, stained with DAPI, mounted in PBS and imaged using a Zeiss LSM-780 inverted confocal microscope with a 63x oil immersion objective. For the description of Cy5-HSP70 mRNA distribution after transfection, at least 100 Cy5-positive cells were visually identified and checked visually for granulation of the labeled mRNA. The experiment was performed in triplicates. The quantification of Cy5-positive cells (transfected with Cy5-HSP70 mRNA +/- benzonase treatment or Cy5-55mer oligo), was performed using CellProfiler as following. Nuclei were detected and cells were identified by propagation from the nuclei. Intensity of Cy5 was measured for each cell and Cy5-positive cells were identified. The experiment was performed in triplicates and at least 300 cells were analyzed per condition and per repetition to determine the percentage of Cy5-positive cells.

V. B. Stress granules microscopy

HeLa cells were seeded in a 12-well plate at 0.1 x 10^6 cells/well on a Poly-L-lysine-coated cover slide. Next day, medium was refreshed and supplemented with 25 mM Hepes NaOH pH 7.4. Cells were kept at 37 °C for 2 h, at 45 °C for 1 h or at 37 °C for 2 h with treatment with 1 mM arsenite for the last 30 min. After incubation or treatment, cells were washed with PBS and fixed with 3.7 % paraformaldehyde in PBS for 9 min at RT. They were then permeabilized with acetone at -20 °C for 5 min, blocked with 1 % BSA in PBS for 1 h at RT and incubated with anti-eIF4E (1:100) in 1 % BSA in PBS at RT for 1 h. Incubation with anti-Rabbit-IgG Alexa Fluor647 conjugate (1:1000) was done in 1 % BSA in PBS at RT for 1 h, followed by three washing steps with PBS and DAPI staining. Slides were mounted in PBS and imaged using a Zeiss LSM-780 inverted confocal microscope with a 63x oil immersion objective. The experiment was performed in triplicates and at least 100 cells were analyzed per condition and per repetition.

To compare SGs formation upon arsenite treatment, HeLa WT and TRMT61A KD cells were seeded in a 12-well plate with Poly-L-lysine coated cover slides at 0.15 x 10^6 cells/well. Next day, medium was replaced by serum-free medium and the cells were kept at 37 °C for 2 h. Arsenite was then added at 0.0625 mM for 30 min at 37 °C. The cells were prepared for microscopy as described previously but using anti-TIAR antibody (1:1000) and imaged similarly. The experiment was performed in triplicates and at least 200 cells were analyzed per condition and per repetition.

Analysis of the pictures was performed using CellProfiler: nuclei were detected, cells were identified by propagation from the nuclei, and SGs were identified and counted within each cell.

V. C. Amyloid microscopy

For aggregation analysis, a construct coding for the amyloid-β peptide (amino-acids 1 to 42) fused to GFP (Aβ-GFP) was used. HeLa cells transfected with Aβ-GFP or control EGFP were fixed 48 h after transfection with 4 % paraformaldehyde in PBS at RT for 1 h and stained with DAPI. Cells were imaged using a Zeiss LSM-780 inverted confocal microscope with a 40x oil immersion objective. Using CellProfiler, nuclei were detected and cells identified by propagation from the nuclei. Fluorescence intensity was measured for each cell. Dead or dying cells were filtered out based on intensity values. The experiment was performed in triplicates and at least 200 EGFP-positive cells were analyzed per condition and per repetition to determine the fraction of cells with aggregates.

V. D. Colocalization of TRMT6/61A and TIAR

8 x 10^6 HeLa cells were transfected with 15 µg Flag-TRMT6 and 15 µg 3xFlag-TRMT61A by electroporation and seeded at 0.5 x 10^6 cells/well in a 12-well plate on Poly-L-lysine-coated slides. 24 h after transfection, medium was replaced by 0 % FBS/DMEM, and cells were kept at 37 °C for 2 h. The cells were then treated with 0.25 mM arsenite at 37 °C for 30 min. After treatment, cells were washed with PBS and fixed with 3.7 % Paraformaldehyde in PBS for 9 min at RT. They were then permeabilized with acetone at -20 °C for 5 min, blocked with 1 % BSA in PBS for 1 h at RT and incubated with anti-TIAR (1:1000) in 1 % BSA in PBS at RT for 1 h. Incubation with anti-Rabbit-IgG Alexa Fluor647 conjugate (1:1000) and anti-Flag M2-Cy3 (1:100) was done in 1 % BSA in PBS at RT for 1 h, followed by three washing steps with PBS and DAPI staining. Slides were mounted in PBS and imaged using a Zeiss LSM-780 inverted confocal microscope with a 63x oil immersion objective. For the analysis of colocalization, ImageJ was used. A line was drawn and fluorescence profiles along the line were measured and exported for each fluorophore.

VI. Mass spectrometry

VI. A. Proteomics

- Sample preparation.

Pulled down proteins were processed on-beads for LC-MS/MS analysis as following. Beads were re-suspended in 50 µl 8 M urea/50 mM Tris HCl pH 8.5, reduced with 10 mM DTT for 30 min and alkylated with 40 mM chloroacetamide for 20 min at 22 °C. Urea was diluted to a final concentration of 2 M with 25 mM Tris HCl pH 8.5, 10 % acetonitrile and proteins were digested with trypsin/lysC mix overnight at 22 °C. Acidified peptides (0.1 % trifluoroacetic acid) were desalted and fractionated on combined C18/SCX stage tips (3 fractions). Peptides were dried and resolved in 1 % acetonitrile, 0.1 % formic acid. LC-MS/MS. LC-MS/MS was performed on a Q Exactive Plus equipped with an ultra-high pressure liquid chromatography unit (Easy-nLC1000) and a Nanospray Flex Ion-Source (all three from Thermo Fisher Scientific). Peptides were separated on an in-house packed column (100 µm inner diameter, 30 cm length, 2.4 µm Reprosil-Pur C18 resin using a gradient from mobile phase A (4 % acetonitrile, 0.1 % formic acid) to 30 % mobile phase B (80 % acetonitrile, 0.1 % formic acid) for 60 min followed by a second step to 60 % B for 30 min, with a flow rate of 300 nl/min. MS data were recorded in data-dependent mode

selecting the 10 most abundant precursor ions for HCD with a normalized collision energy of 30. The full MS scan range was set from 300 to 2000 m/z with a resolution of 70000. Ions with a charge ≥2 were selected for MS/MS scan with a resolution of 17500 and an isolation window of 2 m/z. The maximum ion injection time for the survey scan and the MS/MS scans was 120 ms, and the ion target values were set to 3 x 10^6 and 10^5, respectively. Dynamic exclusion of selected ions was set to 30 s. Data were acquired using Xcalibur software (Thermo Fisher Scientific).

- Data analysis with Max Quant.

MS raw files from five (Hsp70 coding region interactome and Aβ-GFP coaggregators) or three biological replicates (BRaf coding region interactome) of pulldown and background samples were analyzed with Max Quant (version 1.5.3.30) (Cox and Mann, 2008) using default parameters. Enzyme specificity was set to trypsin and lysC and a maximum of 2 missed cleavages were allowed. A minimal peptide length of 7 amino acids was required. Carbamidomethylcysteine was set as a fixed modification, while N-terminal acetylation and methionine oxidation were set as variable modifications. The spectra were searched against the UniProtKB human FASTA database (downloaded in November 2015, 70075 entries) for protein identification with a false discovery rate of 1 %. Unidentified features were matched between runs in a time window of 2 min. In the case of identified peptides that were shared between two or more proteins, these were combined and reported in protein group. Hits in three categories (false positives, only identified by site, and known contaminants) were excluded from further analysis. For label-free quantification (LFQ), the minimum ratio count was set to 1. Data analysis with Perseus. Bioinformatic data analysis was performed using Perseus (version 1.5.2.6) (Tyanova et al., 2016). Proteins identified in the pulldown experiments were further included in the analysis if they were quantified in at least 4 out of 5 biological replicates in at least one group (pulldown/background) for the Hsp70 coding region RNA and Aβ-GFP experimental set-ups and in at least 3 out of 3 biological replicates in at least one group (pulldown/background) for the BRaf coding region RNA control. Missing LFQ values were imputed on the basis of normal distribution with a width of 0.3 and a downshift of 1.8 (1.3 for the Aβ-GFP data set). Proteins enriched in the pulldown (RNA over background binding) were identified by two-sample t-test at a permutation based FDR cutoff of 0.001 and s0 = 0.1 for the Hsp70 coding region interactome, at a p-value cutoff of 0.01 for the BRaf coding region interactome and at an FDR cutoff of 0.05 and s0 = 0.1 for the Aβ- GFP interactome. Categorical

annotations were added in Perseus and a Fisher's exact test with a p value threshold of 0.001 was run for GO (Gene Ontology) term enrichment analysis.

VI. B. Quantification of modified nucleotides

RNA from stress granules or cytosolic mRNAs from heated HeLa cells were resuspended in 10 µl of MS water and digested with 0.05 units of nuclease P1 (Wako) and 0.05 units of bacterial alkaline phosphatase (BAP C75, Takara) in P1 buffer (20 mM ammonium acetate pH 5.3) for 1 h at 37 °C. Samples were store at -20 °C before mass spectrometry. Chromatographic separation of the nucleosides was performed with an Easy-nLC1000 on an in-house packed column (100 µm inner diameter, 50 cm length, 4 µm Synergi Fusion 80 Å pore size using a gradient from mobile phase A (5 mM ammonium formate pH 5.3) to 32 % mobile phase B (100 % acetonitrile) for 50 min followed by a second step to 40 % B for 8 min, with a flow rate of 200 nl/min. Retention times were monitored using 10 nM solutions of nucleoside standards purchased from Sigma Aldrich (main nucleosides) and Carbosynh (N1-methyladenosine and N6-methyladenosine). Nucleosides were injected into a Q Exactive Plus mass spectrometer equipped with a Nanospray Flex Ion-Source and analyzed in the positive mode with a method consisting of full MS and targeted SIM scans. Full scans were acquired with AGC target value of 10^6, resolution of 70.000 and maximum injection time of 100 ms. Adenosine, N1-methyladenosine and N6-methyladenosine were monitored at the respective retention time with a 4-amu isolation window, AGC target value of 2 x 10^5, 140.000 resolution and maximum injection time of 500 ms. The correct identification of N1- and N6-methyladenosines was proved by fragmentation of the parent ion using a normalized collision energy of 30 and recording MS/MS scans at a resolution of 70000, 4.0 m/z isolation window, 2 x 10^5 ACG target and maximum fill time of 120 ms. Manual identification and quantification of nucleosides was performed using Thermo Xcalibur Qual Browser. Extracted ion chromatograms were generated with a deviation of 0.002 Da from the theoretical m/z value and the peaks were integrated using the manual peak annotation function. Absolute amounts of nucleosides were calculated generating an external calibration curve in the range 0.2-3000 fmol by serial dilutions of the nucleoside standards. N1-methyladenosine (m^1A) and N6- methyladenosine (m^6A) amounts were reported as percentage of adenosine (A).

VII. Bioinformatics study

VII. A.Analysis of MS results

pI and molecular weight values were calculated using the Compute pI/MW tool on the ExPASy website. Hydrophobicity and disorder propensity were analyzed with the boxplotter function of cleverSuite (Klus et al., 2014) using Kyte and Doolittle (Kyte and Doolittle, 1982) and TOP-IDB (Campen et al., 2008) scales, respectively. To analyze aggregation propensity the Zyggregator algorithm was used (Tartaglia and Vendruscolo, 2010). To analyze granulation propensity the *cat*GRANULE algorithm was used (Bolognesi et al., 2016). Hsp70 mRNA interactors were compared to the human proteome as provided by Perseus (20592 proteins) and to the human RBPs (Gerstberger et al., 2014). Statistical significance of observed differences was assessed by Mann-Whitney test. GO terms enrichment analysis of mRNAs with m^1A motif enriched in SGs (Khong et al., 2017) and filtered as described above was performed on line with Panther (Mi et al., 2017) using the Overrepresentation Test tool (released 2017-12-05) and the GO ontology database (released 2017-11-28). A binomial test with p-value threshold of 0.05 was run using the set of mRNAs neither enriched nor depleted from SGs as reference. GOslim Molecular Function enrichment analysis of the Aβ-GFP interactome was performed with Panther as described above. As input gene names of Aβ-GFP interactors and of the human genome (all genes in database) were used. FDR cut off for the Fisher's exact test was set to 0.05.

VII. B.Analysis of m^1A motifs in mRNAs

The reference set of human genes (11195 genes) was taken from Khong *et al* (Khong et al., 2017). Ensemble Biomart (version 90) was used to select all transcript variants (69090 transcripts) and to retrieve the cDNA sequences. The unique transcripts were filtered to select those which match the exact length reported in Khong et al (Khong, et al., 2017) (final set of 9301 transcripts). The motifs centered on TTCAA (AGTTCAANNCT, CGTTCAANNCG, GGTTCAANNCC, TGTTCAANNCA) and centered on TTCGA (AGTTCGANNCT, CGTTCGANNCG, GGTTCGANNCC, TGTTCGANNCA) were searched separately in all the sequences. A search algorithm was written in Python for this specific task.

VIII. Statistics

All repetitions in this study were independent biological repetitions performed at least three times if not specified differently. To identify significantly increased proteins in pulldowns (RNA over background binding) in mass spectrometry analyses, a two-sample t-test analysis of grouped biological replicates was performed using a FDR cutoff of 0.001 with s0 = 0.1 and a p-value cutoff of 0.01 for the Hsp70 and B-Raf coding region interactome, respectively and a FDR cutoff of 0.05 with s0 = 0.1 for the Aβ-GFP interactome. Categorical annotation was added in Perseus and a Fisher exact test with a p-value threshold of 0.05 was run for GOslim term enrichment analysis. Statistical significance for categorical readouts in microscopy was analyzed by chi-square analysis. Means and standard deviations were calculated from at least three independent experiments. Unless specified otherwise, statistical significance was analyzed using Student's t-test.

IX. Buffers

Table 4. Buffers.

Buffer	Recipe
Agarose FA Gel (0.6 %)	0.6 % agarose 1 x FA gel buffer 221 mM Formaldehyde 1 x SybrSafe
Agarose gel (1 %)	0.5 g agarose 1 x TAE buffer up to 50 mL SYBR Safe 1:10000
Binding and Washing Buffer (B&W)	5 mM Tris HCl pH 7.5 0.5 mM EDTA 1 M NaCl
Blocking buffer	5 % skim milk in TBS or 5 % BSA in TBST (depending on the compatibility with primary antibody)
Destaining solution	30 % Methanol 10 % Acetic Acid

Buffer	Recipe
Electroporation buffer	135 mM KCl 0.2 mM $CaCl_2$ 2 mM $MgCl_2$ 5 mM EGTA 10 mM Hepes KOH pH7.5
Elution Buffer	20 mM Tris HCl pH 7.5 1 mM EDTA
FA Gel Buffer (10 x)	200 mM MOPS 50 mM Sodium Acetate 10 mM EDTA pH adjusted to 7 with NaOH 246 mM Formaldehyde freshly added
Hypotonic Lysis Buffer (HLB)	10 mM Hepes KOH pH 7.6 10 mM Potassium Acetate 1.5 mM Magnesium Acetate 2 mM DTT (freshly added)
Intracellular buffer	135 mM KCl 0.2 mM $CaCl_2$ 2 mM $MgCl_2$ 5 mM EGTA 10 mM Hepes, pH7.5
Loading Dye (5 x)	80 mM MOPS 20 mM Sodium Acetate 8 mM EDTA 0.16 % saturated Bromophenol Blue solution 886 mM Formaldehyde 20 % Glycerol 30.8 % Formamide

Buffer	Recipe
Low Salt Buffer	20 mM Tris HCl pH 7.5 200 mM LiCl 1 mM EDTA
Lysis Buffer (LB)	10 mM Tris HCl pH 7.4 100 mM KCl 5 mM $MgCl_2$ 0.5 % Sodium Deoxycholate 1 % Triton X-100
Mass Spectrometry Washing Buffer (MS Buffer)	50 mM Tris HCl pH 7.4 150 mM NaCl
PolyA Lysis Buffer	20 mM Tris HCl pH 7.5 500 mM LiCl 0.5 % LiDS 1 mM EDTA 5 mM DTT
Refolding Buffer	100 mM Tris HCl pH 7.6 100 mM NH_4Cl 10 mM $MgCl_2$ 0.1 mM EDTA 1 mM DTT
Resolving gel (10 mL)	10 % Acrylamide/Bis (37.5:1) 0.5 % Sucrose 0.125 M Tris HCl pH 6.8 0.1 % SDS 0.05 % APS 5 µL TEMED H_2O up to 10 mL
Running buffer (5 x)	125 mM Tris 959 mM Glycine 0.5% SDS

Buffer	Recipe
Sample buffer	62.5 mM Tris HCl pH 6.8 2 % SDS 25 % Glycerol 0.01 % Bromophenol blue 5 % β-Mercaptoethanol
SG Lysis Buffer	50 mM Tris HCl pH 7.4 100 mM potassium acetate 2 mM magnesium acetate 0.5 mM DTT 50 µg/mL Heparin 0.5 % NP40 1x SIGMAFAST Protease inhibitor RNasin (1:250)
Solution A	0.1 M NaOH 0.05 M NaCl
Solution B	0.1 M NaCl
Stacking gel (5 mL)	4 % Acrylamide/Bis (37.5:1) 0.375 M Tris HCl pH 8.8 0.1 % SDS 0.05 % APS 5 µL TEMED H_2O up to 5 mL
Staining solution	50 % Methanol 0.05 % Coomassie BB G-250 10 % Acetic Acid
TAE buffer (1 x)	40 mM Tris 20 mM Acetate 1 mM EDTA

Buffer	Recipe
TBE Buffer (5 x)	55.1 g Tris 27.5 g Boric Acid 3.95 g EDTA H_2O up to 1 L
TBE-Urea gel	7 M Urea 6-15 % Acrylamide/Bisacrylamide (29:1) in 1 x TBE Buffer
TBS	100 mM Tris HCl pH 7.5 0.9 % (w/v) NaCl
TBST	TBS + 0.1 % Tween 20
TE Buffer	10 mM Tris HCl pH 8 1 mM EDTA
TFBI	30 mM KOAc 100 mM RbCl 10 mM $CaCl_2$ 50 mM $MnCl_2$ 15 % Glycerol pH adjusted to 5.8 with Acetic Acid
TFBII	10 mM MOPS 75 mM $CaCl_2$ 10 mM RbCl 15 % Glycerol pH adjusted to 6.5 with KOH
Transfer buffer	25 mM Tris 192 mM Glycine 20 % Methanol

Buffer	Recipe
Wash Buffer I	20 mM Tris HCl pH 7.5 500 mM LiCl 0.1 % LiDS 1 mM EDTA 5 mM DTT
Wash Buffer II	20 mM Tris HCl pH 7.5 500 mM LiCl 1 mM EDTA
Washing Buffer	25 mM Tris HCl pH 7.5 10 mM $MgCl_2$ 2 mM DTT

CHAPTER 3: RESULTS

I. Free mRNA interactome in stress conditions

I. A. Free mRNA granulation *in vivo*

Recent publications have highlighted the role of RNA in LLPS and phase transition (Audas et al., 2016; Bounedjah et al., 2014; Fay et al., 2017; Jain and Vale, 2017; Langdon et al., 2018; Mahadevan et al., 2013; Maharana et al., 2018; Van Treeck et al., 2018; Zhang et al., 2015). The formation of membrane-less assemblies composed of both RNA and proteins depends strongly on RNA-RNA and RNA-proteins interactions. They appear as a critical parameter which determines the protein and RNA composition of these assemblies. However, the precise mechanism of their formation remains to be clarified. The first step was to choose an appropriate mRNA template for studying its interactome upon HS.

I. A. 1. Choice of the mRNA probe

As mentioned in the introduction, free mRNA concentration in the cytosol increases upon stress and polysomes disassembly. To study the role of free mRNA under these conditions, we decided to synthesize the coding sequence of HSP70 mRNA *in vitro* and to determine its interactome. In stress conditions, HSP70 mRNA is translated in order to protect the cells from toxic protein aggregation via HSP70 protein. In order to reduce sequence specific bias and make it an unbiased mRNA probe, we excluded the 3' and 5' UTRs which are known to be responsible for the HSP70 translation regulation upon stress (Di-Nocera and Dawid, 1983; Dudler and Travers, 1984; McGarry and Lindquist, 1985). Because these crucial regulatory sequences were deleted, the coding sequence of HSP70 mRNA by itself should not be translated, even in stress conditions. In order to test the behavior of RNA probe, we decided to fluorescently label it and to observe its distribution *in vivo* by microscopy.

I. A. 2. Preparation of fluorescently labeled mRNA

Most commercial RNA labeling kit incorporate fluorescently labeled nucleotides randomly during *in vitro* transcription. The problem of this method is that mRNA is labeled at several sites which would alter its secondary structure and potential interactions with proteins when transfected *in vivo*.

Another possibility would be to label *in vitro* transcribed mRNA with a fluorescent molecule at one end. This should limit the impact of labeling on the structure of the molecule. In collaboration with Dr. Martin Hengesbach and Gerd Hanspach, mRNA was labelled with the fluorescent molecule Cy5 at the 5' end. The procedure required the incorporation of GMP during *in vitro* transcription. Addition of a nucleotide to a transcript during transcription involves several chemical groups. Transcription occurs in the 5' to 3' direction, and polymerization reaction consists in the attack of the 3' hydroxide group of the already incorporated nucleotide on the 5' phosphate group of the next nucleotide to be incorporated. It was shown that GMP can be used as an initiator of mRNA transcripts, but cannot be incorporated in any other position within the RNA molecule because it lacks the triphosphate group (Martin and Coleman, 1989). If added in excess to an *in vitro* transcription reaction, GMP is incorporated in most mRNA molecules synthesized only at the position +1. In the next step by using GMP reactivity, it was possible to label in high yields the mRNA at the 5' end with a Cy5 molecule (Fig. 8).

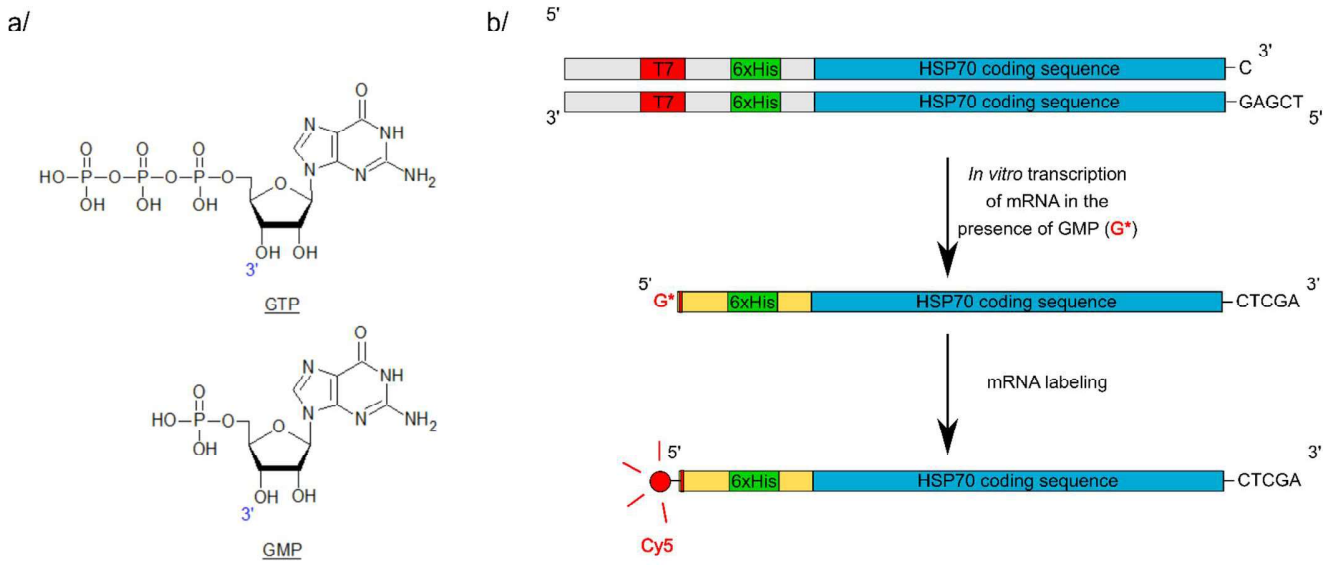

Figure 8. Cy5 labeling of mRNA.
a/ Comparison of GTP and GMP structures. b/ Scheme of Cy5 HSP70 mRNA labeling. A construct containing the T7 promoter followed by 6xHis-tag and the HSP70 coding sequence was used as a template for *in vitro* transcription in the presence of GMP. The generated product was labelled with a fluorescent Cy5 molecule at the 5' end using GMP reactivity.

I. A. 3. Transfection of labelled mRNA into mammalian cells

We first used lipofection to deliver the labeled mRNA into the cytosol of the human cell line HeLa. This method was unsuccessful since the lipidic vesicles remained intact and prevented the release of the mRNA molecules into the cells. Electroporation is another technique for nucleotide transfection that uses an electric field to increase cell membrane permeability. The resulting pores are reversible and allow the nucleotides to cross the plasma membrane of the cells. Although this technique is rather damaging for the cells, it has the advantage to directly deliver the genetic material in the cytosol without any intermediates (Neumann et al., 1982). For this experiment, HeLa cells were electroporated with Cy5-labeled HSP70 mRNA and cells were prepared for microscopy 6 h after electroporation. After paraformaldehyde fixation and DAPI staining, cells were analyzed by confocal microscopy. The fluorescently labeled mRNA formed heterogeneous granular structures (Fig. 9). At least 100 Cy5-positive cells were counted and analyzed visually for the presence of Cy5-labeled granules. Two controls were used to make sure the phenotype was coming from the labelled mRNA and not from the cleaved dye. First, cells were transfected with Cy5-labeled HSP70 mRNA as previously described and treated with benzonase nuclease in order to degrade RNA. The second control was to transfect cells with a short RNA, a 55-bases-oligonucleotide labeled with Cy5, at the same molar amount as HSP70 mRNA. Almost all of the cells transfected with Cy5-labeled HSP70 mRNA (more than 95 %) demonstrated a granular distribution of the signal (Fig. 9 a, b).

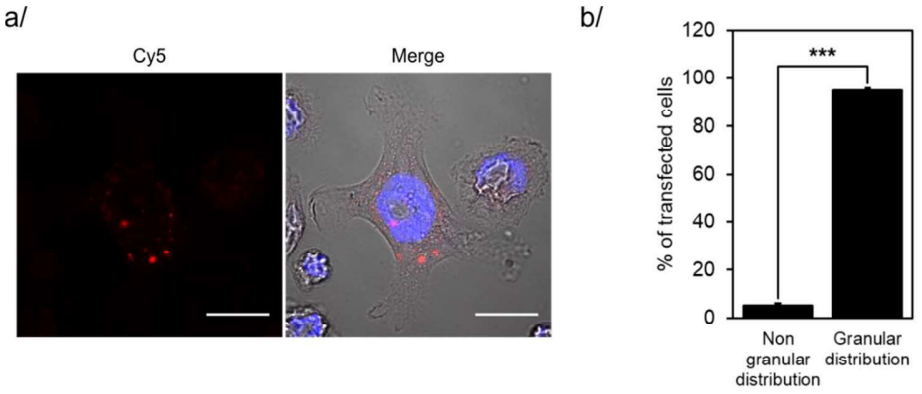

Figure 9. Transfection of cells with Cy5-mRNA by electroporation.
a/ Cy5-labeled HSP70 mRNA (red) distribution in HeLa WT cells 6 h after transfection by electroporation. DAPI staining (blue). Scale bars: 20 µm. b/ Quantification of transfected cells (N = 3, mean +SD). 2-tailed t-test (***: $p<0.001$).

After nuclease treatment, the percentage of Cy5-positive cells was significantly reduced, proving that the degradation of mRNA and release of dye led to the disappearance of the signal. The percentage of positive cells was not reduced to zero upon nuclease treatment most probably because the digestion was incomplete (Fig. 10 a, b). Similarly, cells transfected with a short oligonucleotide showed a strongly reduced percentage of positive cells. The Cy5-positive cells usually demonstrated a different phenotype compared to those transfected with HSP70 mRNA (Fig. 10 a, b). These results provided a strong indication that the granules contained RNA and that RNA was responsible for the granulation.

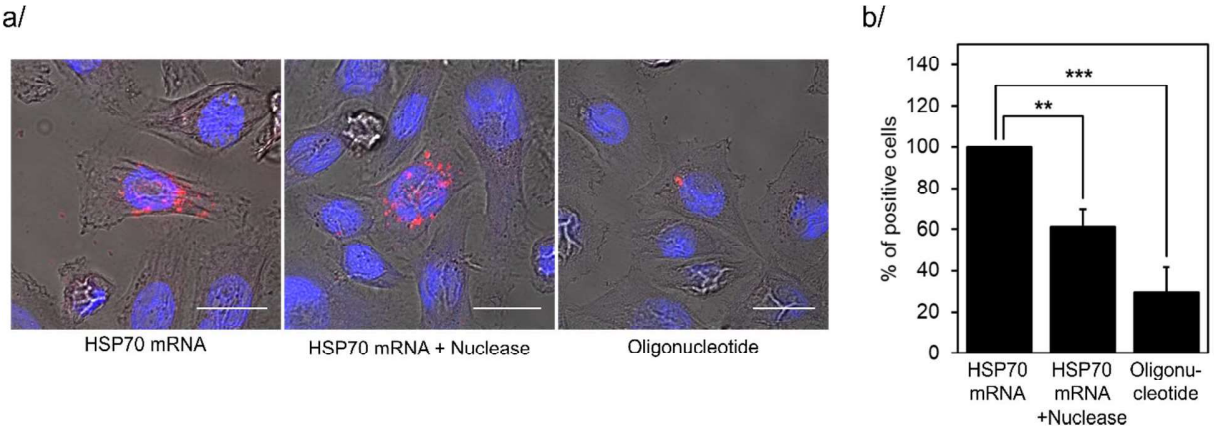

Figure 10. Transfection of cells with Cy5-labeled mRNAs with subsequent nuclease treatment.
a/ Distribution of Cy5-labeled HSP70 mRNA (red) and Cy5-labeled oligonucleotide (red) 6 h after transfection by electroporation. DAPI staining (blue). Scale bars: 20 µm. b/ Quantification of Cy5-positive cells (N = 3mean +SD). 2-tailed t-test (**: $p<0.01$; ***: $p<0.001$).

I. B. Optimization of stress conditions for granulation

In order to understand the potential role of free mRNA in stress conditions, we planned to perform pulldowns of mRNA bait and determine its interactome. The first step was to characterize the stress conditions we would be using.

I. B. 1. Stress response induction

The first indication of stress response induction that we monitored was HSP70 induction. HeLa cells were heat shocked at 45 °C for 0, 30, 60 or 120 min and collected for RNA isolation. These RNAs served as a template for synthesis of complementary DNA (cDNA), to be used for

quantitative PCR (qPCR). We determined the induction of the inducible and constitutive forms of HSP70 (*hspa1a* and *hspa8* genes*)*, and used *gapdh* as an endogenous reference gene. The method of 2^{-ddCt} was used for the estimation of gene expression (Arocho et al., 2006). The results showed that while *hspa8* mRNA levels did not significantly change during HS, *hspa1a* mRNA levels increased and reached a maximal level after 60 min at 45 °C, suggesting an activation of stress response (Fig. 11).

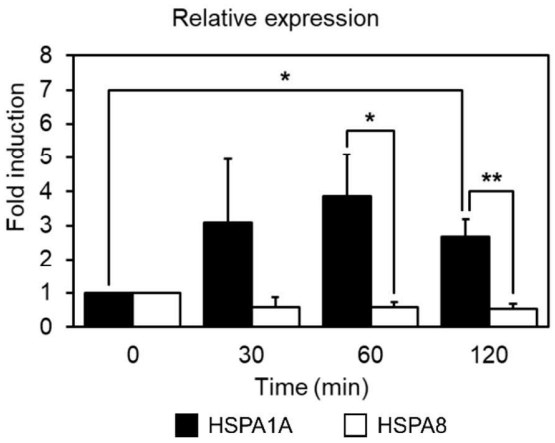

Figure 11. Induction of the constitutive and inducible forms of HSP70 upon heat shock.
Fold induction of *hspa1a* and *hspa8* genes calculated using the 2^{-ddCt} method (N = 3, mean + SD). Two-tailed t-test (*: $p<0.05$; **: $p<0.01$). *gapdh* was used as a reference gene.

The second stress response indicator was the phosphorylation of eIF2α. To assess if our conditions reflected the early stress response phase, before SGs are actually formed, we followed the phosphorylation status of eIF2α during HS. We heated HeLa cells at 45 °C for 0, 30, 60 or 120 min. The cells were then lysed in the presence of phosphatase inhibitors and the amounts of the phosphorylated form of eIF2α and of total eIF2α were assessed by western blotting (Fig. 12). As expected, eIF2α was phosphorylated during HS, which peaked after 30 min.

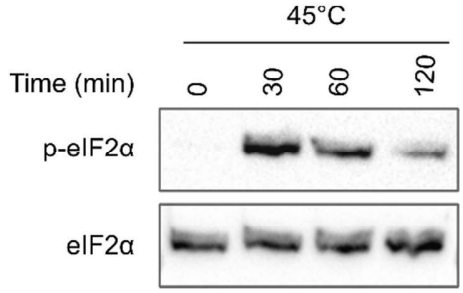

Figure 12. Phosphorylation of eIF2α upon heat shock.
eIF2α levels in cell lysates of cells heated at 45 °C for the indicated time. Phosphorylated (Serine 51) and non-phosphorylated forms of the proteins were detected by western blot using the indicated antibodies. One representative out of three experiments is shown.

Another parameter we needed to check was the formation SGs. Cells were kept at 45 °C for 0 or 60 min. As a positive control, the cells were treated with arsenite for 30 min at 37 °C. After treatment, cells were fixed and stained for microscopy using an antibody against the SG marker eIF4E (Kedersha and Anderson, 2002). The cells were imaged by microscopy using a confocal inversed microscope. Images were analyzed and stress granules counted. The results of three independent experiments were averaged (Fig. 13 a, b). While non-stressed cells did not form SGs, arsenite-treated cells contained in average 13 granules per cell. After 1 h at 45 °C, the distribution of the SG marker protein eIF4E became more granular, yet the number of formed granules was very low compared to the arsenite-treated cells. This indicated that after 1 h HS at 45 °C, the cells were at an early stage of stress response when SGs were being assembled but were not fully formed yet.

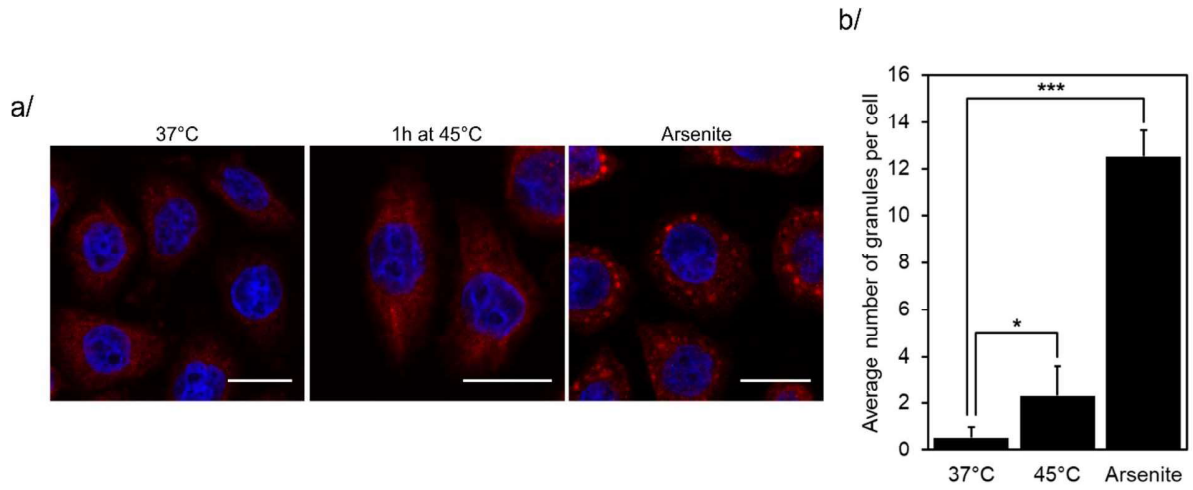

Figure 13. Formation of stress granules upon heat shock.
a/ Immunostaining of eIF4E (red) to detect SGs in cells heated at 45 °C for 1h or treated with 1 mM Arsenite for 30 min at 37 °C. DAPI staining (blue). Scale bars: 20 µm. One representative out of three independent experiments is shown. b/ Quantification of the SGs (N = 3, mean +SD). One-tailed t-test (*: $p<0.05$; ***: $p<0.001$).

I. B. 2. Polysome profiling

Polysome profiling is a technique used to study the translation status of cells by detecting mRNAs association with ribosomes. It is based on a sucrose gradient separation of mRNA-ribosomes complexes by ultracentrifugation. Measurement of OD_{254} along the gradient allows the detection of the complexes. The lightest fraction contains free mRNAs not bound to ribosomes. Then comes

the small ribosomal subunit, followed by the large subunit (40S and 60S in eukaryotes). The fourth fraction contains the intact ribosome (80S) associated with mRNAs and is called monosomal fraction. The following fractions contain mRNAs associated with increasing number of ribosomes and are called polysome fractions. When translation is fully active, polysomes can be detected. If translation is impaired, polysomes are reduced or disappear. HeLa cells were kept at 37 °C or heated at 45 °C for 60 min. Arsenite-treated cells were used as a positive control for translation stop. Lysates were prepared in the presence of cyclohexamide in order to stop translation and prevent ribosome dissociation from mRNAs. Lysates were applied on a sucrose gradient and ultracentifuged in order to separate the different ribosomal fractions. OD_{254} was recorded along the gradient (Fig. 14). Under normal conditions, the 40S, 60S and 80S peaks corresponding to the subunits of the ribosome and to the whole ribosome were visible (Fig. 14 a). Polysomes were detected as well, suggesting an active translation. After arsenite treatment, translation was completely abolished and polysomes could not be detected, while the 80S fraction was prominent (Fig. 14 b). After HS, the 80S fraction became much larger than in normal conditions and the polysomes were strongly reduced, but still detectable (Fig. 14 c). This suggests that translation was reduced, but not completely abolished, thus indicating an early stage of stress response.

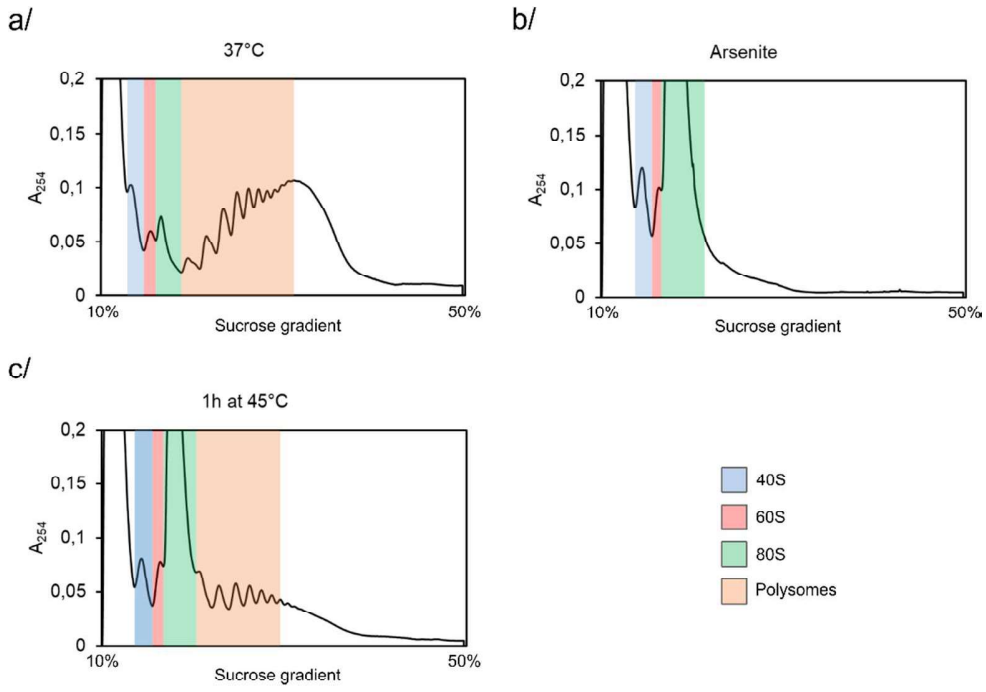

Figure 14. Polysomes profiles during HS.
Polysome profiling of HeLa cells heated at 45 °C for 1 h or treated with 1 mM Arsenite for 30 min. One representative out of three independent experiments is shown.

We analyzed the content of the 80S fraction, where ribosomes can be bound to mRNA, at the frequency of one ribosome per mRNA. The 80S fractions were collected and were normalized to their total RNA content (OD_{254}). The fractions were analyzed by SDS-PAGE and western blotting against S6, a component of the small ribosomal subunit (Fig. 15). The idea behind this experiment was to determine how much of the absorbance at 254 nm was coming from ribosomal RNAs versus from mRNAs associated with ribosomes. The amount of the ribosomal protein S6 detected in the 80S fraction from cells heated at 45 °C was about 2.5 times higher than that from cells kept at 37 °C. The RNA species present in the samples are ribosomal RNAs and mRNAs. Since the total RNA content was equal in both samples, the higher S6 amounts must mean higher fraction of ribosomal RNA and lower fraction of mRNA. We detected less S6, ie less ribosomal RNAs in the 37 °C condition, suggesting that more absorbance signal was coming from mRNAs. This indicates that in normal conditions, more ribosomes were bound to mRNA than after HS. If the mRNA had been released from ribosomes, it should be free in the cytosol. We concluded that the used stress conditions correlated with an increase in free mRNA concentration in the cytosol.

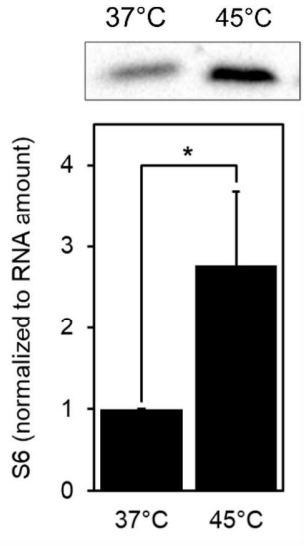

Figure 15. Analysis of the ribosomal 80S fractions.
Ribosome amount in the 80S fraction measured by anti-S6 western blot. 80S fractions were normalized according to the total RNA amount. One out of three independent experiments is shown. Quantification by measurement of bands intensity (mean +SD). Two-tailed t-test (*: $p<0.05$).

I. B. 3. Pulldown of free mRNA

The preparation of the mRNA template was done in several steps. First, the template, a circular plasmid, was linearized using the restriction enzyme XhoI generating a 5' protruding end. This linearized plasmid was used for T7-driven *in vitro* transcription of mRNA. After purification, the

transcript was biotinylated at the 3' end and purified again. In order to study the interactome of free mRNA in stress conditions, we used lysates from HeLa cells heated at 45 °C for 60 min. After a hypotonic lysis and centrifugation to remove debris, the lysate was kept at 4 °C for 3 h in the presence of streptavidin beads conjugated with the biotinylated mRNA. Beads were collected, and bound proteins were identified and quantified by LC-MS/MS.

I. C. Identification of free mRNA interactome

I. C. 1. MS analysis

MS analysis of pulldowns were performed by Dr. Giulia Calloni. 79 proteins were identified (Appendix 1) and found to be significantly enriched on free mRNA (Fig. 16).

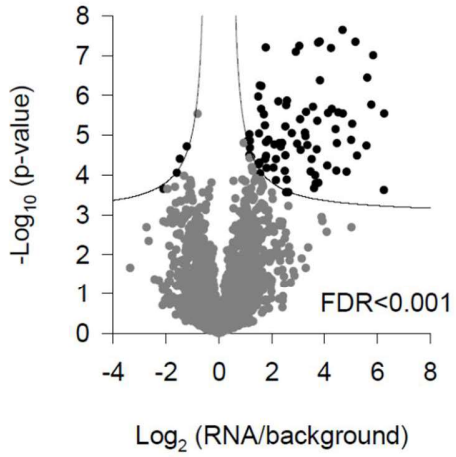

Figure 16. Free mRNA interactome.
Vulcano plot showing the enrichment of interactors pulled down above a significance threshold which is indicated by a black line (False discovery rate (FDR) < 0.001). N = 5 independent experiments.

Among these interactors, only 6 were known to be SGs proteins, indicating an early stage of granulation (Fig. 17).

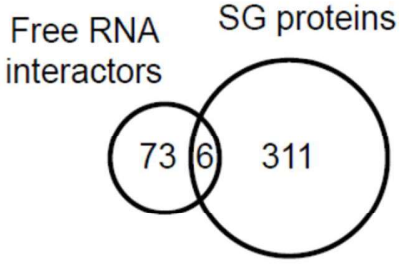

Figure 17. Overlap between identified free mRNA interactors and known stress granules proteins.
Overlap of 6 proteins between the free RNA interactors set and SG proteins.

Among the categories of proteins enriched on free mRNA were nucleic acid binding proteins and RNA-binding proteins as one could have expected (Tab. 5).

Category value	Enrichment	P value
Nucleic acid binding	2.8	7.95×10^{-11}
RNA binding	3.5	1.55×10^{-9}
Nucleolus	3.4	1.24×10^{-7}
Non-membrane-bound organelle	2.1	5.73×10^{-7}
Nuclear part	1.8	1.09×10^{-6}

Table 5. Protein categories enriched in the set of free mRNA interactors.
Functional categories of proteins enriched in the pulldowns with the corresponding enrichment and p values. N=5 independent experiments.

I. C. 2. Control mRNA (B-Raf)

In order to make sure that the identified interactors were not sequence-specific, this experiment was repeated with another mRNA of similar size, B-Raf transcript, depleted of its 3' and 5'UTR. Three repetitions were performed and 58 significant interactors were identified (Appendix 2, Fig. 18).

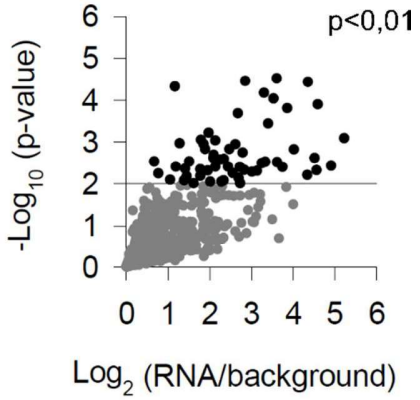

Figure 18. Control mRNA interactome.
Vulcano plot showing the enrichment of interactors pulled down above a significance threshold. N=3 independent experiments. The p value cutoff is indicated.

About half of them overlapped with HSP70 mRNA interactome (Fig. 19). This result reassured us that the sequence specific bias was weak.

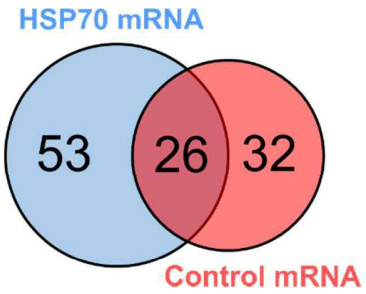

Figure 19. Overlap between the HSP70 mRNA and control mRNA interactomes.
Significant overlap of 26 proteins between the interactor sets of two mRNAs is indicated ($p<4.7x10^{-63}$ based on hypergeometric distribution). N = 3 independent experiments.

I. C. 3. Biochemical verification of MS results

Among the interactors detected, we focused on eIF2 which is a key regulator of translation initiation during stress, and on the methyltransferase TRMT6/61A which is responsible for m^1A deposition on tRNAs and mRNAs

I. C. 3. a. eIF2α interaction with exogenous free mRNA

We verified this interaction under normal and stress conditions and focused on the eIF2α subunit of the complex. After cell lysis, the lysate was incubated in the presence of the biotinylated free mRNA probe. Bound proteins were eluted by benzonase nuclease treatment of the biotinylated mRNA. The protein samples were analyzed by SDS-PAGE and western blotting (Fig. 20). In accordance with mass spectrometry results, eIF2α interacted with naked mRNA after HS (1.4 % of total eIF2α was pulled down). Interestingly, this interaction did not take place with the phosphorylated form of the protein, even though it was prominent in the cytosol. On the other hand, the interaction of free mRNA with eIF2α was weak in non-stressed cells.

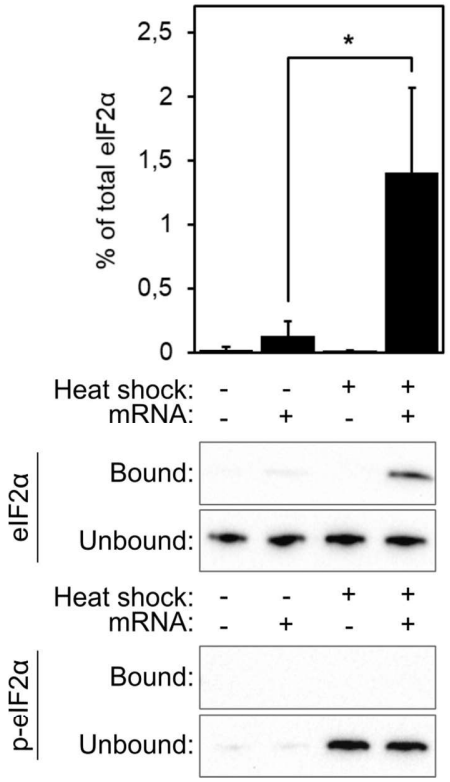

Figure 20. Biochemical verification of free mRNA interaction with eIF2α.
Enrichment of eIF2α in its phosphorylated (Serine 51) or non-phosphorylated forms as determined by western blotting. One representative out of three independent experiments is shown. Quantification by measurement of bands intensity (mean + SD). Two-tailed t-test (*: $p<0,05$).

I. C. 3. b.TRMT6/61A interaction with exogenous free mRNA and endogenous polyA mRNA

The interaction of TRMT6/61A with free mRNA led us to the hypothesis that free mRNA could be methylated upon stress and that this could play a role in SGs assembly. We decided to check if this interaction took place both in normal and in stress conditions. The cells were lysed and the lysate was incubated in the presence of our biotinylated free mRNA probe. Elution of the bound proteins was done by benzonase nuclease treatment of the biotinylated mRNA. The protein samples were analyzed by SDS-PAGE and western blotting (Fig. 21 a). The interaction of naked HSP70 mRNA with TRMT6 was verified under HS, with 5.4 % of total TRMT6 being pulled down in this condition. Like for eIF2α, the interaction was weak in non-stressed cells (1.3 % of total TRMT6 was pulled down). In order to verify that this interaction also took place with endogenous mRNA, we used oligo $d(T)_{25}$ beads to pulldown polyA mRNA and eventually detect associated TRMT6/61A. For comparison, band intensity was normalized to the amount of polyA mRNA bound to the beads (measured using the RNA-specific dye RiboGreen). The amount of TRMT6 bound to polyA mRNA was analyzed by SDS-PAGE and western blotting. We observed that

TRMT6 associated with polyA mRNA under normal conditions (Fig. 21 b). After HS, the amount of TRMT6 associated with polyA mRNA was strongly increased.

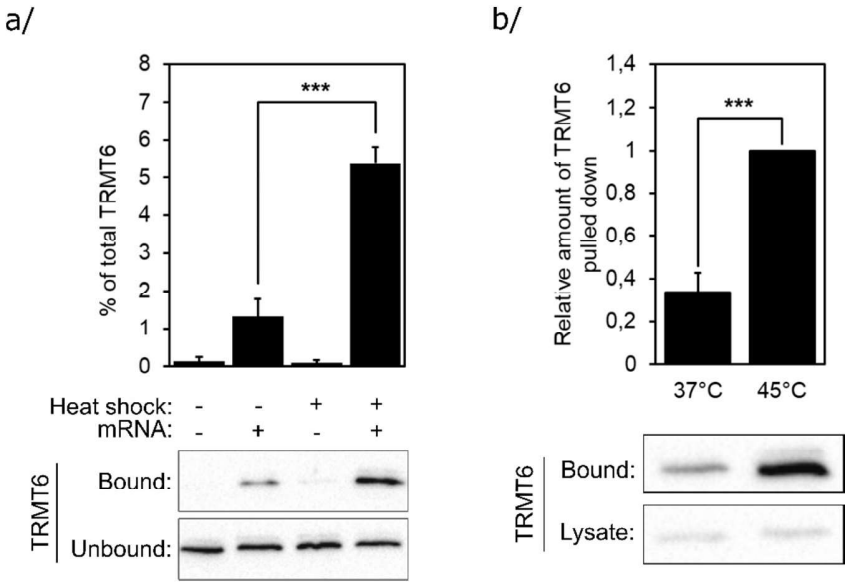

Figure 21. Biochemical verification of free mRNA interaction with TRMT6.
Enrichment of TRMT6 on biotinylated free mRNA (a/) or on polyA mRNA (b/) as determined by western blotting. One representative out of three independent experiments is shown. Quantification by measurement of bands intensity (mean + SD). Two-tailed t-test (***: $p<0.001$).

I. C. 3. c. Co-immunoprecipitation of eIF2α and TRMT6/61A

Co-immunoprecipitation assays were performed to investigate whether eIF2α and TRMT6/61A interacted with each other. Flag-tagged TRMT6 and 3x-Flag-tagged TRMT61A expression constructs were transfected into HeLa cells. The cells were lysed and the tagged proteins were pulled down using anti-Flag affinity beads. After elution using 3xFlag peptides, the bound proteins were analyzed by SDS-PAGE and western blotting (Fig. 22). Under normal conditions, very few eIF2α was pulled down (about 1.5 % of total eIF2α). On the other hand, in the lysate of heat shocked cells heated, the interaction was enhanced (7.3 % of total eIF2α pulled down).

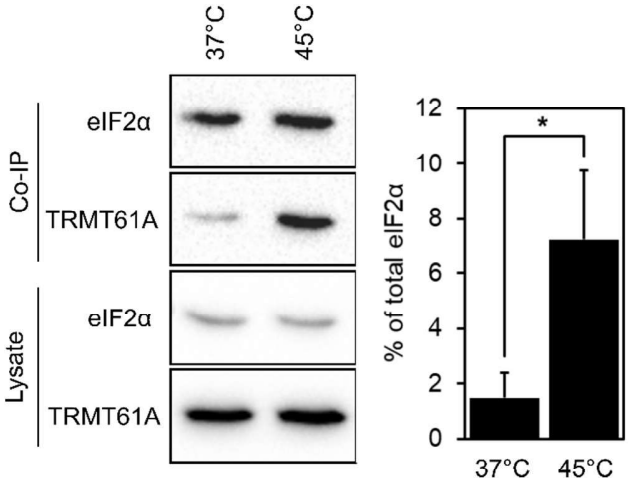

Figure 22. Co-immunoprecipitation of eIF2α and TRMT6/61A.
Association of eIF2α with TRMT6/61A-containing protein complex as assessed by pulldown of Flag-tagged TRMT6/61A and western blotting. One representative out of three independent experiments is shown. Quantification by measurement of bands intensity (mean + SD). Two-tailed t-test (*: $p<0,05$).

To check if RNA was mediating the interaction between eIF2α and TRMT6/61A, we performed co-immunoprecipitations like previously described but pre-treated the lysate with benzonase nuclease (Fig. 23). After benzonase treatment, both at 37 °C and 45 °C, the interaction between eIF2α and TRMT6/61A was abolished. This interaction was thus nucleotide-dependent. However, it remains unclear whether the interaction is mediated by mRNA or tRNA.

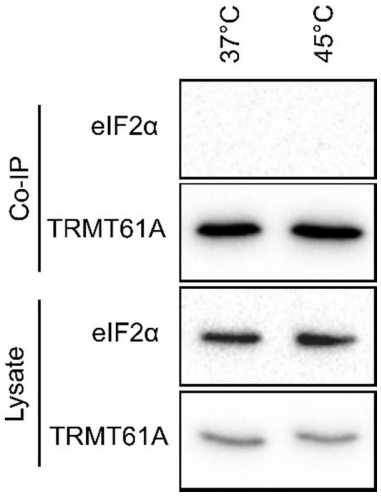

Figure 23. Co-immunoprecipitation of eIF2α and TRMT6/61A after nuclease treatment.
Association of eIF2α with TRMT6/61A-containing protein complex is abolished after nuclease (benzonase) treatment of cell lysate as assessed by pulldown of Flag-tagged TRMT6/61A and western blotting. One representative out of three independent experiments is shown.

I. C. 4. *In vitro* study of TRMT6/61A interaction with HSP70 mRNA

I. C. 4. a. Hypotheses to explain the stronger interaction of TRMT6/61A with RNA after HS

- Competition of tRNA and mRNA for association with TRMT6/61A

One of the TRMT6/61A's substrates is tRNA-iMet. It is also known that under stress, tRNA-iMet is degraded in HeLa cells (Watanabe et al., 2013). A possibility would then be that under normal conditions TRMT6/61A binds preferentially tRNA-iMet over mRNA. Under stress conditions, when tRNA-iMet is degraded, TRMT6/61A would then be free of substrate and able to bind free mRNAs whose concentration in the cytosol increased.

- TRMT6/61A unfolding upon heat changes its affinity to mRNA

Another hypothesis would be that TRMT6/61A unfolds at 45 °C and that this changes binding affinity towards their substrates. Affinity for tRNA-iMet could be reduced while affinity for free mRNA could be increased.

To address these possibilities, *in vitro* analyses using recombinant TRMT6/61A were performed. Furthermore, the *in vitro* reconstitution allowed to test whether the interaction was direct, and whether additional components were needed for temperature effect. For the *in vitro* study of the interaction, we used only biotinylated HSP70 mRNA.

I. C. 4. b. Preparation of recombinant protein

Purification of recombinant human his-tagged TRMT6/61A dimer was performed by Viktor Pfeifer and Adrían Martínez Limón. For this purpose the expression plasmid pET17b-6xHisTrm6-Trm61 was kindly provided by Janet Finer-Moore, UCSF. This expression construct contained both subunits whose expression was induced in *E. Coli* (BL21 strain) cells using IPTG. A 1 mL HisTrap HP affinity chromatography column was used for purification, followed by cleavage of the His tag by HisGST-PreScission protease and size-exclusion chromatography. The heterodimer was isolated and purity was assessed by Coomassie staining of an SDS-PAGE gel (Fig. 24).

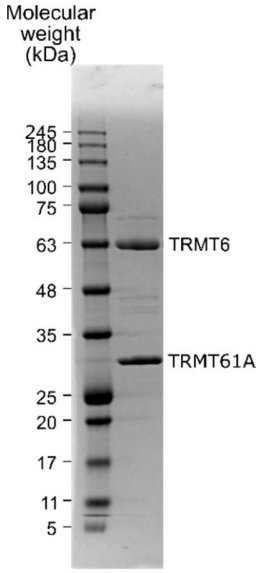

Figure 24. Recombinant TRMT6/61A complex.
Coomassie Blue staining of SDS-PAGE gel to analyze the purity of recombinant methyltransferase TRMT6/61A complex.

I. C. 4. c. TRMT6/61A stability during HS

- Melting

For studying thermal denaturation of TRMT6/61A, the fluorescent dye SYPRO Orange was used. This chemical, which binds hydrophobic regions of proteins, emits low intensity fluorescence in aqueous buffers. When the temperature of a protein in solution increases, it unfolds and exposes hydrophobic regions, which become free to bind SYPRO Orange. This results in an increase in fluorescence and can be used to measure melting transitions of proteins. The method was applied to correlate the increased association of TRMT6/61A and RNA upon HS with structural alteration of the protein. First derivative of the fluorescence change was calculated to visualize transition points. Protein melting analysis of TRMT6/61A without substrate revealed two melting temperatures at 43.5 °C (Tm') and 50.7 °C (Tm), where the major unfolding took place (Fig. 25). Tm' could reflect either a partial local unfolding or a complex dissociation of TRMT6/61A which exists as a tetramer formed by two heterodimers. Addition of unmethylated tRNA-iMet, a TRMT6/61A substrate, slightly increased Tm, but decreased Tm' (Fig. 25). tRNA binds across a heterodimer surface and involves TRMT6 and TRMT61A from the opposing heterodimer. This

suggests that tRNA binding site remained intact at least until 51 °C and that tetramer dissociation around 43 °C is unlikely.

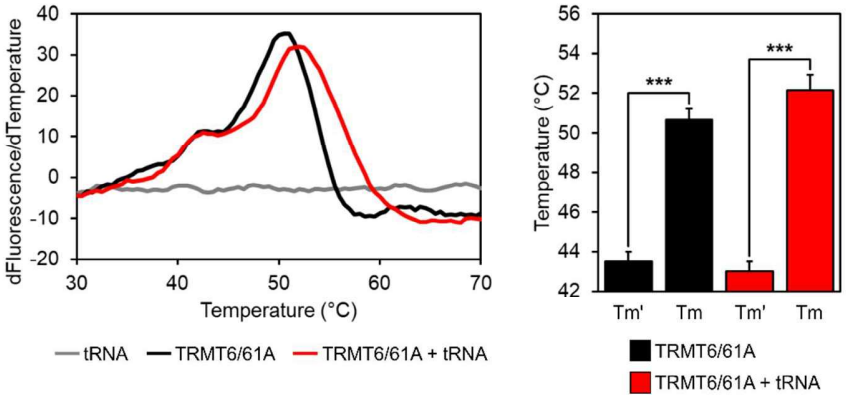

Figure 25. Melting analysis of TRMT6/61A.
Melting analysis of 10 µM recombinant TRMT6/61A in the presence or absence of 10 µM unmethylated tRNA. First derivatives of fluorescence intensity with respect to the temperature are displayed in the left panel. One representative out of three independent experiments is shown. Melting curves indicate two melting points, Tm' and Tm. In the right panel, Tm' and Tm in the presence or absence of tRNA were plotted (N = 3, mean + SD). Two-tailed t-test (***: $p<0.001$).

- Circular dichroism (CD) spectroscopy

This is a standard method used to study protein secondary structure. It involves differential absorption of circularly polarized light by a protein depending on the secondary structure of the sample. The degree of ellipticity (Θ) is the parameter measured by a CD spectrometer and some secondary structures like α-helices and β-sheets display specific values of Θ. CD spectroscopy allows to determine changes of secondary structure under particular conditions. CD spectra revealed no major difference in TRMT6/61A secondary structure between 37 °C and 45 °C (Fig. 26). If at all, HS induces only a subtle local unfolding of TRMT6/61A.

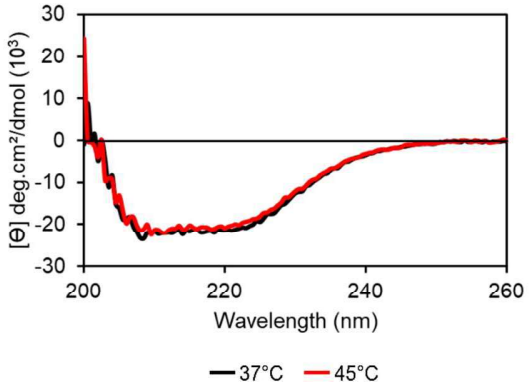

Figure 26. CD spectroscopy analysis of TRMT6/61A. CD spectra of recombinant TRMT6/61A at 5 µM at 37 °C or 45 °C. One representative out of three independent experiments is shown.

- Sensitivity to proteinase K

In order to address minor structural transitions of TRMT6/61A at 45 °C, we studied the protein sensitivity to proteinase K digestion. This protease is non-specific and has a very broad range of substrates. It can be used to study protein unfolding since the amino acids chains become more accessible to the protease when a protein unfolds, which results in a faster hydrolysis rate. After a preliminary experiment to estimate the amount of proteinase K, we incubated 1.5 µM protein at 37 °C or 45 °C and then performed digestion with 0.1 ng/µL proteinase K for 3, 6 or 9 min at the same temperature. Digestion was immediately stopped by PMSF addition. The amounts of remaining protein were assessed by SDS-PAGE and Coomassie staining (Fig. 27). Several conclusions could be made. While the large subunit, TRMT6 was significantly more degraded at 45 °C than 37 °C, the small subunit was insensitive to proteinase K degradation. This differential degradation of the two subunits suggested a partial unfolding of TRMT6 which became then more accessible to the protease, while TRMT61A remained intact. This could also be due to a higher activity of the protease at 45 °C, however TRMT61A was unaffected by proteinase K at 45 °C. Then we concluded that TRMT6 subunits unfolds locally at 45 °C.

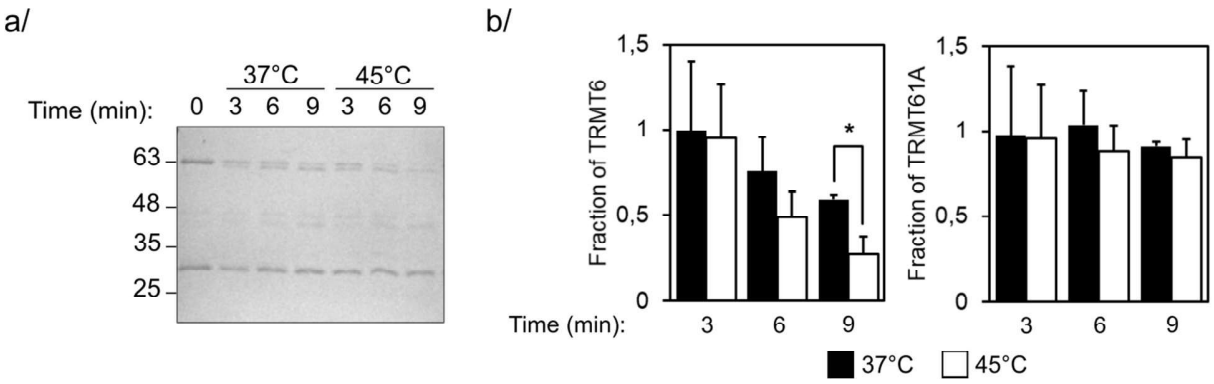

Figure 27. Sensitivity of TRMT6/61A to Proteinase K digestion.
a/ Time course of Proteinase K digestion of recombinant TRMT6/61A complex at 37 °C or 45 °C for the indicated time. Coomassie stained SDS-PAGE gel is shown. One representative out of three independent experiments is shown. b/ Quantification of the remaining TRMT6 (left panel) and TRMT61A (right panel) after digestion (N = 3, mean + SD). Two-tailed t-test (*: $p<0.05$).

In the next step, we decided to verify the direct interaction of mRNA with TRMT6/61A *in vitro* and to check if there is a difference in affinity depending on the temperature.

I. C. 4. d. Optimization of pulldown conditions *in vitro*

In order to check if the interaction between TRMT6/61A and HSP70 mRNA is direct, *in vitro* pulldowns were performed. The effect of tRNA on this interaction was also studied. For this purpose, human tRNA-iMet was prepared *in vitro*.

- tRNA as a substrate

The recombinant protein was of human origin. Therefore we decided to use human tRNA-iMet as a substrate. tRNA was prepared by *in vitro* transcription. The advantage of using *in vitro* transcribed tRNA is that it is unmodified, so it may be a more faithful substrate for TRMT6/61A. Commercial modified tRNA from yeast was used for comparison.

- Estimation of endogenous amounts of TRMT6/61A

In order to be close to *in vivo* conditions, the concentration of endogenous TRMT6/61A in cells was estimated. We used HeLa cell lysate at the concentration used for *ex vivo* pulldowns (5 µg/µL protein concentration), which should represent a circa ten times dilution of cellular concentration as estimated by the cell pellet volume. We used recombinant protein at known concentrations to

estimate the amount of TRMT6/61A in the lysate. According to our estimations, the concentration of TRMT6 in our lysates is about 1 nM (Fig. 28).

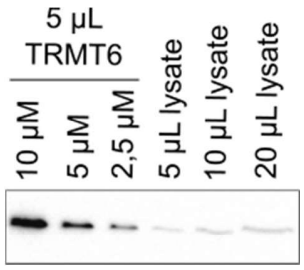

Figure 28. Estimation of endogenous TRMT6 amount in HeLa cells. Amount of TRMT6 detected in HeLa lysate using anti-TRMT6 antibody as determined by western blotting. Known amounts of recombinant TRMT6 were used for comparison. One representative out of three independent experiments is shown.

- Estimation of endogenous amounts of tRNA

In mammalian cells such as HeLa cells, about 15 % of total RNA corresponds to tRNA (Lodish et al., 2000; Westermann et al., 2012). Every HeLa cell contains about 30 pg of total RNA (ThermoFisher Scientific, Macromolecular components of *E. Coli* and HeLa cells) resulting in 4.5 pg tRNA per cell. In the pulldown experiments, approximately 60 million cells were used to prepare 400 µL of lysate. We should then end up with 270 µg tRNA in 400 µL of lysate, or 675 µg tRNA per milliliter of lysate. The average molecular weight of human tRNAs being 25 kDa, the approximate concentration of tRNA in the lysate equals 27 µM. Moreover, there are 49 tRNA isoacceptor families in human (Geslain and Pan, 2010), which suggests that the concentration of every type of tRNA is on average 0.55 µM (not taking into account the relative abundance of each tRNA).

I. C. 4. e. TRMT6/61A-RNA interaction *in vitro*

In order to reconstitute TRMT6/61A interaction *in vitro*, we pre-incubated the protein at 37 °C or 45 °C to simulate HS conditions. The pre-heated protein was then incubated with HSP70 mRNA bound to streptavidin beads. tRNA was added to the protein solution at the same time as the mRNA. The tRNA concentration used was 1 µM. We used both unmodified human tRNA-iMet (*in vitro* transcribed) and modified yeast tRNA (pool of different tRNAs). At 37 °C, the interaction took place, regardless of the presence of tRNA, which excluded the hypothesis of substrate competition (Fig. 29). It showed that a direct interaction between TRMT6/61A and free mRNA takes place without involvement of other proteins. Unexpectedly at 45 °C, the interaction was completely lost,

in contradiction with the *ex vivo* results. It suggests that the local unfolding of TRMT6 is not sufficient to explain the increase of complex affinity for mRNA. We can hypothesize that, even though the direct interaction between HSP70 mRNA and TRMT6/61A can take place, some additional components are missing to explain its increase during HS.

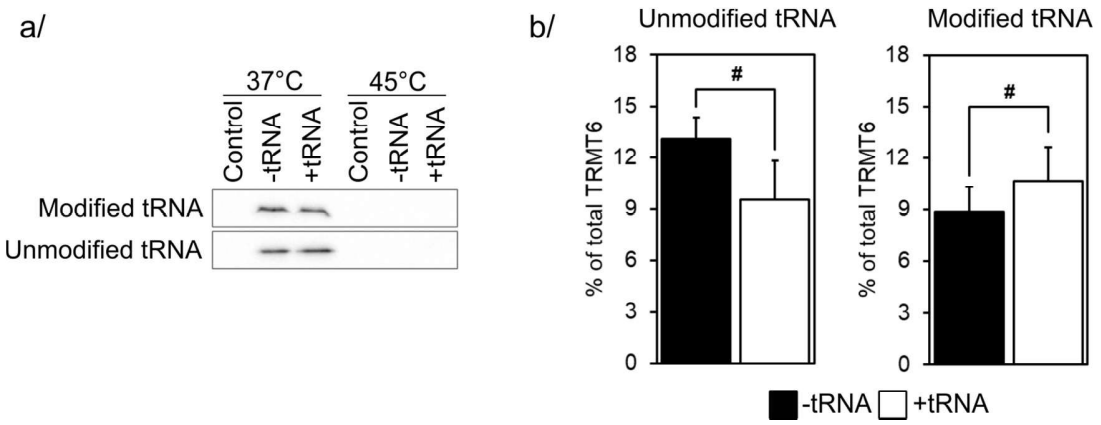

Figure 29. *In vitro* reconstitution of free mRNA interaction with TRMT6/61A.
a/ Direct interaction of recombinant TRMT6/61A with free mRNA *in vitro*. The amounts of TRMT6/61A pulled down by biotinylated HSP70 mRNA were estimated by western blotting using anti-TRMT6 antibody. One representative out of three independent experiments is shown. b/ Quantification (37 °C) by measurement of bands intensity (means + SD). Two-tailed t-test (**#**: non-significant).

II. mRNA sequestration into stress granules

II. A. m^1A motif frequency in mRNAs

Next, the role of the RNA motif recognized by TRMT6/61A was analyzed. The enrichment of the motif in mRNAs from SGs was studied by Riccardo Delli Ponti. For this analysis, the recently published list of mRNAs enriched or depleted from SG was used (Khong et al., 2017). Recently, the motif recognized by TRMT6/61A for the m^1A methylation of adenosine has been identified (Li et al., 2017; Safra et al., 2017). We analyzed the presence of this motif containing a seven-bases-loop stabilized by a stem of at least two bases. The tRNA, mRNA motifs as well as the one used for our analysis are given in the Figure 30 a. The bioinformatics analysis revealed that significantly more mRNAs enriched in SGs contain the motif for methylation than mRNAs depleted from SGs

(about 2.5 times more) (Fig. 30 b). On the other hand, mRNAs that are neither enriched nor depleted from SGs have an intermediate percentage of mRNAs containing this motif. The result suggests that m^1A methylation could be a marker for mRNAs to be selectively targeted to SGs. Methylation of mRNAs by TRMT6/61A could be a way to protect them from degradation during stress by sequestering them into SGs.

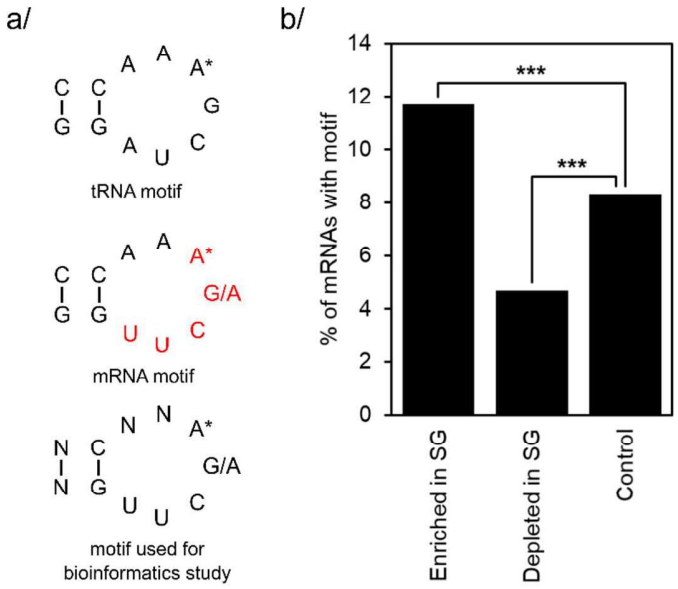

Figure 30. Analysis of m^1A motif presence in mRNAs from stress granules.
a/ tRNA motif recognized by TRMT6/61A for methylation of the adenosine (marked with an asterisk). mRNA motif (red) targeted by TRMT6/61A for methylation of the adenosine. Motif used in this study for identification of mRNA targets of TRMT6/61A. b/ Fractions of mRNA containing the motif enriched or depleted in SGs. The control mRNAs are neither enriched nor depleted in SGs. Chi-square test (***: $p<0.001$).

II. B. TRMT6/61A colocalizes with stress granules

Because the m^1A motif is enriched in mRNAs from SGs, we wondered if the methyltransferase TRMT6/61A could be detected in SGs. To test this possibility, we transfected HeLa cells with Flag-tagged TRMT6 and TRMT61A. The cells were treated with arsenite to induce SGs formation and the subcellular localization of TRMT6/61A was assessed by microscopy, using the SG marker TIAR (Fig. 31). Under normal conditions, both TIAR and TRMT6/61A displayed a homogenous distribution in the cell. Upon arsenite treatment, some cells displayed a clear colocalization of TRMT6/61A and TIAR in SGs. Fluorescence profiles along an indicated line confirmed

TRMT6/61A colocalization with SGs (Fig. 31 b). Interestingly TRMT6/61A has not been identified as a component of SGs yet. It might be that the SG-TRMT6/61A association is labile and thus is disrupted by biochemical isolation used to isolate SGs for high throughput composition analyses.

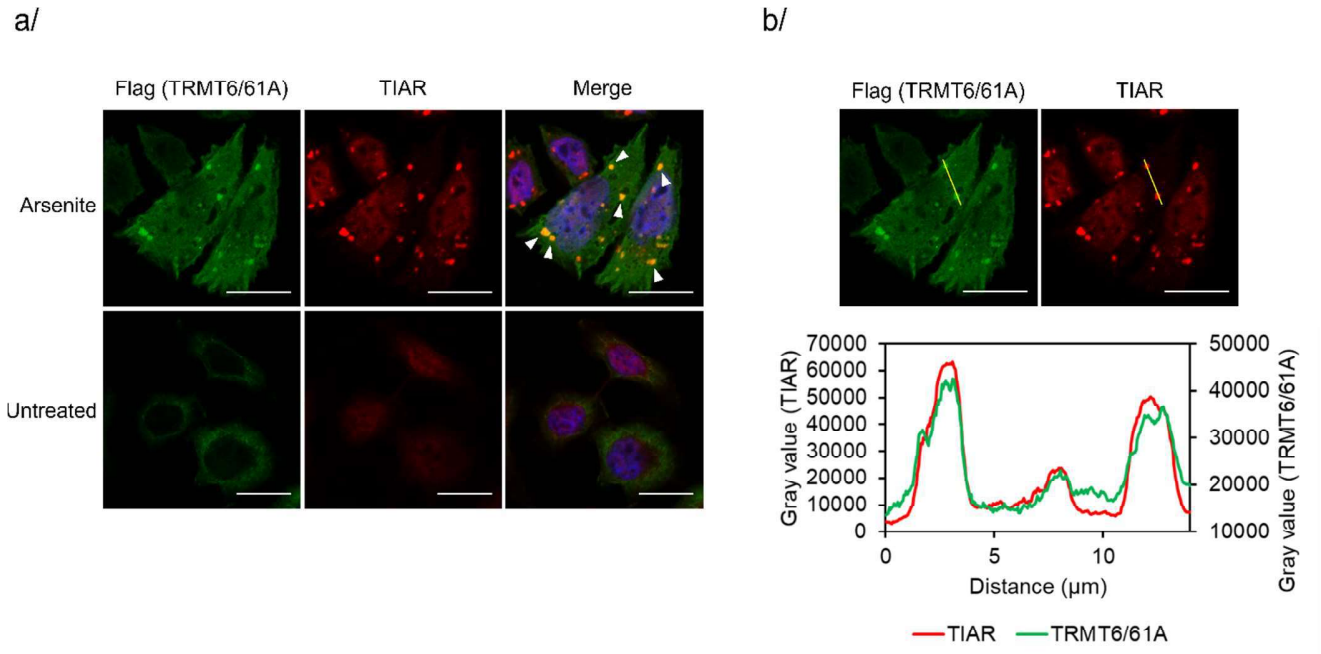

Figure 31. Colocalization of TRMT6/61A and the stress granule marker protein TIAR.
a/ Immunostaining of the SG marker TIAR (red) and of Flag-tagged TRMT6/61A (green) in cells untreated or treated with 0.25 mM arsenite for 30 min. DAPI staining (blue). Colocalization of TRMT6/61A with SGs is indicated with white arrows. Scale bars: 20 µm. One representative out of three independent experiments.
b/ Fluorescence profile for Flag and TIAR signals measured along the line indicated in yellow on the images. N = 3 independent experiments.

II. C. m^1A is enriched on mRNAs from stress granules

To verify biochemically that SGs are enriched in m^1A-containing mRNAs, cells were treated with arsenite and SG cores were isolated. Samples were collected along the purification, as decribed in Figure 32 a, and analyzed by western blotting using antibody against the SGs marker TIAR and anti-GAPDH as a control (Fig. 32 b).

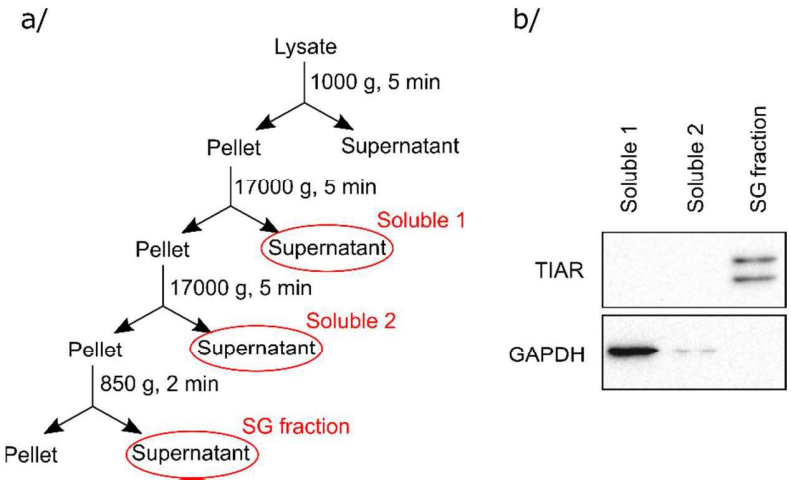

Figure 32. Stress granules isolation.
a/ Scheme of the experimental precedure, adapted from (Khong et al., 2018). The samples collected for western blot analysis are marked in red. b/ The amounts of TIAR and GAPDH in the collected samples were estimated by western blotting. One representative out of three independent experiments is shown.

This analysis confirmed that SGs were effectively enriched in our samples. After purification of RNA from the fraction enriched in SG cores, m^1A and m^6A contents were analyzed by mass spectrometry and compared to cytosolic polyA mRNA (extracted from HeLa cells heated at 45 °C for 60 min). We could observe that, while m^6A content was very similar in SGs-associated RNAs and in total cytosolic mRNAs, m^1A was almost 8 times enriched (Fig. 33).

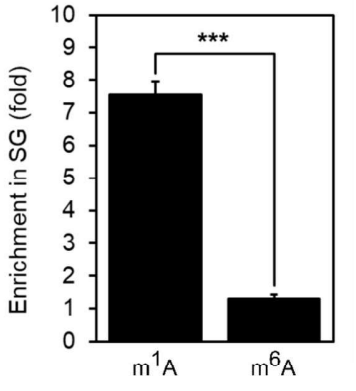

Figure 33. Enrichment of m^1A-containing mRNAs in stress granules.
Increase of fractions of m^1A and m^6A over unmodified adenosine in stress granule mRNAs. The fractions of m^1A and m^6A in cytosolic polyA mRNA were set as 1. N=3 independent experiments (means + SD). Two-tailed t-test (***: $p<0.001$).

II. D. Knock-down (KD) of TRMT61A in HeLa cell line

II. D. 1. Establishment of TRMT61A KD cell lines

Next, TRMT61A knock-down (KD) cell lines were prepared and studied. A pair of double nickase plasmids targeting TRMT61A, each encoding the D10A mutated version of Cas9 and one guide RNA was commercially available. The efficiency of a knock-out (KO) depends on the cell line used, particularly on its ploidy. Targeting a gene in a haploid cell is easier than in a di or triploid cells since several copies of the chromosomes are present and all copies have to be modified. HeLa cells are hypertriploid, therefore knocking out a target gene completely is difficult. Some KD clones were prepared and the expression levels of endogenous TRMT61A was analyzed.

II. D. 2. Characterization of TRMT61A KD cell lines

Expression of TRMT61A in two clones, #11 and #17, was analyzed by western blotting. The clones presented strongly and partially reduced expression of TRMT61A, respectively. These cells lines were not called knock-out (KO), but knock-downs (KD) (Fig. 34). For the next experiments, only the clone with the strong TRMT61A reduction (clone #11) was used unless mentioned otherwise. The viability of the TRMT61A KD cell line was similar to the WT cells. TRMT61A KD cell line grew slightly slower than the WT, however, this difference was minimal. Finally, the translation efficiency of the TRMT61A KD cell line was slightly lower than in the WT cells but this difference was not significant.

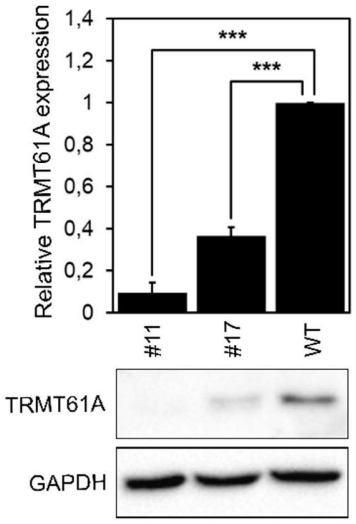

Figure 34. Estimation of TRMT61A amounts in HeLa WT and in the KD cell lines.
Amounts of TRMT61A determined by western blotting using anti-TRMT61A and anti-GAPDH antibodies. One representative out of three independent experiments is shown. Quantification by measurement of bands intensity after normalization to GAPDH (mean + SD). Two-tailed t-test (***: $p<0.001$).

II. D. 3. Levels of m^1A methylation in the KD cell lines

II. D. 3. a. Analysis of m^1A content in tRNAs

Another way to verify the reduction of TRMT61A expression in KD cells is by assessment of the methylation levels of tRNAs. For this purpose, total tRNAs were isolated from WT and KD cells as described (Liu et al., 2016). After nuclease digestion, single nucleotides were quantified by HPLC (Fig. 35). In total tRNAs extracted from HeLa WT cells, a peak corresponding to N1-adenosine could be identified. This peak did not change upon HS but was strongly reduced in tRNAs extracted from HeLa TRMT61A KD cells. m^1A methylation of tRNAs was not completely abolished, probably because of the residual TRMT61A in the KD cell line. This result confirmed the remaining low activity of TRMT61A in the KD cells and the lack of m^1A changes on tRNAs upon HS.

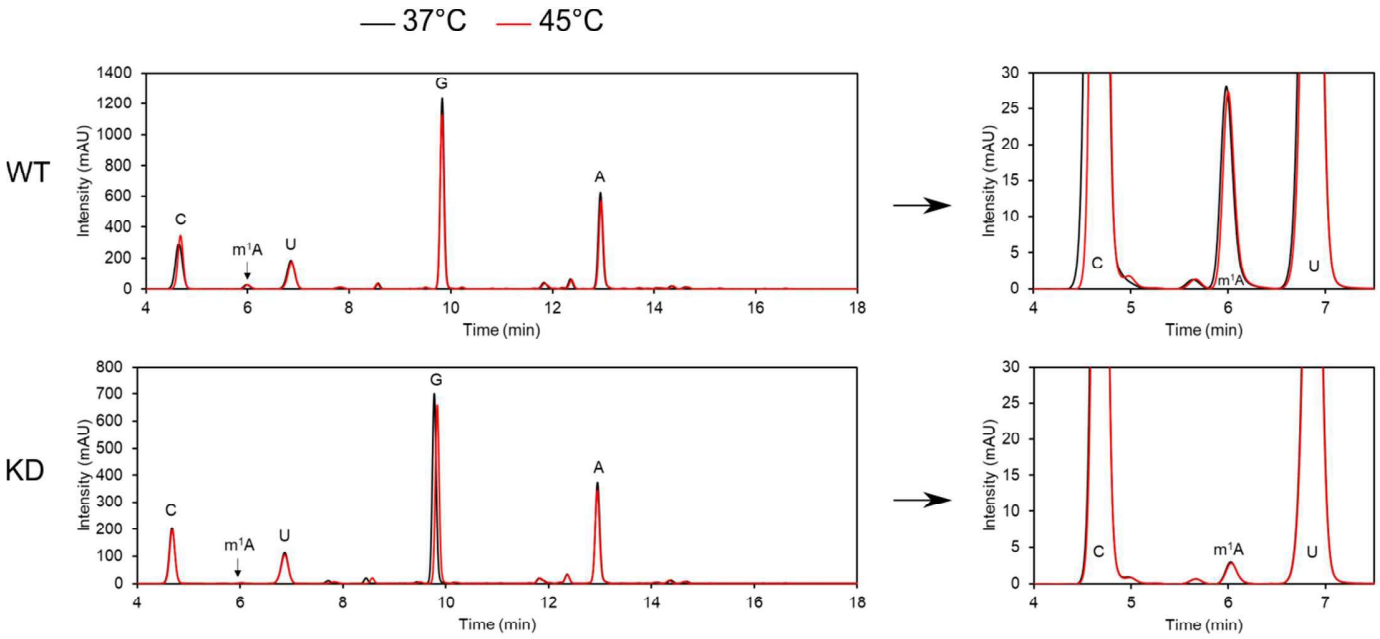

Figure 35. HPLC analysis of nucleosides of endogenous tRNAs.
HPLC analysis of N1-methylated adenosine from cellular tRNAs extracted from HeLa cells WT or TRMT61A KD incubated for 1 h at 37 °C or 45 °C. Right side: close ups.

II. D. 3. b. Quantification of the m^1A methylation in mRNAs

Two recent studies used genetic manipulations to establish TRMT6/61A as the methyl transferase responsible for m^1A methylation of eukaryotic mRNA (Li et al., 2017; Safra et al., 2017). We verified biochemically that mRNAs were less methylated in TRMT61A KD cells. In this assay, polyA mRNAs were pulled down from WT and KD cells using oligo $d(T)_{25}$ beads. These mRNAs, still bound to the beads were incubated with anti-1-methyladenosine or anti-6-methyladenosine antibodies. m^6A was used as a negative control because it is not deposited by TRMT6/61A and should not be reduced in the TRMT61A KD cell line. The bound antibodies were eluted by nuclease digestion of the mRNA and the samples were analyzed by western blotting using species specific antibodies. A scheme of the experiment is given in the Figure 36.

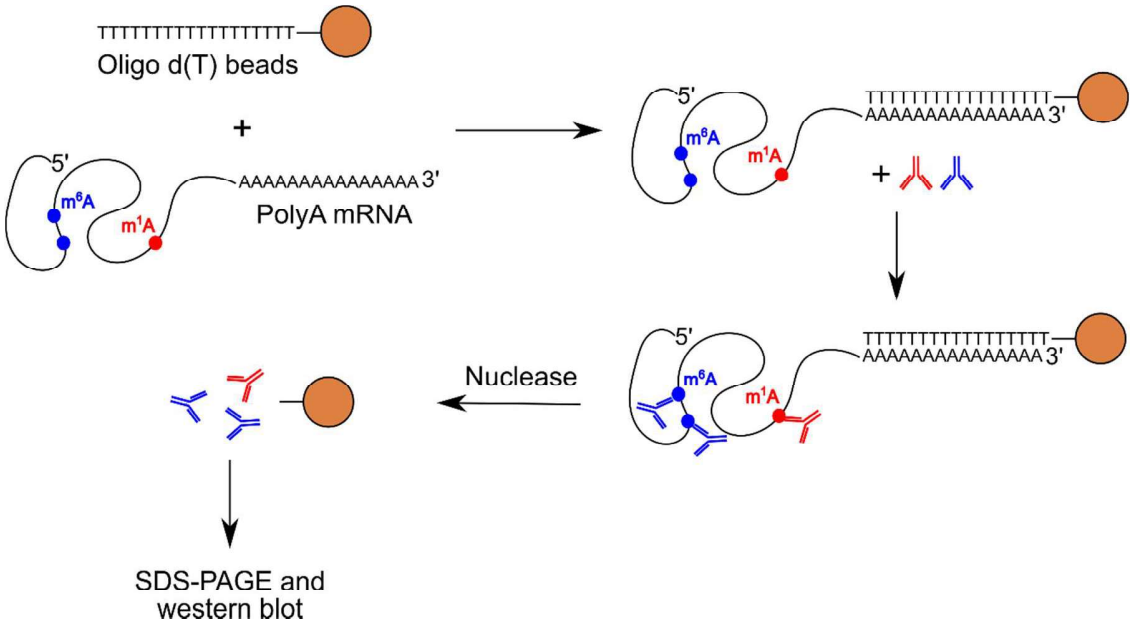

Figure 36. Scheme of the assay used to detect m^1A and m^6A on polyA mRNAs.
Oligo $d(T)_{25}$ beads were used to pull down polyA mRNAs, which were incubated with anti-1-methyladenosine or anti-6-methyladenosine antibodies. The antibodies recognized m^1A and m^6A modifications on polyA mRNAs and were eluted by nuclease digestion of mRNA molecules. They were analyzed by SDS-PAGE and western blotting using species specific antibodies.

In WT cells, m^1A and m^6A signals were slightly, but not significantly, increased upon HS (Fig. 37). This increase upon HS has been reported in the literature and confirms the accuracy of our assay. While m^6A signal in KD was very similar to the WT, m^1A signal was strongly reduced. This result supports the recently published reports claiming that TRMT6/61A is responsible for m^1A methylation of eukaryotic mRNAs (Li et al., 2017; Safra et al., 2017). The residual signal and increase in m^1A upon HS were most probably due to the residual expression of TRMT61A in the KD cell line.

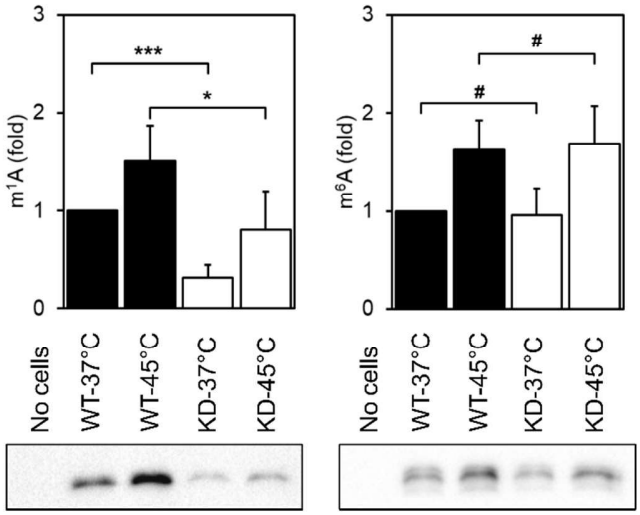

Figure 37. m^1A and m^6A on polyA mRNAs during heat shock.
PolyA mRNA methylation on N1-adenine (left panel) or N6-adenine (right panel) as determined by western blotting (anti-mouse for m^1A and anti-rabbit for m^6A). One representative out of three independent experiments is shown. Quantification by measurement of bands intensity (means + SD). One-tailed t-test (*: $p<0.05$; ***: $p<0.001$; #: not significant).

II. D. 4. Sensitivity of TRMT61A KD cell lines to stress

TRMT6/61A has first been studied in yeast where it was shown to be important during HS (Harashima and Hinnebusch, 1986). We decided to investigate whether the sensitivity to heat and other stresses could be observed in human cells lacking TRMT61A as well. For this assay, two stressors were tested: HS and arsenite treatment. Viability was assessed by an XTT assay after a recovery phase for HS or directly after arsenite treatment (Fig. 38 and 39 respectively). While the two cell lines with reduced TRMT61A expression were tested for heat sensitivity, only the cell line

with the strongest TRMT61A reduction was used for arsenite treatment. TRMT61A KD was less viable after HS. The cell line with the stronger reduction of TRMT61A expression was affected more by HS. This result is in agreement with the observations made in yeast.

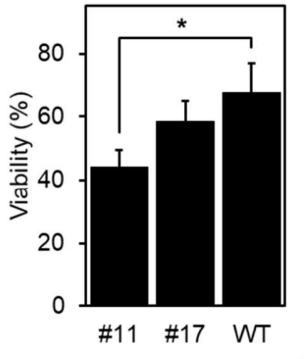

Figure 38. Cell sensitivity to heat shock.
Cell viability of HeLa WT and TRMT61A KD cell lines (clones #11 and #17) assessed by XTT assay. Cells were kept as cell suspension at 45 °C for 2 h and then allowed to recover at 37 °C overnight. Quantification by absorbance measurement. Average values of three independent experiments (mean + SD). Two-tailed t-test (*: $p<0.05$).

Furthermore, the KD cell line was more sensitive to arsenite treatment than the WT. The difference of sensitivity between the WT and the KD increased with increasing arsenite concentration.

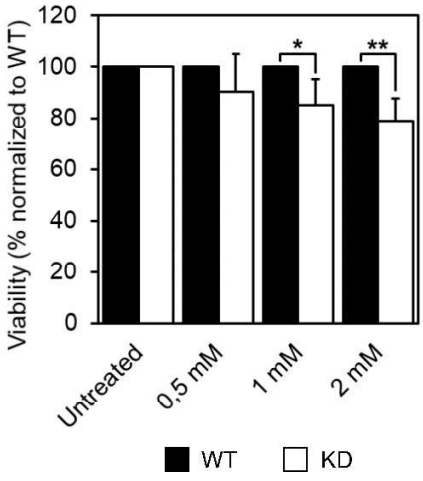

Figure 39. Cell sensitivity to arsenite treatment.
Cell viability of HeLa WT and TRMT61A KD #11 cell lines upon arsenite treatment at the indicated concentration for 30 min at 37 °C. Quantification by absorbance measurement. Average values of three independent experiments (mean + SD). Two-tailed t-test (*: $p<0.05$; **:$p<0.01$).

II. D. 5. Stress granule formation in TRMT61A KD cells

Because TRMT61A KD cells demonstrated an increased sensitivity to arsenite treatment, we wondered whether these cells were able to assemble SGs. Cells were treated with arsenite and SGs were analyzed microscopically. We observed that TRMT61A KD cells assemble significantly less SGs upon arsenite treatment (Fig. 40). Morphologically, SGs in TRMT61A KD cells were larger than in normal cells. This result revealed that cells lacking TRMT61A present defects in SGs assembly.

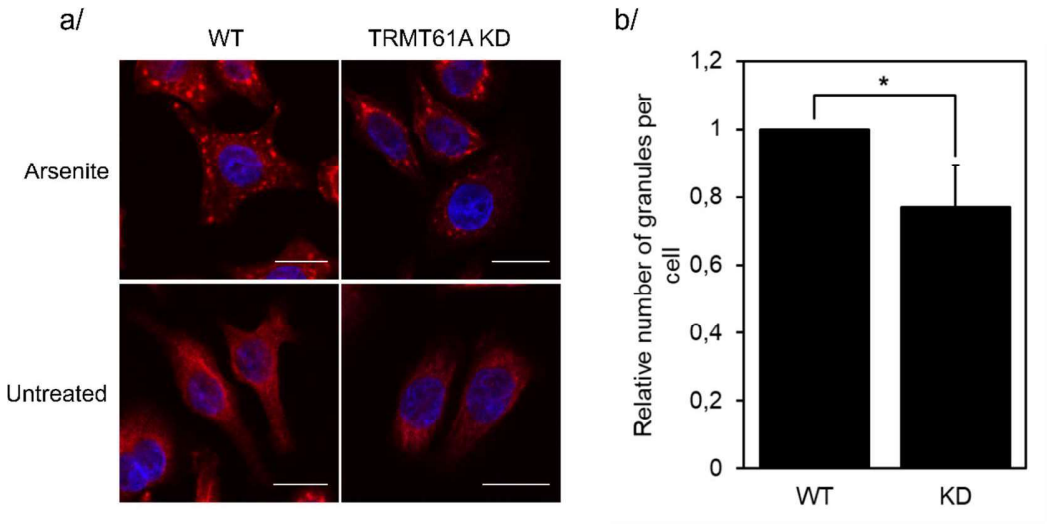

Figure 40. Stress granule assembly in WT and TRMT61A KD cells.
a/ Immunostaining of TIAR (red) to detect SGs in cells treated with 0.0625 mM arsenite for 30 min. Blue, DAPI staining. Scale bars: 20 µm. One representative out of three independent experiments. b/ Quantification of the SGs. N = 3 independent experiments (mean +SD). One-tailed t-test (*: $p<0.05$).

II. E. Functional consequences of mRNA methylation upon heat shock

To verify the effect of m^1A on mRNA sequestration, an m^1A motif was inserted into the 5' UTR of an Ubiquitin-EGFP construct (Fig. 41, Vabulas and Hartl, 2005). The motif was taken from PRUNE1 transcript because it had been experimentally verified earlier (Safra et al., 2017). The Ubiquitin-EGFP (Ub-EGFP) protein is highly unstable and is degraded in normal conditions. It accumulates upon proteasome inhibition and the protein can be detected with a precision of minutes. A control reporter was also prepared in which the adenine was mutated to uridine so that methylation by TRMT6/61A could not take place.

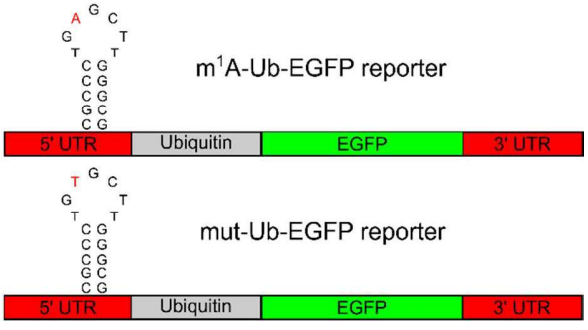

Figure 41. m^1A- and mut-Ub-EGFP reporter constructs.
Schematic view of the m^1A-motif containing Ubiquitin-EGFP reporters. The to-be-methylated adenine on the motif is in red, as well as the mutated base on the control reporter. UTR, untranslated region.

The reporters were transfected into cells and their levels were analyzed by western blot. The accumulation of the protein upon proteasome inhibition was similar for both constructs (Fig. 42).

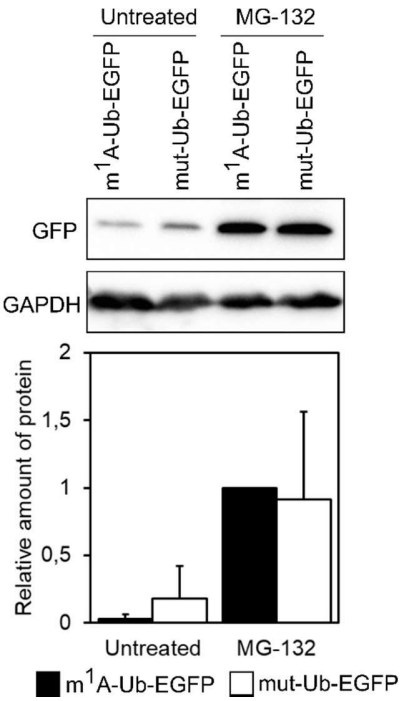

Figure 42. Accumulation of Ub-EGFP upon proteasome inhibition.
Accumulation of Ub-EGFP protein following transfection with m^1A-Ub-EGFP or mut-Ub-EGFP reporters and treatment with 20 μM MG-132 at 37 °C for 3 h. Western blotting was performed using anti-GFP and anti-GAPDH antibodies. One representative out of three independent experiments is shown. Quantification by measurement of bands intensity, normalized to GAPDH amount in the lysates (mean + SD).

Next the accumulation of the protein was checked immediately after HS at 45 °C or after 15 and 30 min of recovery at 37 °C for both constructs (Fig. 43). Before HS, DMEM was supplemented with actinomycin D to inhibit transcription and exclude transcription-based differences. Immediately after HS, the levels of Ub-EGFP were slightly different for both constructs: the construct with the mutated motif produced more protein than the one containing the m^1A motif (Fig. 43). A possible explanation is that upon HS, the m^1A-motif-containing mRNA is very rapidly sequestered, which prevents its translation. On the other hand, the mut-motif-containing mRNA remains in the cytosol, where it can be translated and accumulates during the time when translation is not yet completely inhibited. During recovery at 37 °C, the accumulation of the protein was

significantly faster for m^{1}A-Ub-EGFP construct than for mut-Ub-EGFP construct (Fig. 43). This result suggests that the m^{1}A motif containing mRNA was preserved during HS better than the control mRNA with mutant motif, possibly by being targeted to SGs.

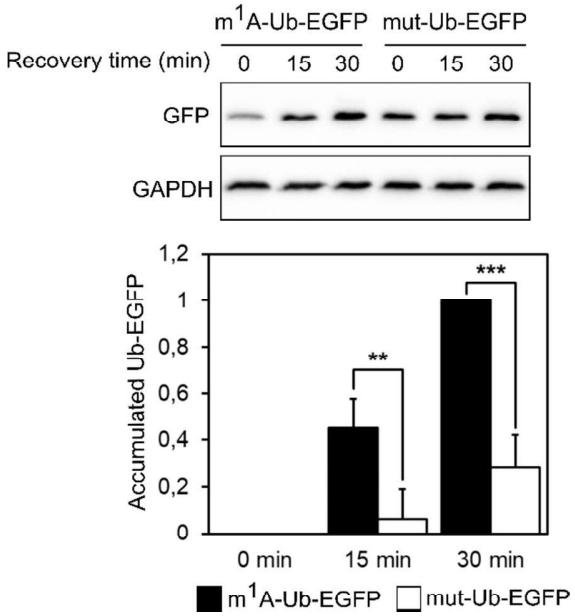

Figure 43. Accumulation of Ub-EGFP after heat shock.
Accumulation of Ub-EGFP protein after 30 min at 45 °C as determined by western blotting using anti-GFP and anti-GAPDH antibodies. 10 µM actinomycin D were added just before HS. Cells were collected directly after HS or after a recovery phase at 37 °C of 15 or 30 min as indicated. One representative out of three independent experiments is shown. Quantification by measurement of bands intensity, normalized to GAPDH amount in the lysates (mean + SD). Two-tailed t-test (**: $p<0.01$; ***: $p<0.001$).

An important control for this experiment was to make sure that mRNA levels were similar in both cases as assessed by qPCR (Fig. 44).

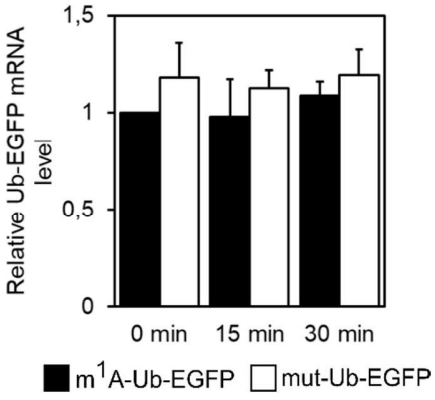

Figure 44. mRNA levels of Ub-EGFP constructs after heat shock.
Accumulation of Ub-EGFP mRNA after 30 min at 45 °C. 10 µM actinomycin D were added just before HS. Cells were collected directly after HS or after a recovery phase at 37 °C of 15 or 30 min as indicated. mRNA levels of the reporters were estimated by qPCR using primers specific for the transfected constructs. Fold induction was calculated using the 2^{-ddCt} method (N = 3, mean + SD).

III. m^{1}A safeguards mRNAs during amyloidogenesis

III. A. Amyloidogenesis is aggravated in TRMT61A KD cell lines

Our results demonstrate an increased sensitivity of cells lacking TRMT61A to acute proteostasis stress. This led us to consider the involvement of N1-adenine methylation in chronic proteostasis stress, such as amyloidogenesis. Links between RNA granulation and neurodegeneration have recently been established (Bosco et al., 2010; Liu-Yesucevitz et al., 2010; Molliex et al., 2015; Vanderweyde et al., 2012; Waelter et al., 2001). Given the potential role of m^{1}A on mRNAs in granulation and in the formation of RNA-protein assemblies, we wondered whether lack of the TRMT61A activity had an effect on protein aggregation and amyloidogenesis.

III. A. 1. Study of Aβ-EGFP accumulation by western blot

For amyloidogenesis study, we used the model of Alzheimer's disease. This neurodegenerative disorder is characterized by abnormal deposits of amyloid β (Aβ) in patients' brain. This 40 to 42 amino-acids-long peptide results from the cleavage of the transmembrane protein amyloid precursor protein (APP) (Goedert and Spillantini, 2006). In order to study the effect of reduced levels of m^{1}A, the A$\beta_{1\text{-}42}$ peptide fused to EGFP was transfected into WT or TRMT61A KD HeLa cells. This aggregating peptide was used to cause a chronic proteostatis stress by triggering amyloidogenesis and amyloid co-aggregation of endogenous proteins. EGFP overexpression was used as a control. Amounts of A$\beta_{1\text{-}42}$-EGFP and EGFP alone were analyzed 48 h after transfection by western blotting using anti-GFP antibody (Fig. 45 a). Earlier time points were inappropriate because aggregates did not have time to accumulate in sufficient amounts. The lower than expected

molecular weight bands suggest partial cleavage of the fusion protein. While only one predominant band was observed in cells transfected with EGFP alone, with no significant difference between the WT and TRMT61A KD cells, a high molecular weight smear appeared above the Aβ-EGFP band (Fig. 45 a). This smear probably corresponded to the accumulation of SDS-insoluble and/or ubiquitinated species and was significantly increased in cells with reduced TRMT61A activity. This could be the result of an impaired capacity of the cells with reduced m^1A to clear amyloid. The amount of GAPDH was reduced in TRMT61A KD cells transfected with Aβ-EGFP compared to the WT, suggesting an increased toxicity. The reintroduction of TRMT6/61A activity in the TRMT61A KD cell line by transient transfection of TRMT6 and TRMT61A constructs partially rescued the observed phenotype by reducing Aβ aggregation (Fig. 45 b). These results indicate that reduced levels of TRMT6/61A methyltransferase impair the clearance Aβ-EGFP aggregates.

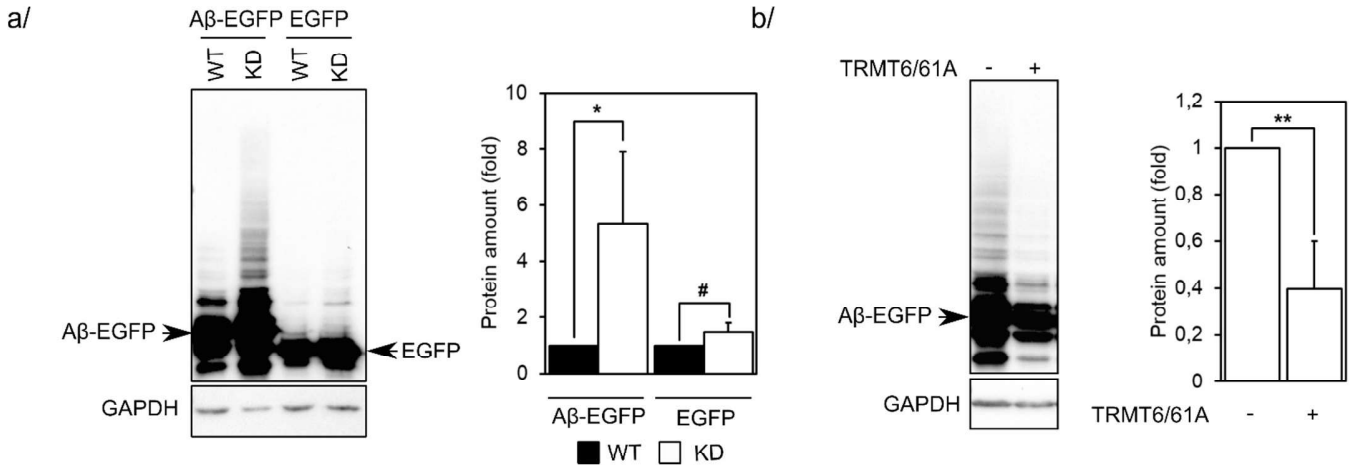

Figure 45. Aβ accumulation in HeLa cells.
a/ Estimation of Aβ-EGFP and EGFP amounts in HeLa WT and TRMT61A-KD cells as determined by western blotting using anti-GFP and anti-GAPDH antibodies. b/ Estimation of Aβ-EGFP amounts in HeLa TRMT61A KD reconstituted with TRMT6/61A. One representative out of three independent experiments is shown. Quantification by measurement of bands intensity, including the actual Aβ-EGFP or EGFP bands with the higher molecular weight smear corresponding to modified species (mean + SD). Two-tailed t-test (*: $p<0.05$; **: $p<0.01$; **#**: not significant).

III. A. 2. Study of Aβ-EGFP accumulation by microscopy

In order to confirm the defect of Aβ-EGFP clearance in TRMT61A KD cells, we used microscopy to visualize the aggregates. The experimental setup was the same as for western blot analysis but the cells were prepared for microscopy and analyzed for GFP signal. At least 200 EGFP-positive

cells were analyzed in each condition and in three independent replicates. Cells with aggregates were identified and quantified. The numbers from three independent replicates were pooled and Chi square test values were calculated (Fig. 46). EGFP and Aβ-EGFP demonstrated very different cellular distributions. While EGFP alone showed a homogenous cytosolic localization, Aβ-EGFP was heterogeneously distributed and aggregates were visually identifiable. Quantification revealed that cells with aggregates were two times more abundant in the TRMT61A KD cells compared to the WT cells. This result confirmed the defect in the clearance of aggregates and suggested an involvement of m^1A modification of mRNAs in cell response to proteostasis stress.

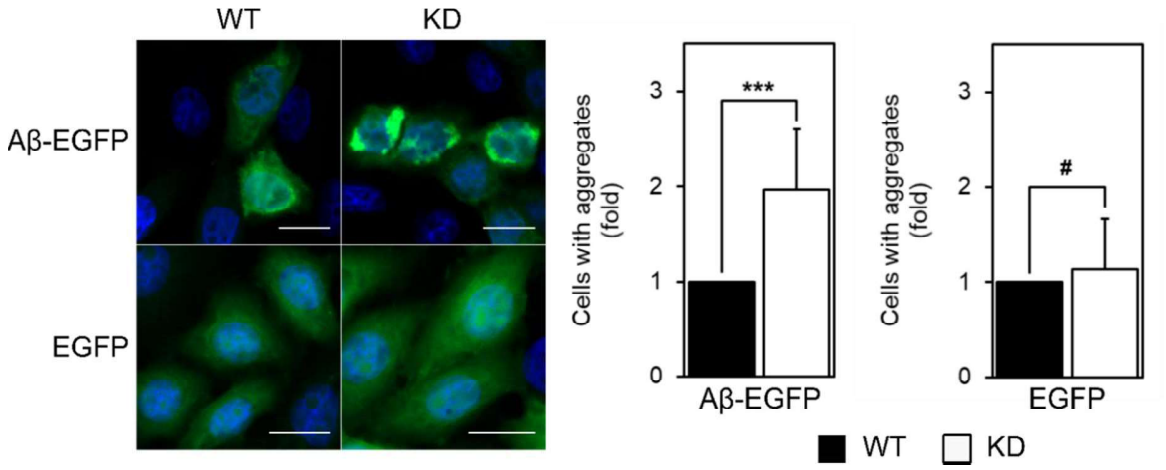

Figure 46. Observation of Aβ aggregates in HeLa cells by immunofluorescence microscopy.
Detection of Aβ-EGFP and EGFP (green) transiently overexpressed in HeLa WT and TRMT61A-KD. Blue, DAPI staining. Scale bar: 20 µm. One representative out of three independent experiments is shown. Quantification by identification of the cells with aggregates among the transfected cells (mean + SD). Chi square test on cumulative data (***: $p<0.001$; #: not significant).

III. B. mRNA co-aggregation with Aβ

III. B. 1. Aβ-EGFP pulldown

To analyze the composition of Aβ aggregates, Aβ-EGFP or EGFP as a negative control were overexpressed in HeLa WT or TRMT61A KD cell lines and aggregates were isolated using GFP nanobodies 24 h after transfection. Label-free MS analyses were performed by Dr. Giulia Calloni (Fig. 47). The number of Aβ-EGFP co-aggregators was strongly increased in the TRMT61A KD cell line compared to the WT, with about three times more co-aggregators identified.

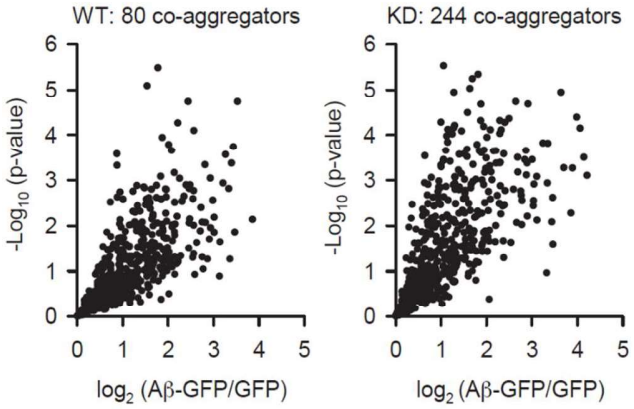

Figure 47. MS analysis of Aβ co-aggregators.
Mass spectrometry analysis of Aβ-EGFP co-aggregators in HeLa WT or TRMT61A KD cells 24 h after transfection of Aβ-EGFP or EGFP. The identified proteins are plotted on x axis according to their enrichment on Aβ-EGFP over EGFP background. The p value is plotted on the y axis. N=5 independent experiments.

A considerable overlap between the co-aggregators in WT and KD cells two sets of proteins was observed (Fig. 48).

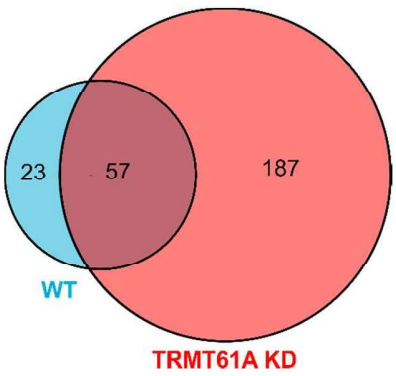

Figure 48. Overlap of Aβ co-aggregators in WT and TRMT61A KD cell lines.
The number of overlapping Aβ-EGFP co-aggregators in the WT and TRMT61A KD cell lines is indicated.

Among the co-aggregators enriched specifically in cells lacking TRMT61A, the top-two enriched category was: “mRNA binding”. This result strongly suggests that mRNA was aberrantly sequestered in the Aβ aggregates (Tab. 6).

Molecular function	FDR
Translation initiation factor activity	1.6×10^{-7}
mRNA binding	3.6×10^{-4}
DNA helicase acitivity	4.7×10^{-3}
Structural constituents of cytoskeleton	4.4×10^{-3}

Table 6. Molecular functions enriched in the set of Aβ co-aggregators in TRMT61A KD cell line.
Gene Ontology (GO) categories enriched among Aβ-EGFP co-aggregators in the TRMT61A KD cell line, but not in the WT cell line. FDR, false discovery rate.

III. B. 2. Mechanism verification: PolyA mRNA pulldown

In order to verify that more mRNA was trapped into aggregates in methylation-deficient cells, we pulled down polyA mRNA from cell lysates from HeLa WT or TRMT61A KD transfected with EGFP or Aβ-EGFP. The proteins bound to polyA mRNA were collected and analyzed by western blotting (Fig. 49). The amounts of mRNA bound to the beads were quantified and compared using RiboGreen reagent but the difference between the WT and the KD for each transfection was negligeable. In both cell lines, EGFP did not associate with polyA mRNA. In the WT cells, Aβ-EGFP associated with polyA mRNA. This result suggested a co-aggregation of mRNA with amyloid. Interestingly, in the TRMT61A KD cell line, Aβ-EGFP was much stronger associated with polyA mRNA. A lack of m^1A-methylation in mRNAs thus resulted in a higher association of mRNA with amyloid. The result suggested that m^1A is necessary to prevent mRNAs entrapment in protein aggregates. In summary, lack of m^1A methylation led to the increased association of mRNAs with the aggregating protein Aβ along with an enhanced Aβ aggregation.

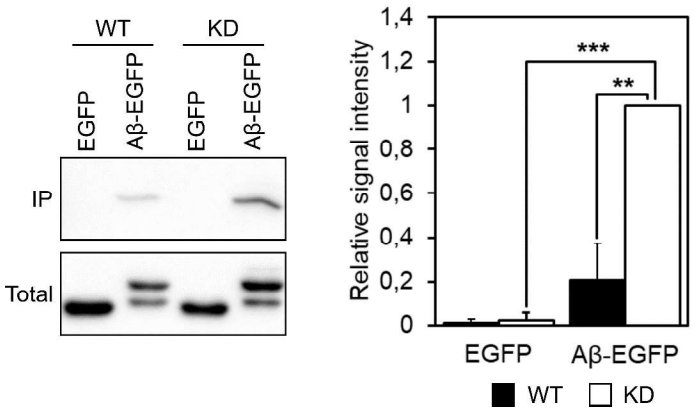

Figure 49. Co-aggregation of polyA mRNA with Aβ.
Estimation of Aβ-EGFP and EGFP amounts in HeLa WT and TRMT61A-KD cells associated with polyA mRNA as determined by western blotting using anti-GFP antibody. One representative out of three independent experiments is shown. Quantification of band intensity normalized to the total amount of EGFP or Aβ-EGFP in the lysates (mean + SD). Two-tailed t-test (**: $p<0.01$;***: $p<0.001$).

III. C. m^{1}A safeguards mRNAs during amyloidogenesis

We then decided to investigate whether the presence of the motif could rescue mRNA from co-aggregation with amyloid and rescues its translation during amyloidogenesis. We used the 3xFlag-NQO1 construct containing the m^{1}A motif (or a mutated control, taken from PRUNE1 transcript (Safra et al., 2017)) presented in the Figure 50.

Figure 50. A scheme of m^{1}A- and mut-NQO1 reporter constructs.
Reporters contain an m^{1}A wild-type (m^{1}A) or mutated (mut) motifs in front of three flag tags and the NQO1 gene.

This construct was co-transfected into HeLa WT cells with increasing amounts of the Aβ-EGFP. The accumulation of the reporter protein was measured by western blotting (Fig. 51).

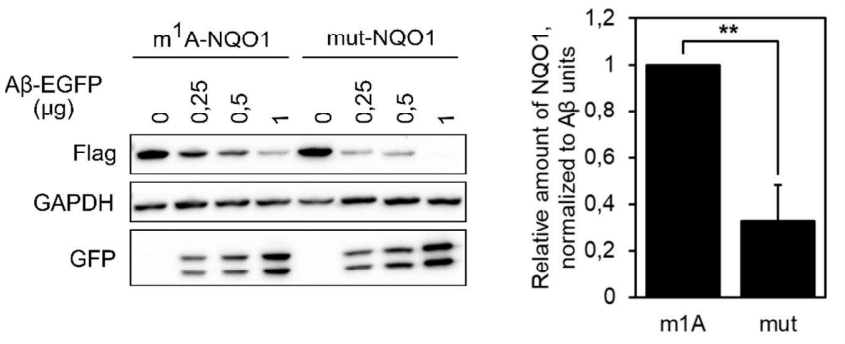

Figure 51. m[1]A- or mut-NQO1 reporter assay in HeLa WT cells.
Estimation of Flag-tagged NQO1 protein amounts synthesized in HeLa WT cells when increasing amounts of Aβ-EGFP were co-transfected as determined by western blotting using the indicated antibodies. One representative out of three independent experiments is shown. Right panel: quantification by measurement of bands intensity, normalized to GAPDH, relative to m[1]A and multiplied by GFP signal in order to take into account the actual amyloid amounts (mean + SD). Two-tailed t-test (**: $p<0.01$).

We also verified mRNA levels of reporter constructs by qPCR to make sure that the motif did not affect mRNA turnover (Fig. 52).

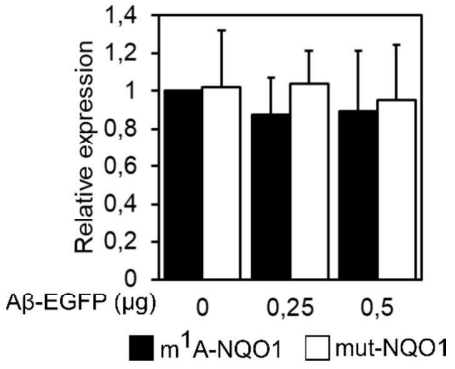

Figure 52. mRNA levels of m[1]A- or mut-NQO1 constructs in HeLa WT cells.
mRNA levels of the reporters as estimated by qPCR using primers specific for the transfected constructs. Fold induction was calculated using the 2^{-ddCt} method (N = 3, mean + SD).

We observed a reduced accumulation of the flag-tagged reporter correlating with the increasing amount of transfected Aβ. This reduction was significantly stronger in the case of the mutated motif although mRNA levels were similar. The result highlights the critical role of the motif in mRNA rescue during amyloidogenesis. The same experiment performed in TRMT61A KD cells did not show any significant difference between the two constructs (Fig. 53), which indicates the central role of the methyltransferase in the safeguarding of mRNAs.

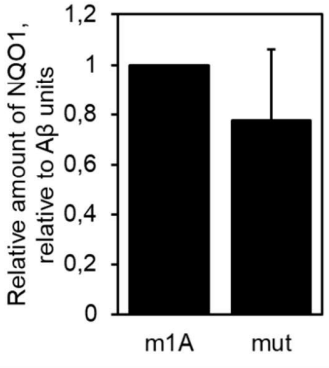

Figure 53. m[1]A- or mut-NQO1 reporter assay in HeLa TRMT61A KD cells. Estimation of Flag-tagged NQO1 protein amounts synthesized in HeLa TRMT61A KD cells when increasing amounts of Aβ-EGFP were co-transfected as determined by western blotting. Quantification as described for HeLa WT cells in Fig. 51 (N = 3, mean + SD).

Finally, the assay was performed in another cell line, the murine melanoma B16F10, in which the difference between the m[1]A and the mutated motifs was significant as well (Fig. 54). This last result strengthens the generality of our finding since it seems to be conserved between cell lines and species.

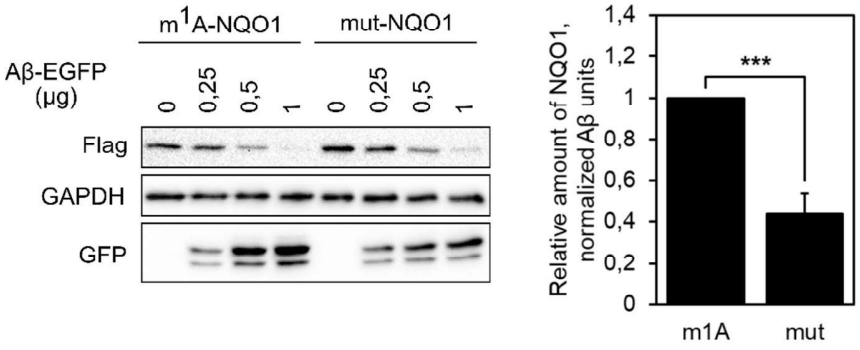

Figure 54. m[1]A- or mut-NQO1 reporter assay in B16F10 cells.
Estimation of Flag-tagged NQO1 protein amounts synthesized in B16F10 cells when increasing amounts of Aβ-EGFP were co-transfected as determined by western blotting using the indicated antibodies. One representative out of three independent experiments is shown. Right panel: quantification by measurement of bands intensity, normalized to GAPDH, relative to m[1]A and multiplied by GFP signal in order to take into account Aβ-EGFP amounts (mean + SD). 2-tailed t-test (***: $p<0.001$).

CHAPTER 4: DISCUSSION

SGs form in cells in response to stress upon eIF2α phosphorylation and translation stop (Kedersha et al., 1999). They are thought to play a role in cell survival, translation regulation and mRNA triage. Although the hypothesis of a liquid-liquid phase separation driving SGs assembly is largely accepted, the details of the molecular mechanism remain unkown (Boeynaems et al., 2018; Brangwynne et al., 2009; Elbaum-Garfinkle et al., 2015; Weber and Brangwynne, 2012). Recent studies highlighted the importance of RNA in this process (Bounedjah et al., 2014). We initiated our project with the hypothesis that free mRNAs trigger SG assembly. We assumed that this happened via specific mRNA-protein interactions during stress response and by means of proteomic analysis defined a set of free mRNA interactors in heated human cytosol. One of these interactors was studied in details and allowed us to connect stress response with the field of epitranscriptomics.

I. Free mRNA granulates spontaneously *in vivo*

In the first part of this work, we designed a free mRNA bait based on HSP70 transcript with deleted 3' and 5' UTR which are known to regulate its translation upon stress. While endogenous HSP70 mRNA is usually excluded from SGs, the free mRNA adopted a granular distribution when transfected into mammalian cells (Fig. 9 and 10). This result reassured us in our experimental strategy and confirmed already published reports which had described the ability of some mRNAs to self-assemble *in vitro* and *in vivo* (Mahadevan et al., 2013; Van Treeck et al., 2018).

II. Free mRNA interactors in mammalian cytosol

In the second part, experimental conditions were optimized in order to study the early phase of stress response in mammalian cells, while SGs are being formed. The condition of 1 h at 45 °C was chosen and displayed full HSP70 induction and eIF2α phosphorylation while polysomes disassembly was only partial, suggesting an early stage of granulation (Fig. 11, 12 and 14). Moreover, analysis of the content of the 80S fraction of polysomes revealed that less mRNA associated with ribosomes in heat shocked cells and suggested the mRNAs had been released and were free in the cytosol (Fig. 15). Observation of heat shocked cells by microscopy showed that almost no SGs were formed under these conditions, indicating an early phase of stress response

(Fig. 13). This setup allowed us to study free mRNA interactome in the time frame when SGs start assembling. Free mRNA pulldowns allowed us to identify 79 interactors (Fig. 16, Appendix 1). Nucleic acid binding proteins and RNA-binding proteins were among the most enriched on free mRNA, which reassured us on the quality of our pulldowns (Tab. 5).

The interaction of free mRNA with eIF2α subunit was verified biochemically and we observed that only the non-phosphorylated form (on Serine 51) of the protein was involved (Fig. 20), even though phosphorylation of eIF2α happened normally. We also showed that this interaction only took place in heat shocked lysate. While eIF2 presence in free mRNA interactome could simply be an indication of the interaction of mRNA with the 43S pre-initiation complex, we excluded this possibility because neither eIF3, eIF1 nor the 40S ribosomal subunits were detected. The fact that the non-phosphorylated form of the protein interacted with free mRNA suggests a functional interaction.

One of the highest-enriched free mRNA interactors was the methyltransferase TRMT6/61A. Although it is a well-known A58 modifier for tRNA, this protein was more recently identified as the methyltransferase responsible for m^1A deposition on mRNAs. We could verify the interaction biochemically, and showed that it is induced by HS (Fig. 21). Furthermore we could verify the interaction of TRMT6/61A with endogenous mRNA during HS using polyA mRNA pulldowns (Fig. 21). Interestingly, free mRNA and TRMT6 could interact directly *in vitro*, but the interaction was lost at 45 °C (Fig. 29). *In vitro* structural studies revealed a local unfolding in the TRMT6 subunit at 45 °C which did not decrease the affinity of the heterodimer for its major substrate tRNA (Fig. 25-27). We could exclude the possibility that the increased interaction of free mRNA with TRMT6/61A was the result of a decreased competition upon tRNA-iMet degradation during HS. Another possibility is that free mRNA and TRMT6/61A could be part of a large multiprotein complex. *Ex vivo* pulldowns revealed that eIF2α and TRMT6/61A interact with each other and that this interaction is RNA dependent (Fig. 22, 23), suggesting that mRNA, eIF2α and TRMT6/61A could be part of a large multiprotein complex. Lack of some key components would explain why we could no reproduce the increased interaction upon HS *in vitro*.

The interaction between the free mRNA and TRMT6/61A was quite unexpected because the mRNA we used does not contain the motif recognized by TRMT6/61A for methylation. Two explanations can be suggested at this point. First, this interaction could be mostly unspecific upon

stress and take place with most free mRNAs available in the cytosol regardless of the presence or absence of the motif. The methylation would then take place only when the methyltransferase encounters the specific motif. The *in vitro* reconstitution of the interaction supports this hypothesis since we showed a direct interaction between HSP70 mRNA and TRMT6/61A (Fig. 29). In this case, the interaction is probably transient and very dynamic, TRMT6/61A going from one mRNA molecule to the other until the suitable methylation motif is recognized by the methyltransferase. A second possibility could be that in the *ex vivo* pulldowns, TRMT6/61A did not interact directly with our probe. Effectively, other free mRNAs containing the m^1A motif may have interacted with TRMT6/61A and brought it to our probe via RNA-RNA or other RNA-protein interactions.

III. m^1A as a tag for targeting mRNAs to stress granules

The bioinformatics analysis revealed that mRNAs enriched in SGs contain significantly more m^1A motifs than mRNAs depleted from SGs, or mRNAs neither enriched nor depleted from SGs (Fig. 30). This result led us to formulate the hypothesis that m^1A methylation of mRNAs could constitute a tag for the mRNAs targeting to SGs.

The observation of overexpressed TRMT6/61A in HeLa cells revealed the colocalization of the methyltransferase with the SG marker TIAR upon arsenite treatment (Fig. 31), while neither TRMT6 nor TRMT61A have been reported as stress granules components. The recruitment of overexpressed TRMT6/61A to SGs might be due to its artificially stabilized interaction with free mRNAs, because of a not normally high concentration of the protein in the cells. Another explanation could be the transient nature of TRMT6-SGs association precluding its preservation during biochemical isolation of SGs.

The functional consequences of m^1A deposition on mRNAs in stress response were analyzed using TRMT61A KD cell lines generated via the CRISPR-Cas9 technique (Fig. 34). Lack of m^1A on mRNAs resulted in an increased sensitivity of the cells to HS and arsenite treatment as assessed by XTT assay (Fig. 38, 39). Heat sensitivity of TRMT6/61A deficient strains was observed in yeast (Watanabe et al., 2013) and was attributed to the strong destabilization of the initiator iMet-tRNA leading to impaired translation. However, transfection with EGFP in the KD cell line did not lead to significantly different protein amounts in WT and TRMT61A KD cell lines (Fig. 45) suggesting that translation was not impaired and that initiator tRNA-iMet destabilization did not constitute a

major issue in our setup. In TRMT61A KD cells, m^1A was, however, significantly reduced on polyA mRNAs (Fig. 37), which allowed us to explore this novel function of the methyltransferase.

In heat shocked cells, an m^1A motif containing mRNA recovered better and was better translated immediately after returning to normal temperature than a control RNA with mutated motif (Fig. 43). A possible explanation is that, in agreement with our bioinformatics analysis, the m^1A-containing mRNA was targeted to SGs and escaped degradation. The colocalization of overexpressed TRMT6/61A with SGs upon arsenite treatment (Fig. 31) supported the hypothesis of a link between m^1A methylation of mRNAs and SG formation. In addition, we could isolate SGs and analyze their m^1A and m^6A content by mass spectrometry. Importantly, while m^6A content in SGs mRNAs was very similar to polyA mRNAs, m^1A was almost 8 times enriched in SGs mRNAs (Fig. 33). We could thus biochemically confirm the results of the bioinformatics analysis and directly support the hypothesis that m^1A is a tag to direct mRNAs to stress granules. Another possibility would be to analyze the localization of endogenous m^1A motif-rich mRNAs using the FISH technique.

IV. TRMT6/61A protects mRNAs from co-aggregation with amyloid

Recently a connection between SGs and neurodegenerative disorders has been proposed, due to the colocalization of some pathological mutants of proteins involved in ALS such as TDP-43 with SGs markers (Liu-Yesucevitz et al., 2010). Because cells lacking TRMT61A demonstrated an increased sensitivity to proteostasis stress (Fig. 38, 39), we compared amyloidogenesis in WT and TRMT61A KD cell lines. Interestingly, cells with reduced levels of TRMT61A demonstrated an increased accumulation of transfected Aβ and an impaired aggregate clearance, which could be observed by western blotting and microscopy (Fig. 45, 46). Analysis of amyloid interactome revealed the co-aggregation of mRNA-binding proteins, suggesting the presence of mRNA in the aggregates (Fig. 47). We could prove this assumption directly by performing polyA mRNA pulldowns and finding an increased association of Aβ with mRNA from cells lacking TRMT61A (Fig. 49). These two results led us to conclude that the lack of m^1A deposition on mRNAs enhanced RNA co-aggregation with amyloids. We could indeed show that an m^1A motif-containing mRNA was rescued and translated more efficiently when co-transfected with Aβ than an mRNA containing a mutated m^1A motif (Fig. 51). This result was further confirmed in another cell line, the murine melanoma B16F10 cell line (Fig. 54).

It remains to understand why m^1A deposition limits mRNAs interaction with protein aggregates. One explanation could be that m^1A induces changes in the secondary structure of mRNAs which make aberrant interactions with aggregating proteins less likely. It is known that the m^1A modification impairs A:U Whatson and Crick base-pairing and induces local melting in mRNAs (Zhou et al., 2016). This type of methylation also introduces a positive charge. Both the positive charge and the changes in mRNA secondary structure could have an influence on mRNAs interactome of proteins and other RNA molecules. Indeed, it was demonstrated that RNA secondary structure directed the specific composition of different types of RNA granules (Langdon et al., 2018). Defects in TRMT6/61A activity could affect mRNA secondary structure such that interactions with aggregation-prone proteins like Aβ are promoted. Another effect of the m^1A-containing mRNAs sequestration into SG is that it limits their exposure to the cytosolic content and prevents co-aggregation with unstable proteins. The increased co-aggregation of mRNA with Aβ that we observed in TRMT61A KD cell lines could simply be a consequence of a reduced sequestration of mRNAs in SGs. The interaction of mRNA molecules with Aβ could be unspecific and happen regardless of their methylation status if they are exposed to these aggregation-prone proteins. m^1A deposition could be a simple way to remove mRNAs from the cytosol and to protect them from stress-induced co-aggregation with proteins.

V. Model and perspectives

We propose a model for free mRNA fate during proteostasis stress (Fig. 55). Upon polysome disassembly, free mRNA is released and exposed to the cytosolic contents. It becomes free to interact with other proteins, including the methyltransferase TRMT6/61A. We propose that TRMT6/61A methylates free mRNAs released in the cytosol upon stress if mRNA contains a specific m^1A motif recognized by the methyltransferase. The m^1A could then be used as a tag to target mRNAs to stress granules and promote their assembly. Upon stress release, SGs rapidly disassemble, thus releasing m^1A-containing mRNAs which could in turn go back to being translating and support cell recovery after stress. On the other hand, mRNAs that lack m^1A methylation could be engulfed by the aggregating proteins generated by conformational stress. Deficiency of the N1-adenine methylation of mRNAs due to the lack of TRMT6/61A could increase the amount of free unpacked mRNAs exposed to misfolded proteins and thus promote amyloidogenesis. The deposition of m^1A on mRNAs could then be a way to protect them during

exposure to stress, to limit their co-aggregation with misfolded proteins and to allow a faster recovery upon stress release.

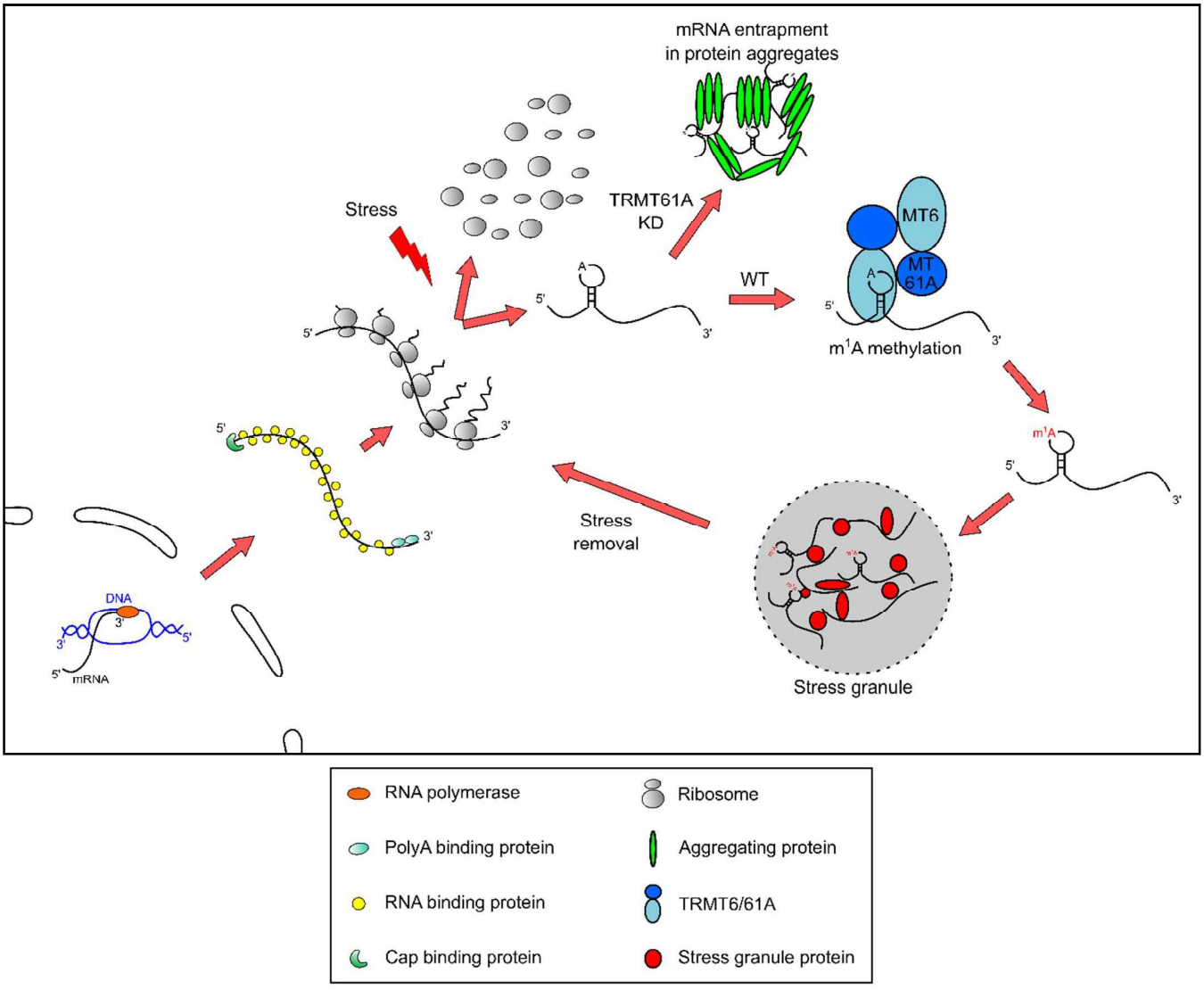

Figure 55. Model for mRNA recruitment to stress granules.
While mRNA is exported to the cytosol, it is covered with RNA-binding proteins which stabilize it and protect is for degradation. The proteins are stripped from the mRNA during translation by ribosomes (polysomes). Upon stress, polysomes disassemble and the mRNA molecules are freed into the cytosol. At this stage, they become able to interact with other proteins present in the cytosol, such as the methyltransferase TRMT6/61A. Upon recognition of a specific motif, TRMT6/61A methylates mRNA to generate m^1A. We propose that the methylated mRNA is directed to SGs and facilitates their assembly. In cells that lack TRMT6/61A, the mRNAs are not methylated, remain unsequestered and become entangled in protein aggregates.

Several questions remain to be addressed. First, a key point would be to study the details of free mRNA release upon different stressors and to investigate mRNA methylation by TRMT6/61A. Our study focused on HS and amyloidegenesis. However, it will be important to explore other pathologically relevant perturbations triggering SGs assembly, like the oxidative stress or amino acids starvation, and to investigate free mRNA release due to translation impairment. While this could be a general stress response mechanism, it could also be specific to HS and amyloidogenesis.

Another important question concerns the mechanism behind the sequestration of m^1A-containing mRNAs into SGs. Specific reader proteins which recognize the mRNA modification should be identified in order to unveil the molecular details behind mRNA recruitment to SGs. Interactome studies of specific m^1A motif-rich mRNAs could provide this information. Effectively, our interactome study was performed using a probe that did not contain the m^1A motif which makes it less suitable for this kind of analysis.

VI. Relevance of RNA granulation and its connection with disease

Stress granules have been connected to several disorders and diseases. The formation of tumors create a stressful environment for the cells which are subject to hypoxia, high levels of Reactive Oxygen Species (ROS) and low nutrient availability. These conditions are favorable for the formation of SGs. Indeed, treatments with chemotherapeutics or radiotherapy cause a sufficient stress to trigger the formation of SGs in some forms of cancer: Sorafenib promotes SGs assembly in hepatocarcinoma cells, and Bortezomib, Cisplastin and Etoposide in glioma cells (Adjibade et al., 2015; de Almeida Souza Vilas-Boas et al., 2016; Hicham Mahboubi and Ursula Stochaj, 2017). This formation of SGs is thought to play a role in the phenomenon of resistance to cancer treatments via the protection from degradation of mRNAs involved in cell proliferation. A study using sarcoma xenografts revealed that the inhibition of SGs formation limited tumors progression and blocked lung metastasis (Somasekharan et al., 2015). Finding practical ways to limit SGs formation upon cancer treatments by chemotherapeutics or radiotherapy could then be of great interest. Targeting TRMT6/61A could allow the manipulation of SGs assembly and limit chemoresistance development.

Another category of disease with SG involvement are neurodegenerative disorders. Some of these diseases are associated with an hyper-formation of SGs, like Alzheimer's disease (Vanderweyde et al., 2012), or with the formation of aberrant SGs like in the case of mutations in TDP-43 involved

in ALS which generate TDP-43-positive SGs that are larger than usual (Dewey et al., 2011). Additionally, these larger granules show reduced motility in neurons (Liu-Yesucevitz et al., 2014). This is problematic since in those cells SGs are constitutive and necessary to transport material along the axons to ensure the local translation (Ainger et al., 1993; Ferrandon et al., 1994; Knowles et al., 1996; Rook et al., 2000). The excessive formation of SGs raises several potential issues. First, the excessive sequestration of mutated aggregating proteins could result in a loss of function, like in the case of TDP-43. On the other hand, SGs not only sequester aggregating proteins but also mRNAs and RNA-binding proteins, which could result in defects in RNA processing and regulation. Finally, SGs are known to sequester some proteins from signaling pathways like TORC which could affect cell growth (Takahara and Maeda, 2012).

Two observations led to the hypothesis that the assembly of SGs promotes the formation of pathological aggregates. First, defects in SGs dynamics could increase neurodegeneration (Shukla and Parker, 2016). SGs contain proteins with prion-like domains, which have a high probability of forming amyloid structures (Li et al., 2013). The high concentration of prion-like domains in SGs correlated with an increased formation or decreased clearance of SGs which could lead to amyloid initiation. Second, several proteins generating pathological aggregates in neurodegenerative disorders colocalize with SGs, like TDP-43, FUS, huntingtin or Tau (Bentmann et al., 2013; Bosco et al., 2010; Liu-Yesucevitz et al., 2010; Waelter et al., 2001). The hypothesis of SGs being precursors or pathological aggregates was proposed (Molliex et al., 2015). If a mutated RNA-binding protein, such as TDP-43 in the case of ALS, is recruited to SGs, it local concentration increases, which facilitates its aggregation. This could be a starting point for a more severe and uncontrolled form of aggregation with the formation of amyloid fibrils. The polymerization into amyloid-like fibers has indeed been observed *in vitro* using cell lysates treated with b-isox, a chemical which precipitates many RNA-binding proteins and RNAs (Han et al., 2012; Kato et al., 2012). In addition, SGs bring RNA-binding proteins and RNA in close proximity, which could promote the aggregation of such proteins, like Tau, which assembles into filaments in the presence of RNA (Kampers et al., 1996). On the other side, in some cases of neurodegeneration, SGs formation is reduced, which correlates with the increased sensitivity of cells to stress. Hexanucleotide repeat expansions in the C9ORF72 gene are associated with ALS and FTD and assumed to be a common genetic cause of the diseases. These repeats result in a reduced expression of the protein in the cells thus resembling a knock-down situation (Maharjan et al., 2017).

Moreover, knocking down C9ORF72 in neuroblastoma cells or in *Caenorhabditis elegans* abolished SGs formation and led to a higher stress sensitivity and increased neurodegeneration (Maharjan et al., 2017; Therrien et al., 2013). These results suggest that the impairment of SGs assembly could also contribute to the progression of neurodegenerative disorders.

These observations highlight the involvement of SGs in diseases such as cancer or neurodegenerative disorders. Manipulating SGs assembly could be of great use in order to limit resistance to cancer treatments or slow down the progression of neurodegeneration. SGs assembly is thought to take place via protein-protein, protein-RNA and RNA-RNA interactions. However, no precise mechanism has been proposed so far. Our study points to the role of post-transcriptional modification of mRNAs by the methyltransferase TRMT6/61A in targeting mRNAs to SGs. Since the defects of mRNA methylation impaired SGs formation and increased amyloidogenesis, stimulating TRMT6/61A activity could possibly limit aggregation. This work suggests the methyltransferase TRMT6/61A as a new target to manipulate SGs formation.

References

Abravaya, K., Myers, M.P., Murphy, S.P., and Morimoto, R.I. (1992). The human heat shock protein hsp70 interacts with HSF, the transcription factor that regulates heat shock gene expression. Genes Dev *6*, 1153–1164.

Adjibade, P., St-Sauveur, V.G., Huberdeau, M.Q., Fournier, M., Savard, A., Coudert, L., Khandjian, E.W., and Mazroui, R. (2015). Sorafenib, a multikinase inhibitor, induces formation of stress granules in hepatocarcinoma cells. Oncotarget *6*, 43927–43943.

Ainger, K., Avossa, D., Morgan, F., Hill, S.J., Barry, C., Barbarese, E., and Carson, J.H. (1993). Transport and Localization of Exogenous Myelin Basic Protein mRNA Microinjected into Oligodendrocytes. J. Cell Biol. *123*, 431–441.

de Almeida Souza Vilas-Boas, F., Mendes da Silva, A., Pires de Sousa, L., Maciel Lima, K., Priscila Vago, J., Bittencourt, L.F.F., Estanislau Dantas, A., Assis Gomes, D., Carvalho Vilela, M., Martins Teixeira, M., et al. (2016). Impairment of stress granule assembly via inhibition of the eIF2alpha phosphorylation sensitizes glioma cells to chemotherapeutic agents. J. Neurooncol. *127*, 253–260.

Ananthan, J., Goldberg, A.L., and Voellmy, R. (1986). Abnormal proteins serve as eukaryotic stress signals and trigger the activation of heat shock genes. Science (80-.). *232*, 522–524.

Anderson, P., and Kedersha, N. (2002). Stressful initiations. J. Cell Sci. *115*, 3227–3234.

Anderson, P., and Kedersha, N. (2006). RNA granules. J. Cell Biol. *172*, 803–808.

Anderson, P., and Kedersha, N. (2008). Stress granules: the Tao of RNA triage. Trends Biochem. Sci. *33*, 141–150.

Anderson, P., Kedersha, N., and Ivanov, P. (2015). Biochimica et Biophysica Acta Stress granules , P-bodies and cancer. BBA - Gene Regul. Mech. *1849*, 861–870.

Arimoto, K., Fukuda, H., Imajoh-Ohmi, S., Saito, H., and Takekawa, M. (2008). Formation of stress granules inhibits apoptosis by suppressing stress-responsive MAPK pathways. Nat. Cell Biol. *10*, 1324–1332.

Arocho, A., Chen, B., Ladanyi, M., and Pan, Q. (2006). Validation of the 2-DeltaDeltaCt calculation as an alternate method of data analysis for quantitative PCR of BCR-ABL P210 transcripts. Diagnostic Mol. Pathol. *15*, 56–61.

Arrigo, A.-P., Suhan, J.P., and Welch, W.J. (1988). Dynamic changes in the structure and intracellular locale of the mammalian low-molecular-weight heat shock protein. Mol. Cell. Biol. *8*, 5059–5071.

Ashraf, S.I., McLoon, A.L., Sclarsic, S.M., and Kunes, S. (2006). Synaptic protein synthesis associated with memory is regulated by the RISC pathway in Drosophila. Cell *124*, 191–205.

Atlas, R., Behar, L., Elliott, E., and Ginzburg, I. (2004). The insulin-like growth factor mRNA binding-protein IMP-1 and the Ras-regulatory protein G3BP associate with tau mRNA and HuD

protein in differentiated P19 neuronal cells. J. Neurochem. *89*, 613–626.

Audas, T.E., Audas, D.E., Jacob, M.D., Ho, J.J.D., Khacho, M., Wang, M., Perera, J.K., Gardiner, C., Bennett, C.A., Head, T., et al. (2016). Adaptation to Stressors by Systemic Protein Amyloidogenesis. Dev. Cell *39*, 155–168.

Baler, R., Dahl, G., and Voellmy, R. (1993). Activation of human heat shock genes is accompanied by oligomerization, modification, and rapid translocation of heat shock transcription factor HSF1. Mol. Cell. Biol. *13*, 2486–2496.

Barbarese, E., Koppel, D.E., Deutscher, M.P., Smith, C.L., Ainger, K., Morgan, F., and Carson, J.H. (1995). Protein translation components are colocalized in granules in oligodendrocytes. J. Cell Sci. *108*, 2781–2790.

Barraud, P., Golinelli-Pimpaneau, B., Atmanene, C., Sanglier, S., Van Dorsselaer, A., Droogmans, L., Dardel, F., and Tisné, C. (2008). Crystal Structure of Thermus thermophilus tRNA m1A58Methyltransferase and Biophysical Characterization of Its Interaction with tRNA. J. Mol. Biol. *377*, 535–550.

Bashkirov, V.I., Scherthan, H., Solinger, J.A., Buerstedde, J.M., and Heyer, W.D. (1997). A mouse cytoplasmic exoribonuclease (mXRN1p) with preference for G4 tetraplex substrates. J. Cell Biol. *136*, 761–773.

Bentmann, E., Haass, C., and Dormann, D. (2013). Stress granules in neurodegeneration - Lessons learnt from TAR DNA binding protein of 43 kDa and fused in sarcoma. FEBS J. *280*, 4348–4370.

Bley, N., Lederer, M., Pfalz, B., Reinke, C., Fuchs, T., Glaß, M., Möller, B., and Hüttelmaier, S. (2015). Stress granules are dispensable for mRNA stabilization during cellular stress. Nucleic Acids Res. *43*.

Boeynaems, S., Alberti, S., Fawzi, N.L., Mittag, T., Polymenidou, M., Rousseau, F., Schymkowitz, J., Shorter, J., Wolozin, B., Van Den Bosch, L., et al. (2018). Protein Phase Separation: A New Phase in Cell Biology. Trends Cell Biol. *28*, 420–435.

Bokar, J.A., Shambaugh, M.E., Polayes, D., Matera, A.G., and Rottman, F.M. (1997). Purification and cDNA cloning of the AdoMet-binding subunit of the human mRNA (N6-adenosine)-methyltransferase. Rna *3*, 1233–1247.

Bolognesi, B., Gotor, N.L., Dhar, R., Cirillo, D., Baldrighi, M., Tartaglia, G.G., and Lehner, B. (2016). A concentration-dependent liquid phase separation can cause toxicity upon increased protein expression. Cell Rep. *16*, 222–232.

Bosco, D.A., Lemay, N., Ko, H.K., Zhou, H., Burke, C., Kwiatkowski, T.J., Sapp, P., Mckenna-Yasek, D., Brown, R.H., and Hayward, L.J. (2010). Mutant FUS proteins that cause amyotrophic lateral sclerosis incorporate into stress granules. Hum. Mol. Genet. *19*, 4160–4175.

Bounedjah, O., Desforges, B., Wu, T. Di, Pioche-Durieu, C., Marco, S., Hamon, L., Curmi, P.A., Guerquin-Kern, J.L., Piétrement, O., and Pastré, D. (2014). Free mRNA in excess upon polysome dissociation is a scaffold for protein multimerization to form stress granules. Nucleic Acids Res. *42*, 8678–8691.

Brandt, F., Carlson, L.A., Hartl, F.U., Baumeister, W., and Grünewald, K. (2010). The Three-

Dimensional Organization of Polyribosomes in Intact Human Cells. Mol. Cell *39*, 560–569.

Brangwynne, C.P., Eckmann, C.R., Courson, D.S., Rybarska, A., Hoege, C., Gharakhani, J., Jülicher, F., and Hyman, A.A. (2009). Germline P Granules Are Liquid Droplets That Localize by Controlled Dissolution/Condensation. Science (80-.). *324*, 1729–1732.

Buchan, J.R., Muhlrad, D., and Parker, R. (2008). P bodies promote stress granule assembly in Saccharomyces cerevisiae. J. Cell Biol. *183*, 441–455.

Campen, A., Williams, R., Brown, C., Meng, J., Uversky, V., and Dunker, A. (2008). TOP-IDP-Scale: A New Amino Acid Scale Measuring Propensity for Intrinsic Disorder. Protein Pept. Lett. *15*, 956–963.

Cherkasov, V., Hofmann, S., Druffel-Augustin, S., Mogk, A., Tyedmers, J., Stoecklin, G., and Bukau, B. (2013). Coordination of translational control and protein homeostasis during severe heat stress. Curr. Biol. *23*, 2452–2462.

Chernov, K.G., Barbet, A., Hamon, L., Ovchinnikov, L.P., Curmi, P.A., and Pastré, D. (2009). Role of microtubules in stress granule assembly: Microtubule dynamical instability favors the formation of micrometric stress granules in cells. J. Biol. Chem. *284*, 36569–36580.

Clemens, M.J., Pain, V.M., Wong, S.-T., and Henshaw, E.C. (1982). Phosphorylation inhibits guanine nucleotide exchange on eukaryotic initiation factor 2. Nature *296*, 93–95.

Cohn, W.E., and Volkin, E. (1951). Nucleoside-5′-phosphates from ribonucleic acid. Nature *167*, 483–484.

Colthurst, D.R., Campbell, D.G., and Proud, C.G. (1987). Structure and regulation of eukaryotic initiation factor eIF-2: Sequence of the site in the α subunit phosphorylated by the haem-controlled repressor and by the double-stranded RNA-activated inhibitor. Eur. J. Biochem. *166*, 357–363.

Deng, J., Harding, H.P., Raught, B., Gingras, A.C., Berlanga, J.J., Scheuner, D., Kaufman, R.J., Ron, D., and Sonenberg, N. (2002). Activation of gcn2 in uv-irradiated cells inhibits translation. Curr. Biol. *12*, 1279–1286.

Desrosiers, R., Friderici, K., and Rottman, F. (1974). Identification of Methylated Nucleosides in Messenger RNA from Novikoff Hepatoma Cells. Proc. Natl. Acad. Sci. *71*, 3971–3975.

Dewey, C.M., Cenik, B., Sephton, C.F., Dries, D.R., Mayer III, P., Good, S.K., Johnson, B.A., Herz, J., and Yu, G. (2011). TDP-43 Is Directed to Stress Granules by Sorbitol, a Novel Physiological Osmotic and Oxidative Stressor. Mol. Cell. Biol. *31*, 1098–1108.

Di-Nocera, P.P., and Dawid, I.B. (1983). Transient expression of genes introduced into cultured-cells of Drosophila. Proc. Natl. Acad. Sci. *80*, 7095–7098.

van Dijk, E., Le Hir, H., and Seraphin, B. (2003). DcpS can act in the 5'-3' mRNA decay pathway in addition to the 3'-5' pathway. Proc. Natl. Acad. Sci. *100*, 12081–12086.

Van Dijk, E., Cougot, N., Meyer, S., Babajko, S., Wahle, E., and Séraphin, B. (2002). Human Dcp2: A catalytically active mRNA decapping enzyme located in specific cytoplasmic structures. EMBO J. *21*, 6915–6924.

Dominissini, D., Moshitch-Moshkovitz, S., Schwartz, S., Salmon-Divon, M., Ungar, L., Osenberg,

S., Cesarkas, K., Jacob-Hirsch, J., Amariglio, N., Kupiec, M., et al. (2012). Topology of the human and mouse m6A RNA methylomes revealed by m6A-seq. Nature *485*, 201–206.

Dominissini, D., Nachtergaele, S., Moshitch-Moshkovitz, S., Peer, E., Kol, N., Ben-Haim, M.S., Dai, Q., Di Segni, A., Salmon-Divon, M., Clark, W.C., et al. (2016). The dynamic N1-methyladenosine methylome in eukaryotic messenger RNA. Nature *530*, 441–446.

Dudler, R., and Travers, A.A. (1984). Upstream elements necessary for optimal function of the hsp 70 promoter in transformed flies. Cell *38*, 391–398.

Eisinger-Mathason, T.S.K., Andrade, J., Groehler, A.L., Clark, D.E., Muratore-Schroeder, T.L., Pasic, L., Smith, J.A., Shabanowitz, J., Hunt, D.F., Macara, I.G., et al. (2008). Codependent Functions of RSK2 and the Apoptosis-Promoting Factor TIA-1 in Stress Granule Assembly and Cell Survival. Mol. Cell *31*, 722–736.

Elbaum-Garfinkle, S., Kim, Y., Szczepaniak, K., Chen, C.C.-H., Eckmann, C.R., Myong, S., and Brangwynne, C.P. (2015). The disordered P granule protein LAF-1 drives phase separation into droplets with tunable viscosity and dynamics. Proc. Natl. Acad. Sci. *112*, 7189–7194.

Eystathioy, T., Chan, E.K.L., Tenenbaum, S.A., Keene, J.D., Griffith, K., and Fritzler, M.J. (2002). A Phosphorylated Cytoplasmic Autoantigen, GW182, Associates with a Unique Population of Human mRNAs within Novel Cytoplasmic Speckles. Mol. Biol. Cell *13*, 1338–1351.

Eystathioy, T., Jakymiw, A., Chan, E.K.L., Séraphin, B., Cougot, N., and Fritzler, M.J. (2003). The GW182 protein colocalizes with mRNA degradation associated proteins hDcp1 and hLSm4 in cytoplasmic GW bodies. RNA *9*, 1171–1173.

Fasken, M.B., and Corbett, A.H. (2009). Mechanisms of nuclear mRNA quality control. RNA Biol. *6*, 237–241.

Fay, M.M., Anderson, P.J., and Ivanov, P. (2017). ALS/FTD-Associated C9ORF72 Repeat RNA Promotes Phase Transitions In Vitro and in Cells. Cell Rep. *21*, 3573–3584.

Ferrandon, D., Elphick, L., Nusslein-Volhard, C., and St Johnston, D. (1994). Staufen protein associates with the 3' UTR of bicoid mRNA to form particles that move in a microtubule dependent manner. Cell *79*, 1221–1232.

Finer-Moore, J., Czudnochowski, N., O'Connell, J.D., Wang, A.L., and Stroud, R.M. (2015). Crystal Structure of the Human tRNA m1A58 Methyltransferase-tRNA3LysComplex: Refolding of Substrate tRNA Allows Access to the Methylation Target. J. Mol. Biol. *427*, 3862–3876.

Gallouzi, I.E., Brennan, C.M., Stenberg, M.G., Swanson, M.S., Eversole, A., Maizels, N., and Steitz, J. a (2000). HuR binding to cytoplasmic mRNA is perturbed by heat shock. Proc. Natl. Acad. Sci. U. S. A. *97*, 3073–3078.

Gerstberger, S., Hafner, M., and Tuschl, T. (2014). A census of human RNA-binding proteins. Nat. Rev. Genet. *15*, 829–845.

Geslain, R., and Pan, T. (2010). Functional analysis of human tRNA isodecoders. J. Mol. Biol. *396*.

Goedert, M., and Spillantini, M.G. (2006). A century of Alzheimer's disease. Science (80-.). *314*, 777–781.

Gowrishankar, G., Winzen, R., Dittrich-Breiholz, O., Redich, N., Kracht, M., and Holtmann, H. (2006). Inhibition of mRNA deadenylation and degradation by different types of cell stress. Biol. Chem. *387*, 323–327.

Greenfield, N., and Fasman, G.D. (1969). Computed Circular Dichroism Spectra for the Evaluation of Protein Conformation. Biochemistry *8*, 4108–4116.

Guelorget, A., Roovers, M., Guérineau, V., Barbey, C., Li, X., and Golinelli-Pimpaneau, B. (2010). Insights into the hyperthermostability and unusual region-specificity of archaeal Pyrococcus abyssi tRNA m1A57/58 methyltransferase. Nucleic Acids Res. *38*, 6206–6218.

Gueydan, C., Droogmans, L., Chalon, P., Huez, G., Caput, D., and Kruys, V. (1999). Identification of TIAR as a protein binding to the translational regulatory AU-rich element of tumor necrosis factor alpha mRNA. J. Biol. Chem. *274*, 2322–2326.

Gupta, A., Kumar, P.H., Dineshkumar, T.K., Varshney, U., and Subramanya, H.S. (2001). Crystal structure of Rv2118c: An AdoMet-dependent methyltransferase from Mycobacterium tuberculosis H37Rv. J. Mol. Biol. *312*, 381–391.

Han, T.W., Kato, M., Xie, S., Wu, L.C., Mirzaei, H., Pei, J., Chen, M., Xie, Y., Allen, J., Xiao, G., et al. (2012). Cell-free formation of RNA granules: Bound RNAs identify features and components of cellular assemblies. Cell *149*, 768–779.

Harashima, S., and Hinnebusch, A. (1986). Multiple GCD genes required for repression of GCN4, a transcriptional activator of amino acid biosynthetic genes in Saccharomyces cerevisiae. Mol. Cell. Biol. *6*, 3990–3998.

Harding, H.P., Zhang, Y., Bertolotti, A., Zeng, H., and Ron, D. (2000). Perk is essential for translational regulation and cell survival during the unfolded protein response. Mol. Cell *5*, 897–904.

Hicham Mahboubi, and Ursula Stochaj (2017). Cytoplasmic stress granules: Dynamic modulators of cell signaling and disease. Biochim. Biophys. Acta *1863*, 884–895.

Hightower, L.E. (1980). Cultured Animal Cells Exposed to Amino Acid Analogues or Puromycin Rapidly Synthesize Several Polypeptides. J. Cell. Physiol. *102*, 407–427.

Hilgers, V., Teixeira, D., and Parker, R. (2006). Translation-independent inhibition of mRNA deadenylation during stress in Saccharomyces cerevisiae. RNA *12*, 1835–1845.

Holcik, M., and Sonenberg, N. (2005). Translational control in stress and apoptosis. Nat. Rev. Mol. Cell Biol. *6*, 318–327.

Holzwarth, G., and Doty, P. (1965). The Ultraviolet Circular Dichroism of Polypeptides. J. Am. Chem. Soc. *87*, 218–228.

Hua, Y., and Zhou, J. (2004). Survival motor neuron protein facilitates assembly of stress granules. FEBS Lett. *572*, 69–74.

Hüttelmaier, S., Zenklusen, D., Lederer, M., Dictenberg, J., Lorenz, M., Meng, X., Bassell, G.J., Condeelis, J., and Singer, R.H. (2005). Spatial regulation of β-actin translation by Src-dependent phosphorylation of ZBP1. Nature *438*, 512–515.

Ingelfinger, D., Arndt-Jovin, D.J., Lührmann, R., and Achsel, T. (2002). The human LSm1-7 proteins colocalize with the mRNA-degrading enzymes Dcp1/2 and Xrnl in distinct cytoplasmic foci. Rna *8*, 1489–1501.

Iwanami, Y., and Brown, G.M. (1968). Methylated bases of ribosomal ribonucleic acid from HeLa cells. Arch. Biochem. Biophys. *126*, 8–15.

Jain, A., and Vale, R.D. (2017). RNA phase transitions in repeat expansion disorders. Nature *546*, 243–247.

Jain, S., Wheeler, J.R., Walters, R.W., Agrawal, A., Barsic, A., and Parker, R. (2016). ATPase-Modulated Stress Granules Contain a Diverse Proteome and Substructure. Cell *164*, 487–498.

Jia, G., Fu, Y., Zhao, X., Dai, Q., Zheng, G., Yang, Y., Yi, C., Lindahl, T., Pan, T., Yang, Y.G., et al. (2011). N6-Methyladenosine in nuclear RNA is a major substrate of the obesity-associated FTO. Nat. Chem. Biol. *7*, 885–887.

Kampers, T., Friedhoff, P., Biernat, J., Mandelkow, E.M., and Mandelkow, E. (1996). RNA stimulates aggregation of microtubule-associated protein tau into Alzheimer-like paired helical filaments. FEBS Lett. *399*, 344–349.

Katahira, J., Sträßer, K., Podtelejnikov, A., Mann, M., Jung, J.U., and Hurt, E. (1999). The Mex67p-mediated nuclear mRNA export pathway is conserved from yeast to human. EMBO J. *18*, 2593–2609.

Kato, M., Han, T.W., Xie, S., Shi, K., Du, X., Wu, L.C., Mirzaei, H., Goldsmith, E.J., Longgood, J., Pei, J., et al. (2012). Cell-free formation of RNA granules: Low complexity sequence domains form dynamic fibers within hydrogels. Cell *149*, 753–767.

Kawakami, a, Tian, Q., Duan, X., Streuli, M., Schlossman, S.F., and Anderson, P. (1992). Identification and functional characterization of a TIA-1-related nucleolysin. Proc. Natl. Acad. Sci. U. S. A. *89*, 8681–8685.

Kedersha, N., and Anderson, P. (2002). Stress granules: sites of mRNA triage that regulate mRNA stability and translatability. Biochem. Soc. Trans. *30*, 963–969.

Kedersha, N., Cho, M.R., Li, W., Yacono, P.W., Chen, S., Gilks, N., Golan, D.E., and Anderson, P. (2000). Dynamic shuttling of TIA-1 accompanies the recruitment of mRNA to mammalian stress granules. J. Cell Biol. *151*, 1257–1268.

Kedersha, N., Chen, S., Gilks, N., Li, W., Miller, I.J., Stahl, J., and Anderson, P. (2002). Evidence That Ternary Complex (eIF2-GTP-tRNAi Met)-Deficient Preinitiation Complexes Are Core Constituents of Mammalian Stress Granules Nancy. Mol. Biol. Cell *13*, 195–210.

Kedersha, N., Stoecklin, G., Ayodele, M., Yacono, P., Lykke-Andersen, J., Fitzler, M.J., Scheuner, D., Kaufman, R.J., Golan, D.E., and Anderson, P. (2005). Stress granules and processing bodies are dynamically linked sites of mRNP remodeling. J. Cell Biol. *169*, 871–884.

Kedersha, N.L., Gupta, M., Li, W., Miller, I., and Anderson, P. (1999). RNA-binding Proteins TIA-1 and TIAR Link the Phosphorylation of eIF-2 alpha to the Assembly of Mammalian Stress Granules. J. Cell Biol. *147*, 1431–1441.

Kelley, P.M., and Schlesinger, M.J. (1978). The effect of Amino Acid Analogues and Heat Shock

on Gene Expression in Chicken Embryo Fibroblasts. Cell *15*, 1277–1286.

Khong, A., Matheny, T., Jain, S., Mitchell, S.F., Wheeler, J.R., Parker, R., Khong, A., Matheny, T., Jain, S., Mitchell, S.F., et al. (2017). The Stress Granule Transcriptome Reveals Principles of mRNA Accumulation in Stress Granules Resource The Stress Granule Transcriptome Reveals Principles of mRNA Accumulation in Stress Granules. Mol. Cell *68*, 808–820.

Khong, A., Jain, S., Matheny, T., Wheeler, J.R., and Parker, R. (2018). Isolation of mammalian stress granule cores for RNA-Seq analysis. Methods *137*, 49–54.

Kiebler, M.A., and Bassell, G.J. (2006). Neuronal RNA Granules: Movers and Makers. Neuron *51*, 685–690.

Kim, W.J., Back, S.H., Kim, V., Ryu, I., and Jang, S.K. (2005). Sequestration of TRAF2 into Stress Granules Interrupts Tumor Necrosis Factor Signaling under Stress Conditions Sequestration of TRAF2 into Stress Granules Interrupts Tumor Necrosis Factor Signaling under Stress Conditions. Mol. Cell. Biol. *25*, 2450–2462.

Kingston, R.E., Schuetz, T.J., and Larin, Z. (1987). Heat-inducible human factor that binds to a human hsp70 promoter. Mol. Cell. Biol. *7*, 1530–1534.

Klus, P., Bolognesi, B., Agostini, F., Marchese, D., Zanzoni, A., and Tartaglia, G.G. (2014). The cleverSuite approach for protein characterization: Predictions of structural properties, solubility, chaperone requirements and RNA-binding abilities. Bioinformatics *30*, 1601–1608.

Knowles, R.B., Sabry, J.H., Martone, M.E., Deerinck, T.J., Ellisman, M.H., Bassell, G.J., and Kosik, K.S. (1996). Translocation of RNA granules in living neurons. J. Neurosci. *16*, 7812–7820.

Kohrmann, M., Luo, M., Kaether, C., DesGroseillers, L., Dotti, C.G., and Kiebler, M.A. (1999). Microtubule-dependent Recruitment of Staufen-Green Fluorescent Protein into Large RNA-containing Granules and Subsequent Dendritic Transport in Living Hippocampal Neurons. Mol. Biol. Cell *10*, 2945–2953.

Krichevsky, A.M., and Kosik, K.S. (2001). Neuronal RNA granules: A link between RNA localization and stimulation-dependent translation. Neuron *32*, 683–696.

Kuratani, M., Yanagisawa, T., Ishii, R., Matsuno, M., Si, S.Y., Katsura, K., Ushikoshi-Nakayama, R., Shibata, R., Shirouzu, M., Bessho, Y., et al. (2014). Crystal structure of tRNA m(1)A58 methyltransferase TrmI from Aquifex aeolicus in complex with S-adenosyl-L-methionine. J. Struct. Funct. Genomics *15*, 173–180.

Kwon, S.H., Zhang, Y., and Matthias, P. (2007). The deacetylase HDAC6 is an essential component of stress granules and plays a critical role in the cellular response to stress. Genes Dev. *21*, 3381–3394.

Kyte, J., and Doolittle, R.F. (1982). A simple method for displaying the hydropathic character of a protein. J. Mol. Biol. *157*, 105–132.

Langdon, E.M., Qiu, Y., Niaki, A.G., McLaughlin, G.A., Weidmann, C., Gerbich, T.M., Smith, J.A., Crutchley, J.M., Termini, C.M., Weeks, K.M., et al. (2018). MRNA structure determines specificity of a polyQ-driven phase separation. Science (80-.). *7432*.

Larson, J.S., Schuetz, T.J., and Kingston, R.E. (1988). Activation in vitro of sequence-specific

DNA binding by a human regulatory factor. Science (80-.). *335*, 372–375.

Lebleu, B., Sen, G.C., Shaila, S., Cabrer, B., and Lengyel, P. (1976). Interferon, double-stranded RNA, and protein phosphorylation. Proc. Natl. Acad. Sci. *73*, 3107–3111.

Li, C., Wen, A., Shen, B., Lu, J., Huang, Y., and Chang, Y. (2011). FastCloning: a highly simplified, purification-free, sequence- and ligation-independent PCR cloning method. BMC Biotechnol. *11*, 92.

Li, P., Banjade, S., Cheng, H.C., Kim, S., Chen, B., Guo, L., Llaguno, M., Hollingsworth, J. V., King, D.S., Banani, S.F., et al. (2012). Phase transitions in the assembly of multivalent signalling proteins. Nature *483*, 336–340.

Li, X., Xiong, X., Zhang, M., Wang, K., Chen, Y., Zhou, J., Mao, Y., Lv, J., Yi, D., Chen, X.W., et al. (2017). Base-Resolution Mapping Reveals Distinct m1A Methylome in Nuclear- and Mitochondrial-Encoded Transcripts. Mol. Cell *68*, 993–1005.e9.

Li, Y.R., King, O.D., Shorter, J., and Gitler, A.D. (2013). Stress granules as crucibles of ALS pathogenesis. J. Cell Biol. *201*, 361–372.

Lin, Y., Protter, D.S.W., Rosen, M.K., and Parker, R. (2015). Formation and Maturation of Phase-Separated Liquid Droplets by RNA-Binding Proteins. Mol. Cell *60*, 208–219.

Liu-Yesucevitz, L., Bilgutay, A., Zhang, Y.J., Vanderwyde, T., Citro, A., Mehta, T., Zaarur, N., McKee, A., Bowser, R., Sherman, M., et al. (2010). Tar DNA binding protein-43 (TDP-43) associates with stress granules: Analysis of cultured cells and pathological brain tissue. PLoS One *5*.

Liu-Yesucevitz, L., Lin, A.Y., Ebata, A., Boon, J.Y., Reid, W., Xu, Y.-F., Kobrin, K., Murphy, G.J., Petrucelli, L., and Wolozin, B. (2014). ALS-Linked Mutations Enlarge TDP-43-Enriched Neuronal RNA Granules in the Dendritic Arbor. J. Neurosci. *34*, 4167–4174.

Liu, F., Clark, W., Luo, G., Wang, X., Fu, Y., Wei, J., Wang, X., Hao, Z., Dai, Q., Zheng, G., et al. (2016). ALKBH1-Mediated tRNA Demethylation Regulates Translation. Cell *167*, 816–828 e16.

Liu, J., Yue, Y., Han, D., Wang, X., Fu, Y., Zhang, L., Jia, G., Yu, M., Lu, Z., Deng, X., et al. (2014). A METTL3-METTL14 complex mediates mammalian nuclear RNA N6-adenosine methylation. Nat. Chem. Biol. *10*, 93–95.

Livak, K.J., and Schmittgen, T.D. (2001). Analysis of relative gene expression data using real-time quantitative PCR and the 2-ΔΔCT method. Methods *25*, 402–408.

Lo, M.C., Aulabaugh, A., Jin, G., Cowling, R., Bard, J., Malamas, M., and Ellestad, G. (2004). Evaluation of fluorescence-based thermal shift assays for hit identification in drug discovery. Anal. Biochem. *332*, 153–159.

Lodish, H., Berk, A., Zipursky, S.. L., Matsudaira, P., Baltimore, D., and Darnell, J. (2000). Molecular Cell Biology, 4th edition (W. H. Freeman).

Loschi, M., Leishman, C.C., Berardone, N., and Boccaccio, G.L. (2009). Dynein and kinesin regulate stress-granule and P-body dynamics. J. Cell Sci. *122*, 3973–3982.

Lu, L., Han, A., and Chen, J. (2001). Translation Initiation Control by Heme-Regulated Eukaryotic Initiation Factor 2 α Kinase in Erythroid Cells under Cytoplasmic Stresses Translation Initiation Control by Heme-Regulated Eukaryotic Initiation Factor 2 ⎵ Kinase in Erythroid Cells under Cytopl. Mol Cell Biol *21*, 7971–7980.

Lu, L., Yi, C., Jian, X., Zheng, G., and He, C. (2010). Structure determination of DNA methylation lesions N1-meA and N3-meC in duplex DNA using a cross-linked protein-DNA system. Nucleic Acids Res. *38*, 4415–4425.

Mahadevan, K., Zhang, H., Akef, A., Cui, X.A., Gueroussov, S., Cenik, C., Roth, F.P., and Palazzo, A.F. (2013). RanBP2/Nup358 Potentiates the Translation of a Subset of mRNAs Encoding Secretory Proteins. PLoS Biol. *11*.

Maharana, S., Wang, J., Papadopoulos, D.K., Richter, D., Pozniakovsky, A., Poser, I., Bickle, M., Rizk, S., Guillén-boixet, J., Franzmann, T., et al. (2018). RNA buffers the phase separation behavior of prion-like RNA binding proteins. Science (80-.). *7366*.

Maharjan, N., Künzli, C., Buthey, K., and Saxena, S. (2017). C9ORF72 Regulates Stress Granule Formation and Its Deficiency Impairs Stress Granule Assembly, Hypersensitizing Cells to Stress. Mol. Neurobiol. *54*, 3062–3077.

Martin, C.T., and Coleman, J.E. (1989). T7 RNA polymerase does not interact with the 5'-phosphate of the initiating nucleotide. Biochemistry *28*, 2760–2762.

Mazroui, R., Di Marco, S., Kaufman, R.J., and Gallouzi, I.-E. (2007). Inhibition of the Ubiquitin-Proteasome System Induces Stress Granule Formation. Mol. Biol. Cell *18*, 2603–2618.

Mcewen, E., Kedersha, N., Song, B., Scheuner, D., Gilks, N., Han, A., Chen, J., Anderson, P., and Kaufman, R.J. (2005). Heme-regulated inhibitor (HRI) kinase-mediated phosphorylation of eukaryotic translation initiation factor 2 (EIF2) inhibits translation, induces stress granule formation, and mediates survival upon arsenite exposure. J. Biol. Chem. *280*, 16925–16933.

McGarry, T.J., and Lindquist, S. (1985). The preferential translation of Drosophila hsp70 mRNA requires sequences in the untranslated leader. Cell *42*, 903–911.

Meyer, K.D., Saletore, Y., Zumbo, P., Elemento, O., Mason, C.E., and Jaffrey, S.R. (2012). Comprehensive analysis of mRNA methylation reveals enrichment in 3′ UTRs and near stop codons. Cell *149*, 1635–1646.

Meyer, K.D., Patil, D.P., Zhou, J., Zinoviev, A., Skabkin, M.A., Elemento, O., Pestova, T. V, Qian, S., and Jaffrey, S.R. (2015). 5' UTR m6A Promotes Cap-Independent Translation. Cell *163*, 999–1010.

Mi, H., Huang, X., Muruganujan, A., Tang, H., Mills, C., Kang, D., and Thomas, P.D. (2017). PANTHER version 11: Expanded annotation data from Gene Ontology and Reactome pathways, and data analysis tool enhancements. Nucleic Acids Res. *45*, D183–D189.

Mokas, S., Mills, J.R., Garreau, C., Fournier, M.-J., Robert, F., Arya, P., Kaufman, R.J., Pelletier, J., and Mazroui, R. (2009). Uncoupling Stress Granule Assembly and Translation Initiation Inhibition. Mol. Clin. Oncol. *20*, 2673–2683.

Mollet, S., Cougot, N., Wilczynska, A., Dautry, F., Kress, M., Bertrand, E., and Weil, D. (2008).

Translationally Repressed mRNA Transiently Cycles through Stress Granules during Stress. Mol. Biol. Cell *19*, 4469–4479.

Molliex, A., Temirov, J., Lee, J., Coughlin, M., Kanagaraj, A.P., Kim, H.J., Mittag, T., and Taylor, J.P. (2015). Phase Separation by Low Complexity Domains Promotes Stress Granule Assembly and Drives Pathological Fibrillization. Cell *163*, 123–133.

Motorin, Y., and Helm, M. (2010). tRNA stabilization by modified nucleotides. Biochemistry *49*, 4934–4944.

Murakami, T., Qamar, S., Lin, J.Q., Schierle, G.S.K., Rees, E., Miyashita, A., Costa, A.R., Dodd, R.B., Chan, F.T.S., Michel, C.H., et al. (2015). ALS/FTD Mutation-Induced Phase Transition of FUS Liquid Droplets and Reversible Hydrogels into Irreversible Hydrogels Impairs RNP Granule Function. Neuron *88*, 678–690.

Nadezhdina, E.S., Lomakin, A.J., Shpilman, A.A., Chudinova, E.M., and Ivanov, P.A. (2010). Microtubules govern stress granule mobility and dynamics. Biochim. Biophys. Acta - Mol. Cell Res. *1803*, 361–371.

Neumann, E., Schaefer-Ridder, M., Wang, Y., and Hofschneider, P.H. (1982). Gene transfer into mouse lyoma cells by electroporation in high electric fields. EMBO J. *1*, 841–845.

Nover, L., Scharf, K.D., and Neumann, D. (1983). Formation of cytoplasmic heat shock granules in tomato cell cultures and leaves. Mol. Cell. Biol. *3*, 1648–1655.

Nover, L., Scharf, K.D., and Neumann, D. (1989). Cytoplasmic heat shock granules are formed from precursor particles and are associated with a specific set of mRNAs. Mol. Cell. Biol. *9*, 1298–1308.

Patel, A., Lee, H.O., Jawerth, L., Maharana, S., Jahnel, M., Hein, M.Y., Stoynov, S., Mahamid, J., Saha, S., Franzmann, T.M., et al. (2015). A Liquid-to-Solid Phase Transition of the ALS Protein FUS Accelerated by Disease Mutation. Cell *162*, 1066–1077.

Pathak, V.K., Schindler, D., and Hershey, J.W. (1988). Generation of a mutant form of protein synthesis initiation factor eIF-2 lacking the site of phosphorylation by eIF-2 kinases. Mol. Cell. Biol. *8*, 993–995.

Peifer, C., Sharma, S., Watzinger, P., Lamberth, S., Kötter, P., and Entian, K.D. (2013). Yeast Rrp8p, a novel methyltransferase responsible for m1A 645 base modification of 25S rRNA. Nucleic Acids Res. *41*, 1151–1163.

Piecyk, M., Wax, S., Beck, A.R.P., Kedersha, N., Gupta, M., Maritim, B., Chen, S., Gueydan, C., Kruys, V., Streuli, M., et al. (2000). TIA-1 is a translational silencer that selectively regulates the expression of TNF-alpha. EMBO *19*, 4154–4163.

Ping, X.L., Sun, B.F., Wang, L., Xiao, W., Yang, X., Wang, W.J., Adhikari, S., Shi, Y., Lv, Y., Chen, Y.S., et al. (2014). Mammalian WTAP is a regulatory subunit of the RNA N6-methyladenosine methyltransferase. Cell Res. *24*, 177–189.

Protter, D.S.W., and Parker, R. (2016). Principles and Properties of Stress Granules. Trends Cell Biol. *26*, 668–679.

Protter, D.S.W., Rao, B.S., Van Treeck, B., Lin, Y., Mizoue, L., Rosen, M.K., and Parker, R.

(2018). Intrinsically Disordered Regions Can Contribute Promiscuous Interactions to RNP Granule Assembly. Cell Rep. *22*, 1401–1412.

Ramaiah, K.V.A., Davies, M. V., Chen, J., and Kaufman, R.J. (1994). Expression of mutant eukaryotic initiation factor 2 alpha subunit (eIF-2 alpha) reduces inhibition of guanine nucleotide exchange activity of eIF-2B mediated by eIF-2 alpha phosphorylation. Mol. Cell. Biol. *14*, 4546–4553.

Ritossa, F. (1962). A New Puffing Pattern Induced by Temperature Shock and DNP in Drosophila. Experientia *18*, 571–573.

Roberts, W.K., Hovanessian, A., Brown, R.E., Clemens, M.J., and Kerr, I.M. (1976). Interferon-mediated protein kinase and low-molecular-weight inhibitor of protein synthesis. Nature *264*, 477–480.

Rook, M.S., Lu, M., and Kosik, K.S. (2000). CaMKIIalpha 3' untranslated region-directed mRNA translocation in living neurons: visualization by GFP linkage. J. Neurosci. *20*, 6385–6393.

Roost, C., Lynch, S.R., Batista, P.J., Qu, K., Chang, H.Y., and Kool, E.T. (2015). Structure and thermodynamics of N6-Methyladenosine in RNA: a spring-loaded base modification. J. Am. Chem. Soc. *137*, 2107–2115.

Roundtree, I.A., Evans, M.E., Pan, T., and He, C. (2017). Dynamic RNA Modifications in Gene Expression Regulation. Cell *169*, 1187–1200.

Rowlands, A.G., Panniers, R., and Henshaw, E.C. (1988). The catalytic mechanism of guanine nucleotide exchange factor action and competitive inhibition by phosphorylated eukaryotic initiation factor 2. J. Biol. Chem. *263*, 5526–5533.

Saavedra, C., Tung, K.S., Amberg, D.C., Hopper, A.K., and Cole, C.N. (1996). Regulation of mRNA export in response to stress in Saccharomyces cerevisiae. Genes Dev. *10*, 1608–1620.

Safra, M., Sas-Chen, A., Nir, R., Winkler, R., Nachshon, A., Bar-Yaacov, D., Erlacher, M., Rossmanith, W., Stern-Ginossar, N., and Schwartz, S. (2017). The m1A landscape on cytosolic and mitochondrial mRNA at single-base resolution. Nature *551*, 251–255.

Saneyoshi, M., Harada, F., and Nishimura, S. (1969). Isolation and characterization of N6-methyladenosine from Escherichia coli valine transfer RNA. BBA Sect. Nucleic Acids Protein Synth. *190*, 264–273.

Schratt, G.M., Tuebing, F., Nigh, E.A., Kane, C.G., Sabatini, M.E., Kiebler, M., and Greenberg, M.E. (2006). A brain-specific microRNA regulates dendritic spine development. Nature *439*, 283–289.

Schwartz, S., Mumbach, M.R., Jovanovic, M., Wang, T., Maciag, K., Bushkin, G.G., Mertins, P., Ter-Ovanesyan, D., Habib, N., Cacchiarelli, D., et al. (2014). Perturbation of m6A writers reveals two distinct classes of mRNA methylation at internal and 5' sites. Cell Rep. *8*, 284–296.

Sharma, S., Watzinger, P., Kötter, P., and Entian, K.D. (2013). Identification of a novel methyltransferase, Bmt2, responsible for the N-1-methyl-adenosine base modification of 25S rRNA in Saccharomyces cerevisiae. Nucleic Acids Res. *41*, 5428–5443.

Sharma, S., Hartmann, J.D., Watzinger, P., Klepper, A., Peifer, C., Kötter, P., Lafontaine, D.L.J.,

and Entian, K.D. (2018). A single N1-methyladenosine on the large ribosomal subunit rRNA impacts locally its structure and the translation of key metabolic enzymes. Sci. Rep. *8*, 1–16.

Shen, S., Li, X.F., Cullen, W.R., Weinfeld, M., and Le, X.C. (2013). Arsenic binding to proteins. Chem. Rev. *113*, 7769–7792.

Shi, Y., Mosser, D.D., and Morimoto, R.I. (1998). Molecular chaperones as HSF1-specific transcriptional repressors. Genes Dev. *12*, 654–666.

Shukla, S., and Parker, R. (2016). Hypo- and Hyper-Assembly Diseases of RNA – Protein Complexes. Trends Mol. Med. *22*, 615–628.

Slobodin, B., Han, R., Calderone, V., Vrielink, J.A.F.O., Loayza-Puch, F., Elkon, R., and Agami, R. (2017). Transcription Impacts the Efficiency of mRNA Translation via Co-transcriptional N6-adenosine Methylation. Cell *169*, 326–337.e12.

Smart, F.M., Edelman, G.M., and Vanderklish, P.W. (2003). BDNF induces translocation of initiation factor 4E to mRNA granules: evidence for a role of synaptic microfilaments and integrins. Proc. Natl. Acad. Sci. U. S. A. *100*, 14403–14408.

Somasekharan, S.P., El-Naggar, A., Leprivier, G., Cheng, H., Hajee, S., Grunewald, T.G.P., Zhang, F., Ng, T., Delattre, O., Evdokimova, V., et al. (2015). YB-1 regulates stress granule formation and tumor progression by translationally activating G3BP1. J. Cell Biol. *208*, 913–929.

Steinberg, T.H., Jones, L.J., Haugland, R.P., and Singer, V.L. (1996). SYPRO Orange and SYPRO Red Protein Gel Stains: One-Step Fluorescent Staining of Denaturing Gels for Detection of Nanogram Lefile:///C:/Users/Patrick/Downloads/Steinberg Gel Staining.pdfvels of Protein. Anal. Biochem. *239*, 223–237.

Stöhr, N., Lederer, M., Reinke, C., Meyer, S., Hatzfeld, M., Singer, R.H., and Hüttelmaier, S. (2006). ZBP1 regulates mRNA stability during cellular stress. J. Cell Biol. *175*, 527–534.

Takahara, T., and Maeda, T. (2012). Transient Sequestration of TORC1 into Stress Granules during Heat Stress. Mol. Cell *47*, 242–252.

Takahashi, M., Higuchi, M., Matsuki, H., Yoshita, M., Ohsawa, T., Oie, M., and Fujii, M. (2013). Stress Granules Inhibit Apoptosis by Reducing Reactive Oxygen Species Production. Mol. Cell. Biol. *33*, 815–829.

Tartaglia, G.G., and Vendruscolo, M. (2010). Proteome-Level Interplay between Folding and Aggregation Propensities of Proteins. J. Mol. Biol. *402*, 919–928.

Taupin, J.L., Tian, Q., Kedersha, N., Robertson, M., and Anderson, P. (1995). The RNA-binding protein TIAR is translocated from the nucleus to the cytoplasm during Fas-mediated apoptotic cell death. Proc. Natl. Acad. Sci. U. S. A. *92*, 1629–1633.

Therrien, M., Rouleau, G.A., Dion, P.A., and Parker, J.A. (2013). Deletion of C9ORF72 results in motor neuron degeneration and stress sensitivity in C. elegans. PLoS One *8*, 1–10.

Thomas, M.G., Martinez Tosar, L.J., Loschi, M., Pasquini, J.M., Correale, J., Kindler, S., and Boccaccio, G.L. (2005). Staufen Recruitment into Stress Granules Does Not Affect Early mRNA Transport in Oligodendrocytes. Mol. Biol. Cell *16*, 405–420.

Tian, B.Q., Taupin, J., Elledge, S., Robertson, M., and Anderson, P. (1995). Fas-activated Serine/Threonine Kinase (FAST) Phosphorylates TIA-1 during Fas-mediated Apoptosis. J. Exp. Med. *182*, 865–874.

Tian, Q., Streuli, M., Saito, H., Schlossman, S.F., and Anderson, P. (1991). A polyadenylate binding protein localized to the granules of cytolytic lymphocytes induces DNA fragmentation in target cells. Cell *67*, 629–639.

Tourrière, H., Chebli, K., Zekri, L., Courselaud, B., Blanchard, J.M., Bertrand, E., and Tazi, J. (2003). The RasGAP-associated endoribonuclease G3BP assembles stress granules. J. Cell Biol. *160*, 823–831.

Van Treeck, B., Protter, D.S.W., Matheny, T., Khong, A., Link, C.D., and Parker, R. (2018). RNA self-assembly contributes to stress granule formation and defining the stress granule transcriptome. Proc. Natl. Acad. Sci. *115*, 2734–2739.

Tutucci, E., and Stutz, F. (2011). Keeping mRNPs in check during assembly and nuclear export. Nat. Rev. Mol. Cell Biol. *12*, 377–384.

Vabulas, R.M., and Hartl, F.U. (2005). Protein Synthesis upon Acute Nutrient restriction Relies on Proteasome Function. Science (80-.). *310*, 1960–1963.

Vanderweyde, T., Yu, H., Varnum, M., Liu-Yesucevitz, L., Citro, A., Ikezu, T., Duff, K., and Wolozin, B. (2012). Contrasting Pathology of the Stress Granule Protein TIA-1 and G3BP in Tauopathies. J. Neurosci. *32*, 8270–8283.

Waelter, S., Boeddrich, A., Lurz, R., Scherzinger, E., Lueder, G., Lehrach, H., and Wanker, E.E. (2001). Accumulation of mutant huntingtin fragments in aggresome-like inclusion bodies as a result of insufficient protein degradation. Mol. Biol. Cell *12*, 1393–1407.

Walters, R.W., Muhlrad, D., Garcia, J., and Parker, R. (2015). Differential effects of Ydj1 and Sis1 on Hsp70-mediated clearance of stress granules in Saccharomyces cerevisiae. Rna *21*, 1660–1671.

Wang, P., Doxtader, K.A., and Nam, Y. (2016). Structural Basis for Cooperative Function of Mettl3 and Mettl14 Methyltransferases. Mol. Cell *63*, 306–317.

Wang, X., Lu, Z., Gomez, A., Hon, G.C., Yue, Y., Han, D., Fu, Y., Parisien, M., Dai, Q., Jia, G., et al. (2014a). N 6-methyladenosine-dependent regulation of messenger RNA stability. Nature *505*, 117–120.

Wang, X., Zhao, B.S., Roundtree, I.A., Lu, Z., Han, D., Ma, H., Weng, X., Chen, K., Shi, H., and He, C. (2015). N6-methyladenosine modulates messenger RNA translation efficiency. Cell *161*, 1388–1399.

Wang, Y., Li, Y., Toth, J.I., Petroski, M.D., Zhang, Z., and Zhao, J.C. (2014b). N6-methyladenosine modification destabilizes developmental regulators in embryonic stem cells. Nat. Cell Biol. *16*, 191–198.

Watanabe, K., Miyagawa, R., Tomikawa, C., Mizuno, R., Takahashi, A., Hori, H., and Ijiri, K. (2013). Degradation of initiator tRNAMet by Xrn1/2 via its accumulation in the nucleus of heat-treated HeLa cells. Nucleic Acids Res. *41*, 4671–4685.

Weber, S.C., and Brangwynne, C.P. (2012). Getting RNA and protein in phase. Cell *149*, 1188–

1191.

Wek, S.A., Zhu, S., and Wek, R.C. (1995). The histidyl-tRNA synthetase-related sequence in the eIF-2 alpha protein kinase GCN2 interacts with tRNA and is required for activation in response to starvation for different amino acids. Mol. Cell. Biol. *15*, 4497–4506.

Westermann, A.J., Gorski, S.A., and Vogel, J. (2012). Dual RNA-seq of pathogen and host. Nat. Rev. Microbiol. *10*, 618–630.

Wheeler, J.R., Matheny, T., Jain, S., Abrisch, R., and Parker, R. (2016). Distinct stages in stress granule assembly and disassembly. Elife *5*, 1–25.

Wilczynska, A., Aigueperse, C., Kress, M., Dautry, F., and Weil, D. (2005). The translational regulator CPEB1 provides a link between dcp1 bodies and stress granules. J. Cell Sci. *118*, 981–992.

Wolozin, B. (2014). Physiological Protein Aggregation Run Amuck: Stress Granules and the Genesis of Neurodegenerative Disease. Discov. Med. *17*, 47–52.

Xiao, W., Adhikari, S., Dahal, U., Chen, Y.-S., Hao, Y.-J., Sun, B.-F., Sun, H.-Y., Li, A., Ping, X.-L., Lai, W.-Y., et al. (2016). Nuclear m 6 A Reader YTHDC1 Regulates mRNA Splicing. Mol. Cell *61*, 507–519.

Yang, J., Sharma, S., Watzinger, P., Hartmann, J.D., Kötter, P., and Entian, K.D. (2016). Mapping of complete set of ribose and base modifications of yeast rRNA by RP-HPLC and mung bean nuclease assay. PLoS One *11*, 1–18.

Zander, G., Hackmann, A., Bender, L., Becker, D., Lingner, T., Salinas, G., and Krebber, H. (2016). MRNA quality control is bypassed for immediate export of stress-responsive transcripts. Nature *540*, 593–596.

Zhang, H., Elbaum-Garfinkle, S., Langdon, E.M., Taylor, N., Occhipinti, P., Bridges, A.A., Brangwynne, C.P., and Gladfelter, A.S. (2015). RNA Controls PolyQ Protein Phase Transitions. Mol. Cell *60*, 220–230.

Zhao, B.S., Roundtree, I.A., and He, C. (2017). Post-transcriptional gene regulation by mRNA modifications. Nat. Rev. Mol. Cell Biol. *18*, 31–42.

Zheng, G., Dahl, J.A., Niu, Y., Fedorcsak, P., Huang, C.M., Li, C.J., Vågbø, C.B., Shi, Y., Wang, W.L., Song, S.H., et al. (2013). ALKBH5 Is a Mammalian RNA Demethylase that Impacts RNA Metabolism and Mouse Fertility. Mol. Cell *49*, 18–29.

Zhou, H., Kimsey, I.J., Nikolova, E.N., Sathyamoorthy, B., Grazioli, G., McSally, J., Bai, T., Wunderlich, C.H., Kreutz, C., Andricioaei, I., et al. (2016). m1A and m1G disrupt A-RNA structure through the intrinsic instability of Hoogsteen base pairs. Nat. Struct. Mol. Biol. *23*, 803–810.

Zou, J., Guo, Y., Guettouche, T., Smith, D.F., and Voellmy, R. (1998). Repression of heat shock transcription factor HSF1 activation by HSP90 (HSP90 complex) that forms a stress-sensitive complex with HSF1. Cell *94*, 471–480.

Statement of personal contributions

Except when stated otherwise by reference or acknowledgment, the work presented was generated by myself under the supervision of my advisors during my doctoral studies. All contributions from colleagues are explicitly indicated:

Fig. 9 and Fig. 10: Transfection of cells with Cy5-mRNA by electroporation: The *in vitro* transcription of mRNA was done by myself. Gerd Hanspach (Institute for Organic Chemistry and Chemical Biology; Goethe University Frankfurt) labelled the mRNA molecules with a Cy5 molecule. I performed the transfection of cells with mRNA and microscopy analysis.

Fig. 16 and Fig. 18: Free mRNA interactome: I prepared the biotinylated mRNA and performed the free mRNA pulldowns. Dr. Giulia Calloni (Buchmann Institute for Molecular Life Sciences; Goethe University Frankfurt) processed the samples for MS measurement and performed the MS analysis.

Fig. 24: Purified recombinant TRMT6/61A: Adrían Martínez Limón (Buchmann Institute for Molecular Life Sciences; Goethe University Frankfurt) and Viktor Pfeifer (Intern student) purified the protein complex.

Fig. 25 and 26: *In vitro* study of TRMT6/61A stability at 45 °C: Adrían Martínez Limón performed the melting experiment and the CD spectroscopy analysis. The TRMT6/61A susbtrate (unmethylated tRNA) was transcribed *in vitro*, purified and refolded by myself.

Fig. 30: Study of m^1A motif presence in mRNAs: The analysis of m^1A motif enrichment was performed by Riccardo Delli Ponti (Centre for Genomic Regulation (CRG); Barcelona, Spain).

Fig. 33: Enrichment of m^1A-containing mRNAs in stress granules: I isolated the stress granules, performed the western blot analysis and the RNA extraction. Dr. Giulia Calloni processed the samples for MS measurement and performed the MS analysis.

Fig. 35: HPLC analysis of nucleosides of endogenous tRNAs: I performed the tRNA isolation. Dr. Giulia Calloni processed the samples and analyzed nucleosides content by HPLC.

Fig. 47: MS analysis of Aβ co-aggregators: I performed the GFP pulldowns. Dr. Giulia Calloni processed the samples and performed the MS analysis.

Appendix 1 and 2: List of mRNA interactors identified by label-free quantitative mass spectrometry: As specified for related Fig. 16 & Fig. 18.

Appendix 3: List of Aβ-EGFP interactors identified by label-free quantitative mass spectrometry: As specified for related Fig. 47.

Appendix 1: List of HSP70 mRNA interactors identified by LFQ mass spectrometry

Table 7. List of HSP70 mRNA interactors.
Data from five independent replicates are shown.
Label-free quantification (LFQ) mRNA/BG: LFQ of mRNA sample over background.

Protein names	Gene names	AVG mRNA/BG	Sequence coverage [%]
Replication factor C subunit 1	RFC1	146.34	17.4
TRMT61A	TRMT61A	87.77	33.9
Round spermatid basic protein 1	RSBN1	76.47	17.4
Arf-GAP with GTPase, ANK repeat and PH-containing protein 1	AGAP1	61.59	16.2
RNA 3-terminal phosphate cyclase	RTCA	59.78	43.7
Methenyltetrahydrofolate synthase domain-containing protein	MTHFSD	53.41	49.1
TRMT6	TRMT6	42.31	35.2
N-acetyltransferase 10	NAT10	40.05	49.7
DnaJ homolog subfamily C member 21	DNAJC21	39.13	48.6
E3 ubiquitin-protein ligase RBBP6	RBBP6	38.83	4.9
N-acylneuraminate cytidylyltransferase	CMAS	35.44	28.8
Ribosomal RNA small subunit methyltransferase NEP1	EMG1	31.13	39.3
Kinesin-like protein;Kinesin-like protein KIF23	KIF23	29.51	13.2
PHD finger protein 3	PHF3	28.87	19.2
Far upstream element-binding protein 1	FUBP1	28.68	56
Kinesin-like protein KIF2A	KIF2A	27.25	51
Lysine-rich nucleolar protein 1	KNOP1	27.03	21.4
Transforming acidic coiled-coil-containing protein 2	TACC2	21.99	32.9
THO complex subunit 5 homolog	THOC5	20.97	21.4
SLAIN motif-containing protein 2	SLAIN2	19.53	60.6
Zinc finger CCCH domain-containing protein 8	ZC3H8	17.08	25.6
Helicase-like transcription factor	HLTF	14.92	31.4
SPATS2-like protein	SPATS2L	14.89	51.6
Mediator of RNA polymerase II transcription subunit 1	MED1	14.73	13
CAP-Gly domain-containing linker protein 2	CLIP2	14.57	47.9
Serine/arginine-rich splicing factor 3	SRSF3	13.91	44.5
p21-activated protein kinase-interacting protein 1	PAK1IP1	13.86	40.6
Zinc finger protein 787	ZNF787	13.71	3.1
Microtubule-associated protein	MAP4	13.23	48.7
Zinc finger C2HC domain-containing protein 1A	ZC2HC1A	12.35	56
Uncharacterized protein KIAA1522	KIAA1522	11.05	48.2
Zinc finger protein 346	ZNF346	10.65	50.7
THO complex subunit 4	ALYREF	10.54	39.8
Nucleolin	NCL	9.84	41.5
GAS2-like protein 3	GAS2L3	9.75	15.1
Spermatogenesis-associated serine-rich protein 2	SPATS2	8.46	72.1
Serine/arginine-rich splicing factor 7	SRSF7	7.93	56.2
Mediator of RNA polymerase II transcription subunit 24	MED24	7.87	9.4
Heterogeneous nuclear ribonucleoprotein D-like	HNRNPDL	7.65	27.3
RRP15-like protein	RRP15	7.35	8.2

Protein names	Gene names	AVG mRNA/BG	Sequence coverage [%]
Ribonuclease P protein subunit p30	RPP30	6.88	19
SAFB-like transcription modulator	SLTM	6.34	9.1
Putative ATP-dependent RNA helicase DHX57	DHX57	6.34	61.1
Cytoplasmic FMR1-interacting protein 2	CYFIP2	6.32	30.8
ATP-dependent RNA helicase DDX24	DDX24	6.29	15.3
Regulator of nonsense transcripts 3B	UPF3B	6.14	38.3
Cytoskeleton-associated protein 5	CKAP5	6.13	61.3
ATP-dependent RNA helicase A	DHX9	5.33	57.5
Ribosome-binding protein 1	RRBP1	5.20	48.4
Eukaryotic translation initiation factor 2 subunit 2	EIF2S2	4.93	75.1
Regulator of nonsense transcripts 2	UPF2	4.92	55.7
Signal recognition particle 9 kDa protein	SRP9	4.85	55.8
Protein LSM14 homolog A	LSM14A	4.66	40
Signal recognition particle 14 kDa protein	SRP14	4.37	68.4
Proline/serine-rich coiled-coil protein 1	PSRC1	4.34	14.3
Interleukin enhancer-binding factor 3	ILF3	3.85	63.5
Heterogeneous nuclear ribonucleoprotein D0	HNRNPD	3.58	27
Transforming acidic coiled-coil-containing protein 1	TACC1	3.57	41.7
Eukaryotic translation initiation factor 2 subunit 1	EIF2S1	3.55	75.6
ATP-dependent RNA helicase DHX36	DHX36	3.49	57.5
Centrosomal protein of 170 kDa	CEP170	3.47	41.4
Spliceosome RNA helicase DDX39B	DDX39B	3.41	43.2
Interleukin enhancer-binding factor 2	ILF2	3.32	75.3
Heterogeneous nuclear ribonucleoprotein A3	HNRNPA3	3.08	48.1
Replication protein A 70 kDa DNA-binding subunit	RPA1	3.08	61.2
Adenomatous polyposis coli protein	APC	3.01	27.7
Endoribonuclease Dicer	DICER1	2.96	27.6
Eukaryotic translation initiation factor 2 subunit 3	EIF2S3	2.96	63.8
SRSF protein kinase 2	SRPK2	2.94	40
Casein kinase I isoform delta	CSNK1D	2.94	28.2
TRMT1-like protein	TRMT1L	2.84	8.9
Cold-inducible RNA-binding protein	CIRBP	2.83	31.2
MAP/microtubule affinity-regulating kinase 3	MARK3	2.34	37.2
ATP-binding cassette sub-family F member 1	ABCF1	2.31	55.6
Microtubule cross-linking factor 1	MTCL1	2.27	51.7
Eukaryotic translation initiation factor 5B	EIF5B	2.26	45
WD repeat-containing protein 24	WDR24	2.24	38.4
Echinoderm microtubule-associated protein-like 3	EML3	2.17	28.9
Calmodulin-regulated spectrin-associated protein 2	CAMSAP2	2.06	37.1

Appendix 2: List of B-Raf mRNA interactors identified by LFQ mass spectrometry

Table 8. List of B-Raf mRNA interactors.
Data from three independent replicates are shown.
LFQ PD/BG: LFQ of pulldown sample over background.

Protein name	Gene name	AVG PD/BG	Sequence coverage [%]
Kinesin-like protein KIF2A	KIF2A	109.23	9.5
Biorientation of chromosomes in cell division protein 1-like 1	BOD1L1	39.48	0.4
Septin-11	SEPT11	36.14	8.3
THO complex subunit 4	ALYREF	30.55	24.6
Zinc finger CCHC domain-containing protein 8	ZCCHC8	27.10	8.8
Spliceosome RNA helicase DDX39B	DDX39B	27.07	13.7
SPATS2-like protein	SPATS2L	24.31	30.8
Protein FAM98A	FAM98A	20.68	20.2
tRNA (adenine(58)-N(1))-methyltransferase non-catalytic subunit TRM6	TRMT6	17.46	7.6
Serrate RNA effector molecule homolog	SRRT	17.36	3.8
KH domain-containing, RNA-binding, signal transduction-associated protein 1	KHDRBS1	16.46	6.3
Methenyltetrahydrofolate synthase domain-containing protein	MTHFSD	15.13	25.0
UPF0568 protein C14orf166	C14orf166	12.36	75.8
Heterogeneous nuclear ribonucleoprotein A/B	HNRNPAB	12.13	18.6
tRNA-splicing ligase RtcB homolog	RTCB	12.04	59.4
ATP-dependent RNA helicase DDX1	DDX1	10.95	46.4
PHD finger protein 3	PHF3	10.51	5.1
Interleukin enhancer-binding factor 2	ILF2	10.01	25.0
Protein SCAF11	SCAF11	10.01	2.4
Far upstream element-binding protein 1	FUBP1	8.92	18.8
Nucleolin	NCL	8.07	27.6
Ras-related protein Rab-5A	RAB5A	7.43	15.8
Spermatogenesis-associated serine-rich protein 2	SPATS2	7.26	33.9
Putative ATP-dependent RNA helicase DHX57	DHX57	7.22	21.1
RRP15-like protein	RRP15	6.92	11.7
Interleukin enhancer-binding factor 3	ILF3	6.88	22.3
DnaJ homolog subfamily C member 21	DNAJC21	6.56	21.7
Caprin-1	CAPRIN1	6.47	30.2
Signal recognition particle 9 kDa protein	SRP9	6.18	38.4
U1 small nuclear ribonucleoprotein C	SNRPC	5.54	7.6
SLAIN motif-containing protein 2	SLAIN2	5.53	18.1
Signal recognition particle 14 kDa protein	SRP14	5.41	30.4
Heterogeneous nuclear ribonucleoprotein A1	HNRNPA1	5.34	31.9
Regulator of nonsense transcripts 2	UPF2	5.29	10.2
Rac GTPase-activating protein 1	RACGAP1	5.25	4.1
Serine/arginine-rich splicing factor 3	SRSF3	4.66	11.0
ATP-dependent RNA helicase DHX36	DHX36	4.60	26.2
Ras GTPase-activating protein-binding protein 1	G3BP1	4.60	53.9
Heterogeneous nuclear ribonucleoprotein D-like	HNRNPDL	4.52	14.3

Protein name	Gene name	AVG PD/BG	Sequence coverage [%]
RNA-binding motif protein, X chromosome	RBMX	4.29	40.2
Centrosomal protein of 170 kDa	CEP170	4.00	9.4
Regulator of nonsense transcripts 3B	UPF3B	3.91	21.3
Heterogeneous nuclear ribonucleoprotein Q	SYNCRIP	3.81	46.9
7SK snRNA methylphosphate capping enzyme	MEPCE	3.64	2.8
RNA-binding protein 24;RNA-binding protein 38	RBM24	3.60	16.2
Glycogen phosphorylase, liver form	PYGL	3.58	1.1
Protein LSM14 homolog A	LSM14A	3.45	11.0
Heterogeneous nuclear ribonucleoproteins A2/B1	HNRNPA2B1	3.06	46.7
Tudor domain-containing protein 3	TDRD3	2.85	21.7
Protein PRRC2C	PRRC2C	2.73	32.0
Eukaryotic translation initiation factor 2 subunit 3	EIF2S3	2.73	41.5
Nuclear factor 1;Nuclear factor 1 X-type	NFIX	2.70	15.8
WD repeat-containing protein 82	WDR82	2.43	15.0
TOX high mobility group box family member 4	TOX4	2.31	7.9
Putative ATP-dependent RNA helicase DHX30	DHX30	2.24	8.2
DAZ-associated protein 1	DAZAP1	2.10	24.9
Antigen KI-67	MKI67	1.72	0.4
Fragile X mental retardation protein 1	FMR1	1.60	9.5

Appendix 3: List of Aβ-EGFP interactors identified by LFQ mass spectrometry

Table 9. List of Aβ-EGFP interactors.
Data from five independent replicates are shown.
LFQ PD/BG: LFQ of pulldown sample over background.

Protein name	Gene name	AVG PD/BG	Sequence coverage [%]
Amyloid beta A4 protein	APP	1181.74	1.8
Sideroflexin-1	SFXN1	34.51	33.9
60S ribosomal protein L21	RPL21	24.57	39.1
Plectin	PLEC	22.36	7.6
Nicotinamide phosphoribosyltransferase	NAMPT	16.73	38.5
60S ribosomal protein L27	RPL27	15.70	30.9
DNA replication licensing factor MCM6	MCM6	15.17	9.6
Insulin-like growth factor 2 mRNA-binding protein 1	IGF2BP1	14.25	18.2
U1 small nuclear ribonucleoprotein 70 kDa	SNRNP70	14.12	36.2
Non-POU domain-containing octamer-binding protein	NONO	13.19	27.8
Eukaryotic translation initiation factor 4 gamma 1	EIF4G1	13.14	8.5
Glutamate--cysteine ligase regulatory subunit	GCLM	12.83	14.2
Heterogeneous nuclear ribonucleoprotein A0	HNRNPA0	11.37	21
Regulator of nonsense transcripts 1	UPF1	10.61	3
28 kDa heat- and acid-stable phosphoprotein	PDAP1	10.08	22.7
Mitochondrial 2-oxoglutarate/malate carrier protein	SLC25A11	9.96	20.3
Transforming protein RhoA	RHOA	9.57	13.5
Erlin-1	ERLIN1	8.63	14.2
Cytochrome b-c1 complex subunit 2, mitochondrial	UQCRC2	8.63	31.6
60S ribosomal protein L8	RPL8	8.37	24.4
Staphylococcal nuclease domain-containing protein 1	SND1	8.16	20.3
ATP-dependent RNA helicase A	DHX9	7.95	10.5
Tubulin alpha-4A chain	TUBA4A	7.74	56.7
Splicing factor, proline- and glutamine-rich	SFPQ	7.52	6.2
Eukaryotic translation initiation factor 3 subunit L	EIF3L	7.16	18
Transcription factor BTF3	BTF3	7.09	7.3
Translational activator GCN1	GCN1L1	6.74	5.5
Proteasome-associated protein ECM29 homolog	KIAA0368	6.63	2.1
ATP-binding cassette sub-family E member 1	ABCE1	6.58	10.5
Alanine--tRNA ligase, cytoplasmic	AARS	6.45	3.1
Clathrin interactor 1	CLINT1	6.25	6.7
Calpain-2 catalytic subunit	CAPN2	6.15	5.9
Vigilin	HDLBP	6.00	7.1
Heat shock 70 kDa protein 1B	HSPA1B	5.94	44.2
HCLS1-associated protein X-1	HAX1	5.76	39.7
MARCKS-related protein	MARCKSL1	5.64	14.4
Mitochondrial import inner membrane translocase TIM50	TIMM50	5.51	13
60S ribosomal protein L15	RPL15	5.48	28.4
Cell division cycle protein 123 homolog	CDC123	5.37	16.6
Filamin-C	FLNC	5.00	19.3

Protein name	Gene name	AVG PD/BG	Sequence coverage [%]
Replication factor C subunit 3	RFC3	4.93	3.9
Signal recognition particle 14 kDa protein	SRP14	4.84	47.1
LIM domain only protein 7	LMO7	4.57	8.9
Smoothelin	SMTN	4.55	5.7
Pyruvate carboxylase, mitochondrial	PC	4.26	2.1
Pre-mRNA-processing factor 6	PRPF6	4.20	6.7
Double-stranded RNA-specific adenosine deaminase	ADAR	4.19	3.8
Cytochrome c oxidase subunit NDUFA4	NDUFA4	4.06	22.2
KH-containing, RNA-binding, signal transduction protein 1	KHDRBS1	4.04	6.3
Succinate dehydrogenase [ubiquinone] flavoprotein subunit	SDHA	4.04	5
Ras GTPase-activating protein-binding protein 2	G3BP2	3.96	7.5
Calreticulin	CALR	3.96	18.9
60S ribosomal protein L23	RPL23	3.87	29.3
DNA-dependent protein kinase catalytic subunit	PRKDC	3.87	15.8
CDKN2A-interacting protein	CDKN2AIP	3.83	24.7
60S acidic ribosomal protein P0	RPLP0	3.61	29.7
Keratin, type I cytoskeletal 18	KRT18	3.52	76.3
Replication factor C subunit 1	RFC1	3.49	2.3
Centrosomal protein of 170 kDa	CEP170	3.48	2.2
Protein phosphatase 1G	PPM1G	3.47	4
Receptor protein-tyrosine kinase	EGFR	3.42	1.8
tRNA (cytosine(34)-C(5))-methyltransferase	NSUN2	3.38	24.4
Nuclease-sensitive element-binding protein 1	YBX1	3.38	40.1
Mitochondrial ribonuclease P protein 1	TRMT10C	3.27	17.4
Stress-70 protein, mitochondrial	HSPA9	3.24	24.2
Structural maintenance of chromosomes protein 4	SMC4	3.12	5
Serrate RNA effector molecule homolog	SRRT	3.04	11.6
ADP/ATP translocase 2	SLC25A5	2.98	43.3
40S ribosomal protein S9	RPS9	2.95	44.3
Ribosomal protein L19;60S ribosomal protein L19	RPL19	2.80	15
La-related protein 1	LARP1	2.67	5.7
Coatomer subunit gamma-1	COPG1	2.63	19.9
Heat shock protein beta-1	HSPB1	2.60	44.9
Ensconsin	MAP7	2.56	7.1
Adenylate kinase 4, mitochondrial	AK4	2.52	9.4
Tubulin alpha-1B chain	TUBA1B	2.04	58.5
Signal recognition particle receptor subunit beta	SRPRB	1.99	11.2
Heat shock cognate 71 kDa protein	HSPA8	1.91	54.2
Heat shock protein HSP 90-beta	HSP90AB1	1.88	43.6
Bifunctional glutamate/proline--tRNA ligase	EPRS	1.85	14.9

Appendix 4: Plasmids prepared and/or used in the thesis

pcDNA3.1-Hygro
Expression: mammalian
Source: 1-71, Vabulas lab
Used for: Empty plasmid used for adjusting DNA amounts in transfections experiments
Bacterial resistance gene: Ampicillin

pUb(h)EΔ
Expression: Mammalian
Source: 1-383, Vabulas lab
Used for: Preparation of 1-1008 and 1-1009
Bacterial resistance gene: Kanamycin

p3F-NQO1
Expression: Mammalian
Source: 1-874, Vabulas lab.
Used for: Preparation of 1-1010 and 1-1011.
Bacterial resistance gene: Ampicillin

pRBS-3xF-BRAF
Expression: Mammalian
Source: 1-894, modification of the plasmid pB-Raf (a gift from Dustin Maly, Addgene, plasmid 40775) by addition of a RBS sequence and of two extra flag tags suing the primers F-BRAF-fw and rev and pcDNA3-RBS-fw and rev.
Used for: *In vitro* transcription of B-Raf mRNA.
Bacterial resistance gene: Ampicillin

pcDNA3.1-eGFP
Expression: Mammalian
Source: 1-949, Vabulas lab
Used for: Overexpression in mammalian cells
Bacterial resistance gene: Ampicillin

pAβ-eGFP
Expression: Mammalian
Source: 1-950, Vabulas lab
Used for: Overexpression in mammalian cells
Bacterial resistance gene: Ampicillin

pTRMT6-FLAG
Expression: Mammalian
Source: 1-953, Vabulas lab
Used for: Overexpression in mammalian cells
Bacterial resistance gene: Ampicillin

pTRMT61A-FLAG
Expression: mammalian
Source: 1-954, Vabulas lab
Used for: Overexpression in mammalian cells
Bacterial resistance gene: Ampicillin

pTRMT61A-3xF
Expression: mammalian
Source: 1-967, cloned from 1-954 using the primers FLAG-TRMT6/61A-fw and rev
Used for: Insertion of 2 extra flag tags for better antibody detection sensitivity
Bacterial resistance gene: Ampicillin

CRISPR-TRMT61A-GFP and **CRISPR-TRMT61A-Puro**
Expression: Mammalian
Source: 1-998 and 1-999, Vabulas lab
Used for: generation of TRMT61A knock-out/knock-down cell lines (double nickase plasmids mix)
Bacterial resistance gene: Ampicillin

pm1A-Ub-EGFP
Expression: Mammalian
Source: 1-1008, cloned from pUb(h)EΔ (Vabulas lab) using the primers m1A-1-383-fw and rev
Description: Insertion of an m^1A motif at the 5' of an Ubiquitin-EGFP construct (PRUNE-1 gene m^1A motif described by Safra et al., 2017)
Bacterial resistance gene: Kanamycin

pm1A-Ub-EGFP-mut
Expression: Mammalian
Source: 1-1009, cloned from pUb(h)EΔ (Vabulas lab) using the primers m1A-1-383-fw-CTRL and rev-CTRL
Description: Insertion of a mutated m^1A motif (T instead of the A to be methylated) at the 5' of an Ubiquitin-EGFP construct (PRUNE gene m^1A motif described by Safra et al., 2017)
Bacterial resistance gene: Kanamycin

pm1A-3F-NQO1
Expression: Mammalian
Source: 1-1010, cloned from p3F-NQO1 (1-874) using the primers m1A-1-874-fw and rev.
Description: Insertion of an m^1A motif at the 5' of a 3F-NQO1 construct (PRUNE gene m^1A motif described by Safra et al, Nature, 2017)
Bacterial resistance gene: Ampicillin

pm1A-mut-3F-NQO1
Expression: Mammalian
Source: 1-1011, cloned from p3F-NQO1 (1-874) using the primers m1A-CTRL-1-874-fw and rev.
Description: Insertion of a mutated m^1A motif (T instead of the A to be methylated) at the 5' of a 3F-NQO1 construct (PRUNE gene m^1A motif described by Safra et al, Nature, 2017)
Bacterial resistance gene: Ampicillin

pT7-HSP70
Expression: bacterial
Source: 2-67, Vabulas lab
Used for: *in vitro* transcription of HPS70 mRNA, as a template.
Bacterial resistance gene: Ampicillin

phis-TRMT6/TRMT61a
Expression: bacterial
Source: 2-239, Vabulas lab
Used for: Purification of recombinant TRMT6/TRMT61A.
Bacterial resistance gene: Ampicillin

Appendix 5: Chemicals and reagents

Table 10. Chemicals and reagents.

Chemical/Reagent/Kit	Company	Reference
1-Ethyl-3-(3-dimethylaminopropyl)carbodiimid*hydrochloride (EDC)	Alfa Aesar	A10807
2-chloroacetamide	Sigma-Aldrich	22790
2-mercaptoethanol	Sigma-Aldrich	M3148
2-propanol (MS grade)	Fisher Scientific	A461-212
Aceton	Roth	9372.1
Acetic acid	Roth	3738.5
Acetonitrile (MS grade)	Fisher Scientific	A955-1
Acrylamide/Bisacrylamide (30 % ; 37.5 :1)	Roth	3029.1
Acrylamide/Bisacrylamide (29 :1)	Sigma-Aldrich	A2792
Actinomycin D	Enzo Life Sciences	BML-GR300
Adenosine	Sigma-Aldrich	A9251
Agarose	Biozym	840014
Albumin fraction V	Roth	8076.3
AllIN HIFI DNA Polymerase	HighQu	HLE0201
Amersham Cy5 monoreactive dye pack	GE Healthcare	PA25001
Ammonium acetate	Roth	7869.2
Ammoniumperoxodisulfate (APS)	Roth	9592.2
Ampicillin sodium salt	Sigma-Aldrich	A0166
Ampliscribe T7 high yield transcription kit	Epicenter	AS3107
Anti-Flag M2 affinity gel	Sigma-Aldrich	A2220
Arsenite (III) oxide (As_2O_3)	Sigma-Aldrich	202673
ATP disodium salt hydrate	Sigma-Aldrich	A26209
Bacterial Alcaline Phosphatase (BAP C75)	Takara	2120A
Benzonase	Merck	71205-3
Boric Acid	Fluka	15665
Bradford reagent	Sigma-Aldrich	B6916
Brilliant Blue R250	Roth	46255
Bromphenol Blue	Roth	A512.2
Calcium chloride dihydrate	Roth	T885.2
Chloroform	Roth	7331.2
Cycloheximide	Sigma-Aldrich	C7698
Cystine	Sigma-Aldrich	C8755
Cytidine	Sigma-Aldrich	C122106
DAPI	Sigma-Aldrich	1246530100
DMEM (Debulcco's Modified Eagle's Medium)	Sigma-Aldrich	D5671
DMSO	Sigma-Aldrich	D4540
DNA Gel loading dye	New England Biolabs	B7024S

Chemical/Reagent/Kit	Company	Reference
DpnI	New England Biolabs	R0176S
DTT (Dithiothreitol)	Roth	6908.2
Dynabeads M-280 Streptavidin	ThermoFisher Scientific	11205D
EDTA (Ethylendiamintetraacetic acid)	Sigma-Aldrich	E9884
EGTA (Ethylene glycol-bis(2-aminoethylether)-N,N,N',N'-tetraacetic acid)	Roth	3054.3
Ethylenediamine	Sigma-Aldrich	03550
Ethanol	Roth	K928.4
Fetal Bovine Serum	Sigma-Aldrich	F0804
Flag (3x) peptide	Sigma-Aldrich	F4799
Formaldehyde solution (36.5-38 %)	Sigma-Aldrich	F8775
Formic acid	Fisher chemicals	A117-50
GelRed	Biotium	41003
GeneJET Plasmid Miniprep kit	ThermoFisher Scientific	K0503
GenElute HP Endotoxin-Free Plasmid Maxiprep kit	Sigma-Aldrich	NA0410-1KT
GFP Trap Magnetic Agarose	Chromotek	gtma
Glutamine	Gibco	25030-024
Glycerin	Roth	3783.5
Glycin	Roth	3908.3
GMP	Sigma-Aldrich	G8377
Guanosine	Sigma-Aldrich	G6752
Hepes (N-2-Hydroxyethyl piperazine-N'-2-ethane sulphonic acid)	Roth	9105.3
Herculase II Fusion DNA polymerase	Agilent	600675
Hydrochloric acid 32 %	Roth	P074.1
Hygromycin B Hydrochloride from*Streptomyces	Sigma-Aldrich	H3274
Imidazole ($C_3H_4N_2$)	Sigma-Aldrich	56749
Isopropyl alcohol	Sigma-Aldrich	33539
Kanamycin	Sigma-Aldrich	K1377
KiCqStart SYBR Green qPCR ReadyMix	Sigma-Aldrich	KCQS00
LB-medium	Roth	X964
LB-agar	Roth	X965
Lipofectamine RNAiMax	ThermoFisher Scientific	13778
Lithium Chloride	Sigma-Aldrich	L9650
Lithium Dodecyl Sulfate	Sigma-Aldrich	L9781
Low range ssRNA ladder	New England Biolabs	N0364S
Magnesium acetate tetrahydrate	Roth	0275.1
Magnesium chloride hexahydrate	Roth	A537.4
Magnesium sulfate heptahydrate	Roth	T888.1

Chemical/Reagent/Kit	Company	Reference
Manganese II chloride tetrahydrate	Roth	T881.1
MegaClear transcription clean up kit	ThermoFisher Scientific	AM1908
MEM non-essential aminoacids	Gibco	11140-35
Methanol	Roth	CP43.4
Methanol (MS grade)	Fisher Scientific	A456-1
Methionine	Sigma-Aldrich	M9625
MG-132	Enzo Life Sciences	BML-PI102-0025
Milk powder	Roth	T145.3
mirVana miRNA isolation kit	ThermoFisher Scientific	AM1560
MOPS (3-(N-Morpholino)propanesulfonic acid)	Roth	6979.4
N1-methylated adenosine	Carbosynth	NM03697
N1-Methyl-ATP	Trilink	N1042
N6-methylated adenosine	Carbosynth	NM32281
N6-Methyl-ATP	Trilink	N1013
Nuclease P1	Wako Chemicals	145-08221
Oligo d(T)25 magnetic beads	New England Biolabs	S1419S
Opti-MEM	Gibco	31985062
Paraformaldehyde	Sigma-Aldrich	158127
Penicillin/Streptomycin	Sigma-Aldrich	P4333
Phenol/Chloroform Isoamylalcohol pH 4-5	Sigma-Aldrich	77619
Phenol/Chloroform Isoamylalcohol pH 8	ThermoFisher Scientific	17908
Phosphatase Inhibitor cocktail 2	Sigma-Aldrich	P5726
Phusion High fidelity DNA polymerase	New England Biolabs	M0530
Pierce 3´end RNA biotinylation Kit	ThermoFisher Scientific	20160
PMS (phenazine methosulfate)	Sigma-Aldrich	P9625
PMSF (Phenylmethylsulfonylfluorid)	Roth	6367.2
Polyethylenimine, 25 kDa, linear (PEI)	Polysciences Inc.	#23966
Poly-L-lysine	Sigma-Aldrich	P8920
Potassium Acetate	AppliChem	A3625
Potassium Chloride	Roth	6781.2
Potassium Hydroxide	Roth	6751.1
Pre-coated TLC-sheets ALUGRAM SIL G/UV_{254}	Macherey-Nagel	818133
Protein ladder	HighQu	PRL0202
Proteinase K	Sigma-Aldrich	P2308
Puromycin aminonucleoside	Sigma-Aldrich	P8833
Reprosil-Pur C18 resin	Dr Maisch GmbH	R124.aq
RevertAid RT kit	ThermoFisher Scientific	K1691
RiboGreen	ThermoFisher Scientific	R11491

Chemical/Reagent/Kit	Company	Reference
RNA loading dye	New England Biolabs	B0363S
RNAsin	Promega	N2515
RNeasy mini kit	Qiagen	74104
Rubidium Chloride	Sigma-Aldrich	83979
SDS (Sodium Dodecyl Sulfate)	Roth	CN30.3
SIGMAFAST protease inhibitor tablets	Sigma-Aldrich	S8820
Sodium Chloride	Roth	3957.2
Sodium Deoxycholate	AppliChem	A1531
Sodium Hydroxyde	Roth	6771.1
Sucrose	Sigma-Aldrich	S0389
SuperSignal West Pico PLUS Chemiluminescent Substrate	Thermo Fisher Scientific	34577
SYBR Safe	Thermo Fisher Scientific	S33102
SYPRO Orange	Sigma-Aldrich	S5692
TCA (Trichloroacetic acid)	Sigma-Aldrich	T6399
TEMED (Tetramethylethylenediamine)	Roth	2367.3
Trifluoroacetic acid	Sigma-Aldrich	299537
Triton X-100	Sigma-Aldrich	T8787
Trizma base (2-Amino-2-(hydroxymethyl)-1,3-propanediol)	Sigma-Aldrich	T1503
Trizol	Life Technologies	15596
Trypsin/Lys-C Mix, Mass spec grade	Promega	V5073
Trypsin-EDTA solution	Sigma-Aldrich	T4049
Tween 20	Sigma-Aldrich	P1379
Urea (CH_4N_2O)	Roth	2317.4
Uridine	Sigma-Aldrich	U3750
Water (MS grade)	Fisher Scientific	W6-212
XbaI	New England Biolabs	R0145
XhoI	New England Biolabs	R0146
XmnI	New England Biolabs	R0194
XTT sodium salt	Sigma-Aldrich	X4626

Appendix 6: Antibodies

Table 11. Antibodies.

Antibody	Company	Reference	Dilution
Alexa Fluor 647-conjugated anti-Rabbit IgG	Cell Signaling	#4414	1:1000 in 1 % BSA/PBS (immunofluorescence)
Anti-1-methyladenosine (m^1A)	MBL	D345-3	1:100 in 1 % Tween 20/PBS (detection of m^1A on polyA mRNAs)
Anti-N^6-methyladenosine (m^6A)	MBL	RN131P	1:100 in 1 % Tween 20/PBS (detection of m^6A on polyA mRNAs)
Anti-eIF2α	Cell Signaling	#9722	1:1000 (western blot)
Anti-eIF2α (phosphor-Ser51)	Cell Signaling	#3398	1:1000 (western blot)
Anti-eIF4E	Cell Signaling	#9742S	1:100 in 1 % BSA/PBS (immunofluorescence)
Anti-Flag	Sigma-Aldrich	F1804	1:1000 (western blot)
Anti-Flag M2-Cy3	Sigma-Aldrich	A9594	1:100 in 1 % BSA/PBS (immunofluorescence)
Anti-GAPDH	Cell Signaling	#2118S	1:1000 (western blot)
Anti-GFP	Sigma-Aldrich	11814460001	1:1000 (western blot)
Anti-S6	Santa Cruz Biotechnology, Inc.	sc-74459	1:100 (western blot)
Anti-TIAR	Cell Signaling	#8509	1:1000 in 1 % BSA/PBS (immunofluorescence)
Anti-TRMT6	Bethyl	A303-008A	1:500 (western blot)
Anti-TRMT61A	Santa Cruz Biotechnology, Inc.	sc-107105	1:100 (western blot)
HRP-conjugated anti-Goat IgG	Sigma-Aldrich	A4174	1:5000 (western blot)
HRP-conjugated anti-Mouse IgG	Sigma-Aldrich	A9044	1:5000 (western blot)
HRP-conjugated anti-Rabbit IgG	Cell Signaling	#7074	1:5000 (western blot)